Chiral Cavities with Amino Acid Derived Ligands and their Interactions with Chiral and Achiral Guests

A
Thesis Submitted
In Partial Fulfillment of the Requirement
for the Degree of

DOCTOR OF PHILOSOPHY

By

Subash Chandra Sahoo

Department of Chemistry
Indian Institute of Technology Guwahati
Guwahati-781039
March-2010

Dedicated to my Parents

and

Brother (Basudev Sahoo)

****** Subash

INDIAN INSTITUTE OF TECHNOLOGY GUWAHATI

Department of Chemistry

STATEMENT

I hereby declare that the matter embodied in this thesis is the result of investigations carried out by me in the Department of Chemistry, Indian Institute of Technology Guwahati, India under the supervision of Dr Manabendra Ray, Associate Professor, Department of Chemistry, Indian Institute of Technology Guwahati, India.

In keeping with the general practice of reporting observations, due acknowledgements have been made wherever the work described is based on the findings of other investigations.

March, 2010

I. I. T. Guwahati

Subash Chandra Sahoo

Dr.Manabendra Ray
Associate Professor
Indian Institute of Technology Guwahati
Department of Chemistry
Tel. 91 361 258 2310
Fax.91 361 258 2349

CERTIFICATE

This is to certify that Mr. Subash Chandra Sahoo has been working under my supervision since July 2005. I am forwarding his thesis, entitled, "**Chiral Cavities with Amino acid derived Ligands and their Interactions with Chiral and Achiral Guests"** being submitted for the degree of Doctorate of Philosophy of this Institute. I certify that he has fulfilled all the requirements according to the rules of this Institute, and that the investigations embodied in this thesis have not been submitted elsewhere for a degree.

March- 2010

I. I. T. Guwahati

Dr. Manabendra Ray
Supervisor

Acknowledgement

During the period of my Ph.D work I have been guided and supported by many people and that gives me a pleasant opportunity to express my gratitude to all of them. First and foremost, with a deepest sense of gratitude, I wish to express my sincere thanks to my supervisor, Dr. Manabendra Ray for his excellent guidance, constant encouragements and moral supports at each and every step of my research work. I am so fortunate to utter that his enthusiasm and fundamental view on research and his efforts in producing high quality work, which have made a deep impression on me. His confidence in doing lab work, scientific thinking, valuable suggestions, discussions and the creative way of scientific presentation inspired me to gain more knowledge in the field of inorganic chemistry and crystal engineering. As his third student I find myself privileged to have worked under his kind guidance.

My sincere thanks are due to all my doctoral committee members for their constant inspiration and valuable suggestions. I am grateful to Dr. Gopal Das and Dr. B. K. Patel for their insightful advices and valuable scientific hints. My sincere thanks are due to all other faculty members in the Department of Chemistry for their help and encouragement and the non-teaching staffs of the Department for their technical support.

I am thankful to Indian Institute of Technology Guwahati for providing me with the infrastructure and facilities for research. My sincere thanks to Mr. Chandan Borgohain, Mr. K. Senapathy and Mr. Kh. Kesho Singh of Central Instruments facility, IIT-Guwahati for their help in all the characterizations (SEM, NMR, EPR, VSM, and LCMS) required during my research work. I am grateful to IACS, Kolkata and CDRI, Lucknow for elemental analysis whenever I need during my research work. I am grateful to Babulai da mounting crystals and Subal da for their help.

My heartfelt thanks to Siva Murru, Saitanya Bharadwaj and Rajendra Pamula for their help, support, and as good neighbors and best friends. I would never forget to thank my seniors; Meher bhai, Padhi Bhai, Laxmi Bhai, and Biswa Bhai for their constant help and support whenever I need. I will always remember the wonderful time I had spent with them. My sincere thanks to my lab senior Dr. Rik Rani Koner and my lab juniors Mrigendra Dubey and S. H. Faizi for their timely help and support during my entire research period.

My special thanks to Himansu for his eternal help and support. Thanks to Bigyana, Sontosh, Annu and Rosy for their timely help and support.

I would like to express my appreciation to my other friends in the campus, Jugal, Smruti, Deba, Nihar, Mussawir, Readdy, Ramesh, Suri, Zia, Jasmini, and my all 2005 Ph.D batch mates for the wonderful time I had with them. My sincere thanks to super seniors; Sarala Didi, Babu da, Martha Bhai, Tara bhai, for their help and support. I express my honest appreciation to Sraban bahi, Mamta appa, Manu bhai and Amit Sir for providing homely feeling by inviting for lunch and dinner during holidays.

The financial support from Council of Scientific and Industrial Research (UGC), New Delhi for JRF and SRF is duly acknowledged. I also thank Indian Institute of Technology, Guwahati for the initial financial support as JRF.

I am grateful to Futu Bhai for his honest help and support for my study. I am also thankful to Mira Bhauja and their family members for their help and support. I am so grateful to express my sincere thanks to my best friend Hemanta and his family for timely help and support. He and his friendship is god gift for me and I myself felt lucky to have a friend like him.

Finally, my Ph. D endeavor could not be completed without the endless love and blessings from my parents and grandparents. I wish to express my sincere gratitude to my sisters (Manu & Sabita) and parents especially to father. He is the main soul and inspiration for each and every step during my childhood which gave me strength and right path to go ahead in spite of my poverty. Along with my family I wish to express my sincere gratitude to grandparent family; especially Bada papa, Bada maa, Kasi Bbahi, and Puni for their enormous support and help. I found privileged to be part of their family. I am highly indebted to thank my elder brother Basu Bhai, June Nani and Bubun Bhai for their constant inspiration, insightful advices, and encouragement for my higher studies and unwavering faith on me, which always encourages me to go ahead. At last but not least, my thanks to Mitu bahuja for his endless love and blessings for me.

Abstract

In this thesis we have attempted to explore the synthesis of small molecular weight complexes having guest binding site within a cavity. During the course we have explored two different sets of amino acid derived ligands (Figure 1) and systematically synthesized number of Cu(II) and Ni(II) complexes via two different approaches were we would able to form cavity capable of binding external guest either through metal coordination or H-bonding. We have used amino acid derivative ligands, as it is the easiest and cost effective way to incorporate chirality in the host due to availability of pure L-amino acids from the natural source. Further studies with external guest we were able to separate enantiomers from a racemic mixture with one of the host. This particular result constitutes a rare example of chiral separation through non-covalent interaction between a host and guest where host-guest adducts are structurally characterized.

The thesis has been divided in to six chapters. Chapter wise summary of the work are given below.

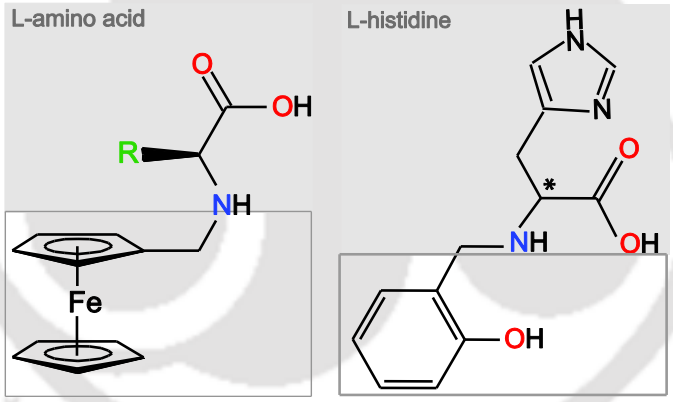

Figure 1 The chiral amino acid derived ligands used in this thesis.

Chapter 1: *Introduction*

This chapter summarizes a brief literature review on different types of organic or inorganic base macrocyclic receptors used for guest recognition particularly keeping the view of importance of chirality.

Chapter 2: *Ferrocene substitution in amino acids enhances the axial binding in Cu(II) bis-complexes and separates the hydrophobic and hydrophilic region in the lattice.*

This chapter describe the synthesis, characterization and electrochemical properties of a set of ferrocenylmethyl substituted L-amino acid ligands and their Cu(II) complexes. It was

observed that the two ligands organize around Cu(II) in a C_2 symmetry such that both amino acid residues stay on the same side of the Cu(II) coordination plane. Structural characterization of the complexes of L-methionine (Figure 2) and L-asparagine derived ligands showed axial coordination of weak thioether and amide respectively to Cu(II). We like to note that usually methionine thioether does not bind in synthetic Cu(II) complexes. Coordination of the thioether group of L-methionine to copper (2.791Å) is shorter than observed in the electron transfer protein plastocyanin (2.9Å). The characterization of *bis*-complexes with L-serine and L-threonine derivatives showed axial coordination of water with a shorter Cu–O bond length compared to that observed in the corresponding amino acid complexes. The structures also revealed separation of the hydrophilic and hydrophobic regions due to amino acid and ferrocene respectively which resulted in the formation of interesting H-bonded networks (Figure 2).

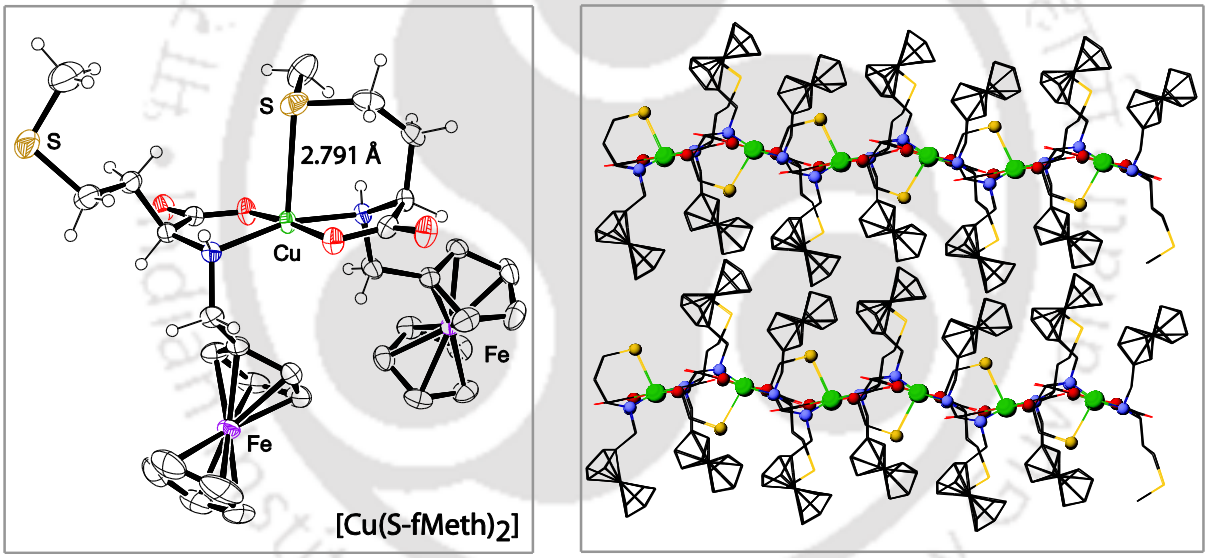

Figure 2. Molecular and lattice structure of Cu(II) complex of ferrocenylmethyl-L-methionine ligand.

Chapter 3: *Formation of a narrow chiral cavity in Cu(II) bis-complexes of ferrocenylmethyl L-tyrosine derivative and its inter action with achiral guests.*

The tendency of ferrocenylmethyl substituted amino acids to organize around Cu(II) in a C_2 symmetry, as observed in Chapter 2, was utilized to form a narrow chiral cavity employing ferrocenylmethyl-L-tyrosine ligand. The structural characterization of $[Cu^{II}(S\text{-fTyr})_2(MeCN)_2]$ and subsequently other adducts prepared from it by substituting MeCN showed that planar

heterocyclic N-donors as guests stabilized the cavity, while polar water molecules destroyed it (Figure 3). Electrochemical properties of the complexes showed a shift of Cu^{II}/Cu^{I} potentials depending on the strength of the guest binding inside the cavity.

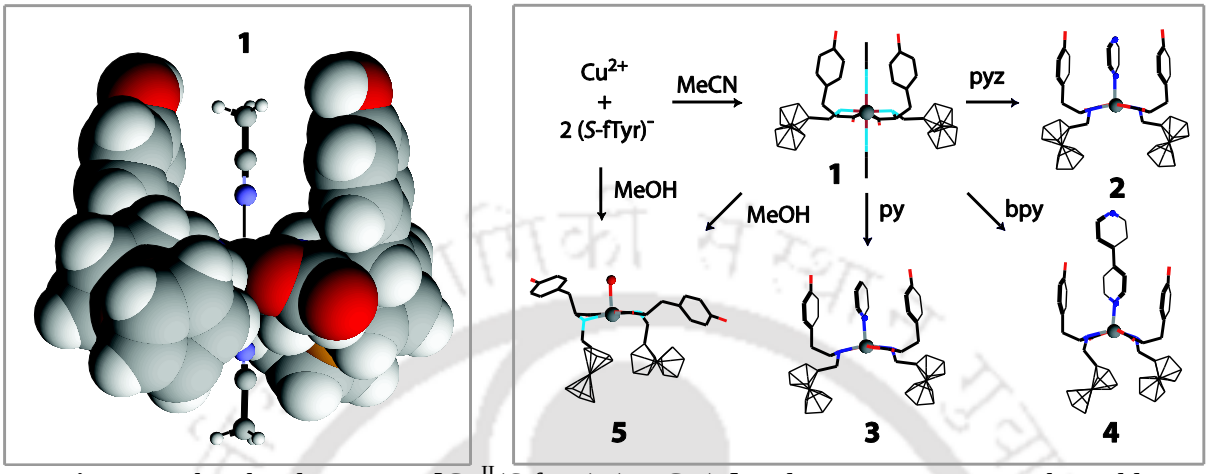

Figure 3 The chiral cavity in $[Cu^{II}(S\text{-fTyr})_2(MeCN)_2]$ and its conversion to other adducts.

Chapter 4: *Effect of ligand chirality and co-ligand on structure and electrochemical properties of bis-Copper(II) complexes of ferrocenyl-methyl-L-leucine.*

In this chapter we further explored the cavity formation with ferrocenylmethyl-L-Leucine derivative, effect of ligand chirality on the structure and effect of substituting one of the ligand on electrochemical properties of the Cu^{II}/Cu^{I}. All the complexes were structurally characterized. Structure of $[Cu^{II}(S\text{-fLeu})_2(H2O)]$ showed that unlike the tyrosine derivative in Chapter 3, the cavity was not formed due to the rotation of the leucine isopropyl groups. Both the homochiral complexes show similar properties but a dramatic change in physical and chemical was observed for the racemic *bis*-complex. The effect of chirality on the structure shown in Figure 4. Poor solubility of the racemic complexes as compared to pure *bis*-complexes, not only limit their solution studies but also crystallographic characterization. On the other hand, after substituting one of the ligand in the pure *bis*-complex by N-donor heterocyclic ligands, Cu^{II}/Cu^{I} potential of the complexes shifted remarkably towards positive.

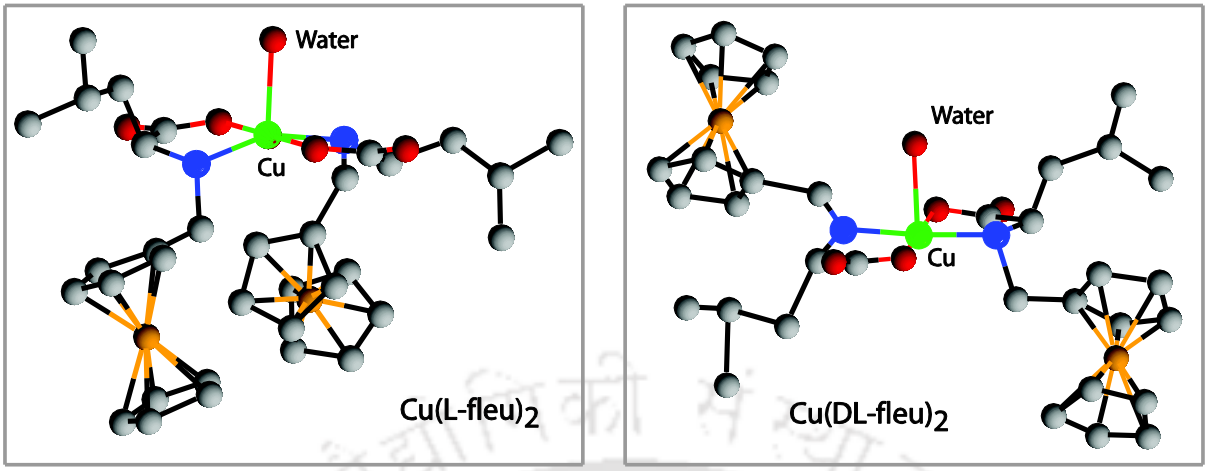

Figure 4. The structures of Cu(II) complex with L and racemic leucine derivative illustrating the effect of ligand chirality on the structure.

Chapter 5: *Synthesis and characterization of binuclear Ni(II) complexes with cations inside the metallocavity.*

The results presented in the earlier chapters showed the cavity formed with ferrocenylmethyl amino acid derivatives with Cu(II) form either narrow cavity or no cavity at all. The narrowness of the cavity formed with tyrosine derivative limits the choice of guest molecules and we were unable to find a chiral guest suitable to fit in the cavity. Because of this we looked at salicylaldehyde derivative of L-histidine reported earlier from our group.[1] The reported complex $[Fe^{III}_2(OH)(L^{L\text{-}his})_2(CH_3COO)]$ had a cavity formed around bridging acetate group and two carboxylate aligned on the other side. In this chapter we have synthesized and characterized a set of complex with the general formula $M[Ni^{II}_2(L^{L\text{-}his})_2(CH_3COO)]$ where M^+ was varied with K^+, Cs^+, NH_4^+ and R-NH_3^+ (where R= $Ph(CH_3)CH$-). The structure with K^+ showed the formation of a cavity around two aligned carboxylate. The K^+ remained bound to the carboxylates. In NH_4^+ complex NH_4^+ is found to be H-bonded to the carboxylate inside the cavity. The crystals of complex with alkyl ammonium salt did not diffract well but poorly resolved structure showed formation of channels in the lattice where the alkyl ammonium ions remained inside the channels (Figure 5).

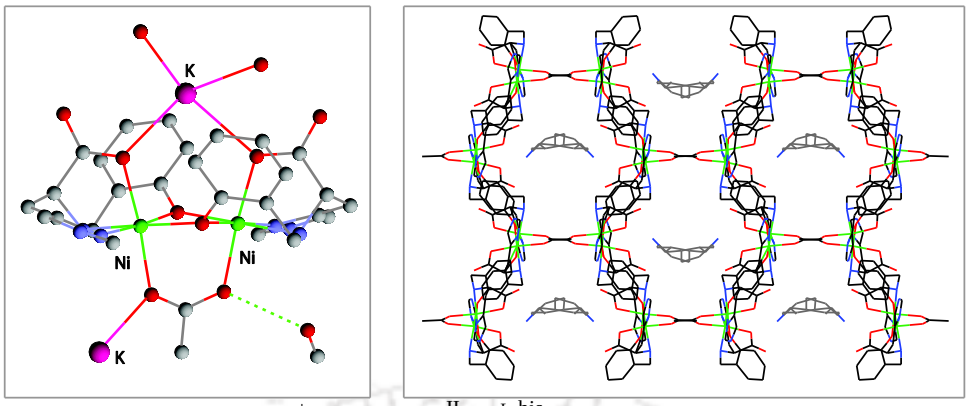

Figure 5. The chiral cavity in K^+ salt of $[Ni^{II}_2(L^{L\text{-}his})_2(CH_3COO)]^-$ and the channels formed in chiral amine salt .

Chapter 6: *Chiral recognition and resolution of amino alcohols through well defined interaction inside metallocavity.*

In this chapter we have structurally characterized a monomeric Ni(II) complex which transforms to dinuclear complex in presence of a base. Results presented in Chapter 5 showed that the $[Ni^{II}_2(L^{L\text{-}his})_2(CH_3COO)]^-$ binds ammonium ion inside the cavity through H-bond but alkyl derivatives does not crystallizes well. In this chapter we employed amino alcohols as guest expecting that the presence of alcoholic OH might assist in H-bonding and thereby improving the quality of crystals. Using the base assisted transformation of mononuclear to dinuclear complex we have been successful in separation of enantiomers of amino alcohols (Figure 6). Structural characterization of the host-guest adduct clearly showed that the cavity in $[Ni^{II}_2(L^{L\text{-}his})_2(CH_3COO)]^-$ can recognize three out of four groups around chiral centre of the amino alcohols through non-covalent interactions.

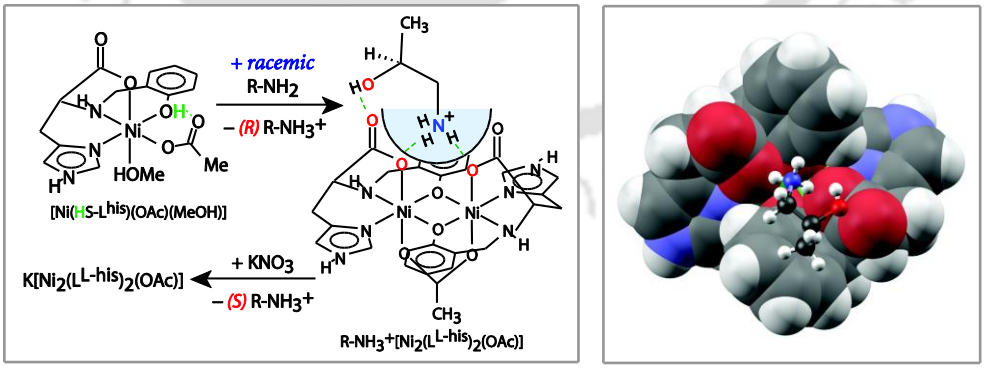

Figure 6 The schematic representation of the conversion of the complexes during the chiral separation and the space filling model showing orientation of the chiral ion inside metallocavity

Contents

Chapter 1

Pair of molecules that are mirror images of each other but not superimposable are chiral and the pair of molecules are called enantiomeric pair (Figure 1). Geometrically these molecules lack an internal plane of symmetry. The word chiral comes from the Greek cheir, meaning "the hand" because of the similar relationship between our left and right hand. Awareness about this type of molecules started in the mid 19th century when Louis Pasteur manually separated two different forms of crystals of sodium ammonium tartrate. Lord Kelvin in 1904 first defined chirality as - *any geometrical figure, or group of points is chiral and has chirality if its image in a plane mirror, ideally realized, cannot be brought to coincide with itself.*

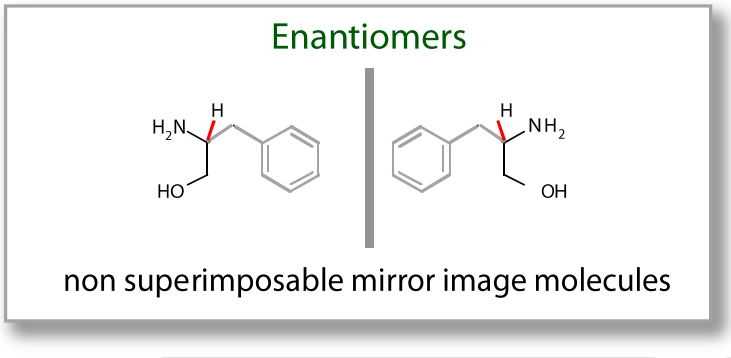

Figure 1.1 Showing palm of hands as well as mirror images of a molecule from my presentation.

Chirality of chemical substances is ever-present in nature and the essential substances that form living organisms such as amino acids and sugars are chiral and usually exist as pure enantiomeric forms. Biological chiral discrimination is an important phenomenon in amino acids or sugars, where one enantiomer is exclusively selected by nature over the other. The understanding of homochirality in nature is therefore important for the understanding of life. Even though enantiomers are indistinguishable in most inanimate environment, chiral compounds exhibit different properties in biochemical systems due to their natural asymmetry. For example, α-limonene and linalool have different smell depending on the chirality[1a]. Later, chiral discrimination is very important in the pharmaceutical industry, where one enantiomer may have a different pathway in the body, or it may be toxic (Table 1.1)[1]. For example one enantiomer of antidepressant drug methylphenidate is 13 times more potent [1b] over its isomer.

Table 1.1 Molecules with chirality of variable functionality.

Chiral isomers	Distinguished properties	Chiral isomers	Distinguished properties
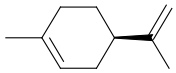 R-(+)- Limonene 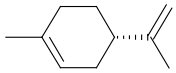 S-(-)- Limonene	Orange smell Lemon smell	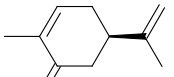 S-(+)- Carvone 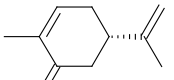 R-(-)- Carvone	Spearmint smell Caraway seeds
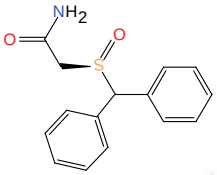 Armodafinil (R- isomer) 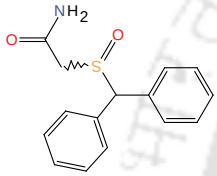 Modafinil (Racemic- isomer)	Use: Sleep disorder No effect	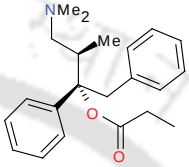 Darvon 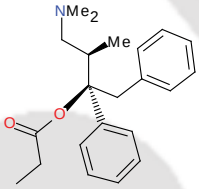 Novrad	Painkiller Anti-cough agent
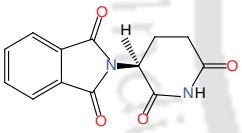 S- Thalidomide 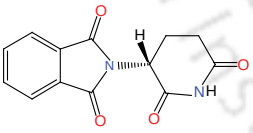 R- Thalidomide	Causes birth defects Cures morning sickness.	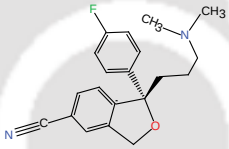 Escitalopram (S- isomer) 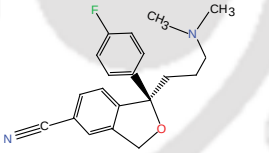 Citalopram (R- isomer)	Use: Depression/anxiety disorder in adults Decreases binding of S-isomer.
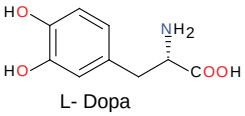 L- Dopa 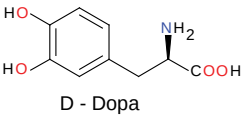 D - Dopa	Restoring nerve function Highly toxic	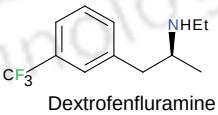 Dextrofenfluramine 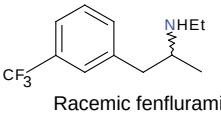 Racemic fenfluramine	Appetite suppressant Undesirable side effects
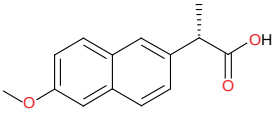 Naproxen (S - isomer)	Use : Anti-inflammatory *S*-isomer is 28 times more active	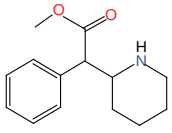 Methylphenidate	Use: Attention deficiency disorder D-isomer is 13 times more active

The enantiomer D-*threo*-methylphenidate, Ritalin®, is currently marketed as a racemate even though the other enantiomer is not effective. The worldwide market for single enantimer forms of chiral drugs exceeded US $200 billion in 2008 and still growing [2]. There are several methods for obtaining enantiomerically pure components such as extensive use of chromatographically techniques, biotransformation, diasterioisomeric crystallization and enantioselective synthesis[3]. Despite the availability of such methods, obtaining optically pure compounds remain a synthetically and commercially challenging task owing to the chemical similarity of the enantiomers. Often resolution of recemic mixture is more economical than asymmetric synthesis.

Usually chirality in organic molecules originates from the presence of at least one sp^3 hybridized carbon where all the four groups attached to the carbon are different. Ideally, recognition of an enantiomer requires recognition of three out of four different groups around sp^3 hybridized carbon centre.[4] As the chemical groups around a chiral carbon varies from compound to compound, so is the design of the receptors varies accordingly (Table 1.2) [5].

Recognition of the groups in biological receptors often use non-covalent interactions. For example, noradrenaline which functions both as a hormone as well as neurotransmitter is recognized by β-adrenergic receptors using non-covalent interactions (Figure 1.2).[6] Involving H-bond and other weak interaction in the recognition process have the advantage of easy recovery of the guest but the very nature of lability of the guest makes the isolation and characterization of host-guest complexes more difficult.

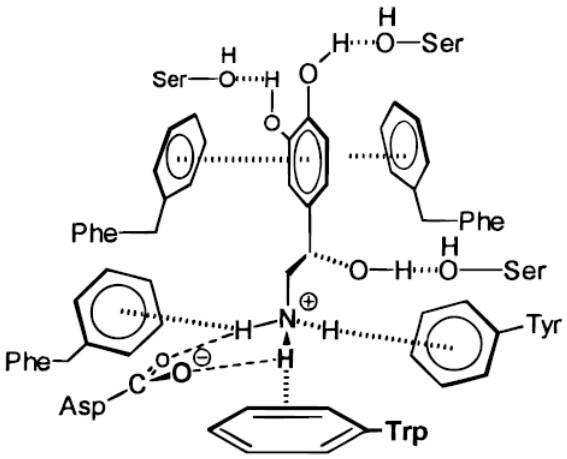

Figure 1.2 β-adrenergic receptors.

Table 1.2 Selected examples of receptors with what they recognizes

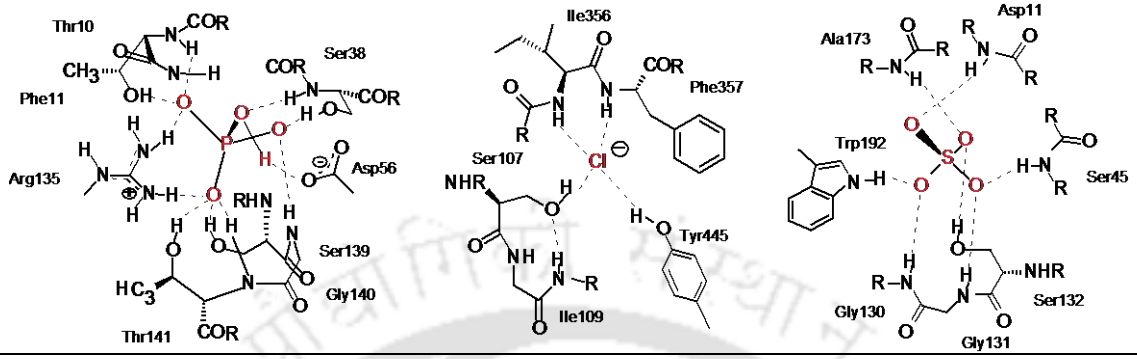	
Chem. Soc. Rev. **2009**, *38*, 585. (**A**)	
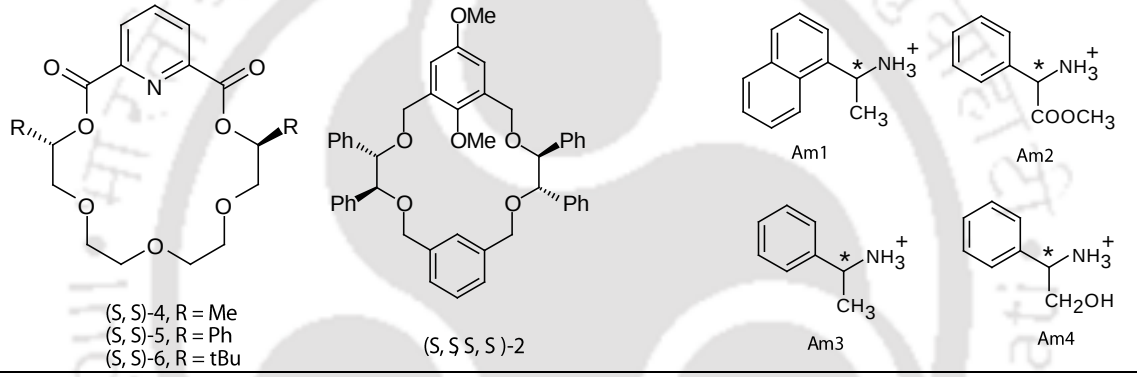	
Chem. Rev. **1997**, *97*, 3319. (**B**)	
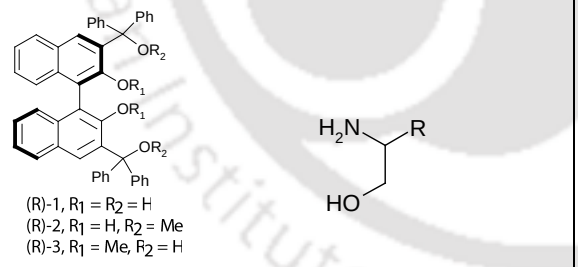	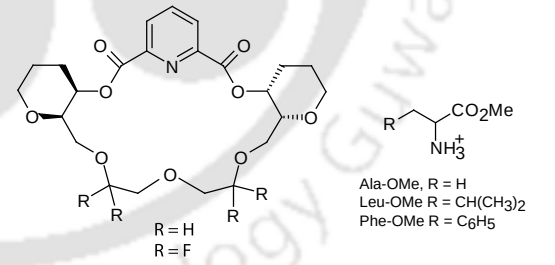
J. Org. Chem. **2007**, *72*, 97. (**C**)	*Angew chem. Int., Ed*. **2009**, *48*, 7803. (**D**)
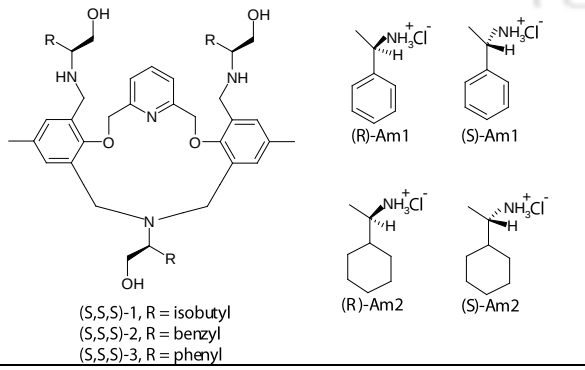	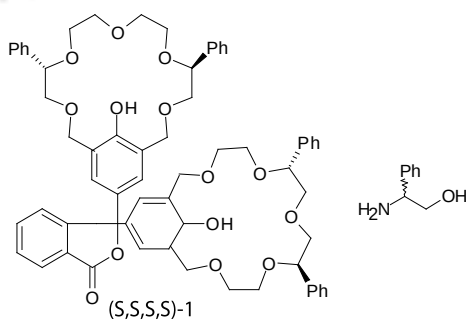
Tetrahedron: Asym. **2009**, *20*, 1541. (**E**)	*J. Org. Chem*. **2005**, *70*, 4609. (**F**)

Table 1.3 Organic macrocyclic receptors for recognition of various chiral molecules.

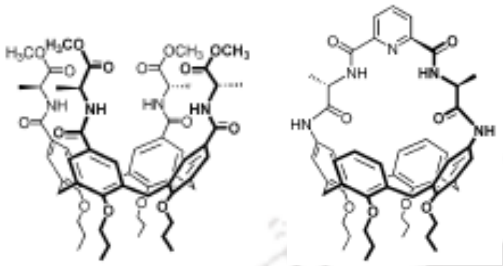

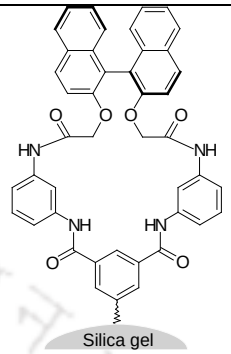

Chem. Soc. Rev. **2007**, *36*, 254. (**A**)

Org. Lett. **2008**, *10*, 2365. (**B**)

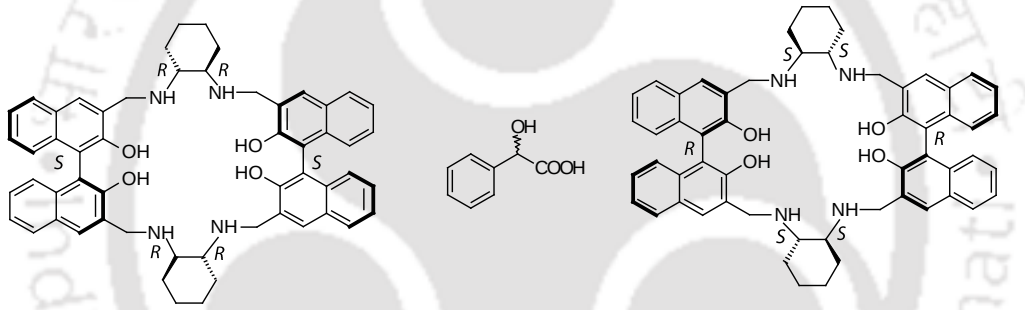

Angew. Chem., Int. Ed. **2005**, *44*, 1690. (**C**)

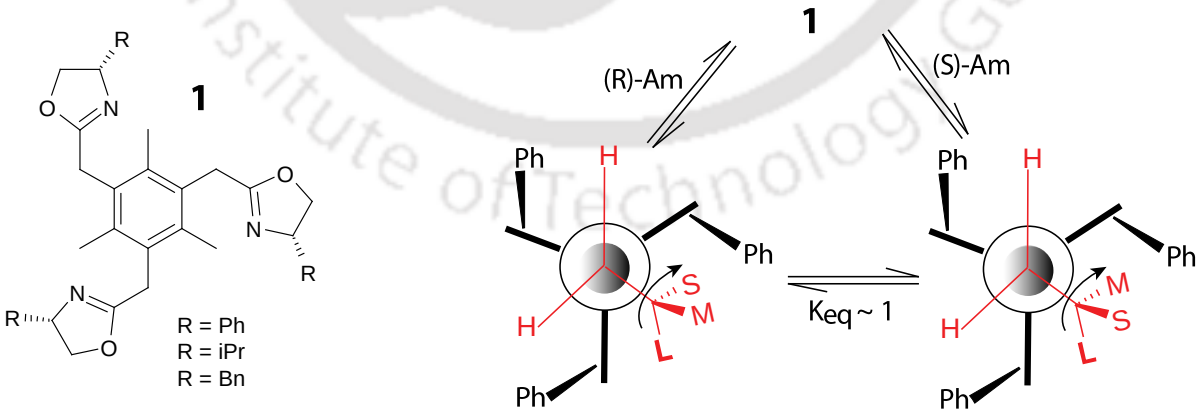

Chem. Rev. **2008**, *108*, 1. (**D**)

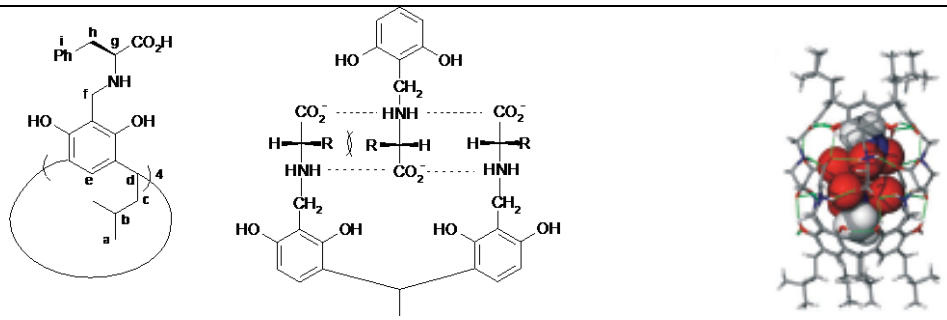

Chem. Commum. **2009**, 1959. (**F**)

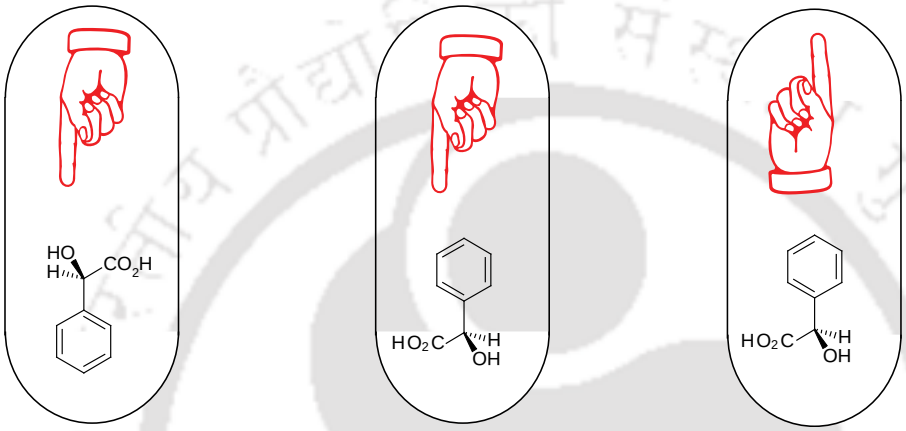

J. Am. Chem. Soc. **2003**, *125*, 6239. (**G**)

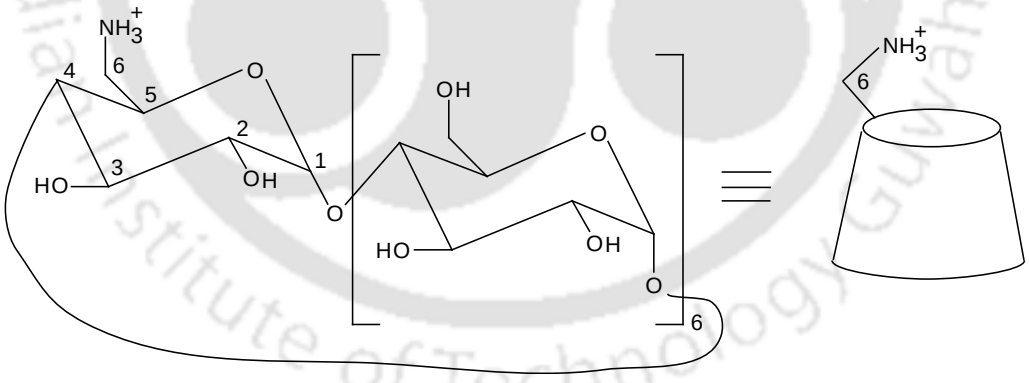

J. Am. Chem. Soc. **2002**, *124*, 813. (**H**)

Recognition and separation of enantiomers using synthesized hosts has been approached from diverse angles (Table 1.3)[7] including few rigid metallo organic frame work (Table 1.4).[8, 9]

While separation using chiral adsorbant as stationary phase has been progressed substantially[7b-d], the understanding of recognition at the molecular level is limited to molecular modelling due to the difficulty in structural characterization of large organic or MOF hosts.[10] For example, in a nobable work Kubo and co-workers[11a] showed chirality of an amino alcohol showed different colour upon addition to a large chiral host (Table 4, Figure A). While the receptor has been characterized using NMR, the mechanism of the recognition was proposed based on the molecular modelling.

In another notable example, Kim and co-workers used structurally characterized porous channels (Table 1.5, Figure C) of a chiral metal complex as host to enhance stereo selectivity of an organic reaction but the structural characterization with adduct was not possible.[11b]

Low-molecular weight rigid host would, in principle, facilitate structural characterization but it is challenging to accommodate three different recognition sites within a small host. Chin and co-workers, using a chiral Co(III) complex as host, showed the chiral interaction between the host and chiral guest in a set of structurally characterized covalently bonded host-guest complexes but chiral separation was not possible as the interactions were weak due to the open nature of the cavity (Table 1.5, Figure B).[12]

Earlier our group reported [synthesis] of large chiral host out of metal complexes using a set of chiral amino acid based ligands.[13] Synthesis of host using assembly of organic precursors or metallo organic assemblies being pursued by others as well [7,9]

In another notable example, Kim and co-workers used structurally characterized porous channels (Table 1.5, Figure C) of a chiral metal complex as host to enhance stereo selectivity of an organic reaction but the structural characterization with adduct was not possible.[11b]

Table 1.4 MOF based macrocyclic receptors for recognition of various chiral molecules.

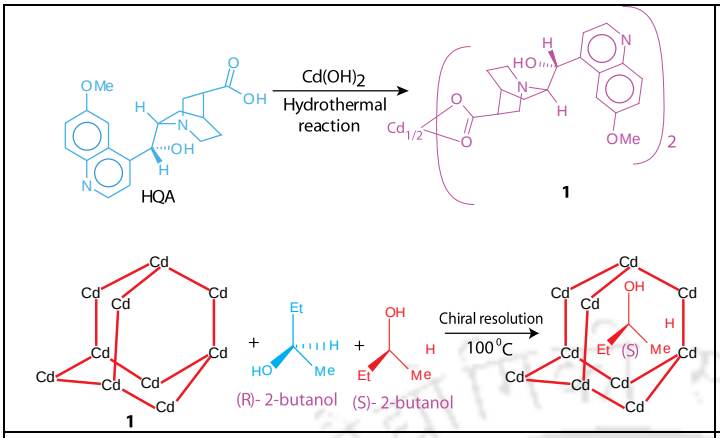	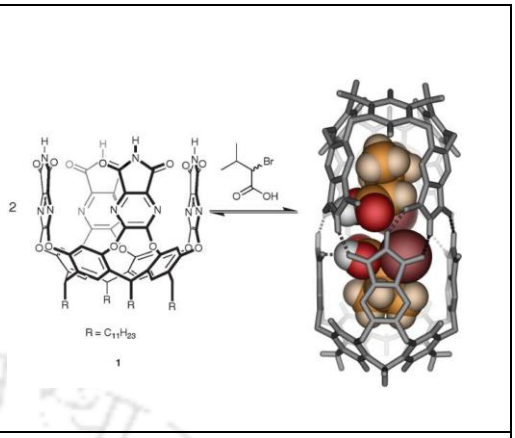
Angew. Chem. Int. Ed. **2001,** *113*, 4554. (**A**)	*Chem. Commun.* **2005**, 3667. (B)
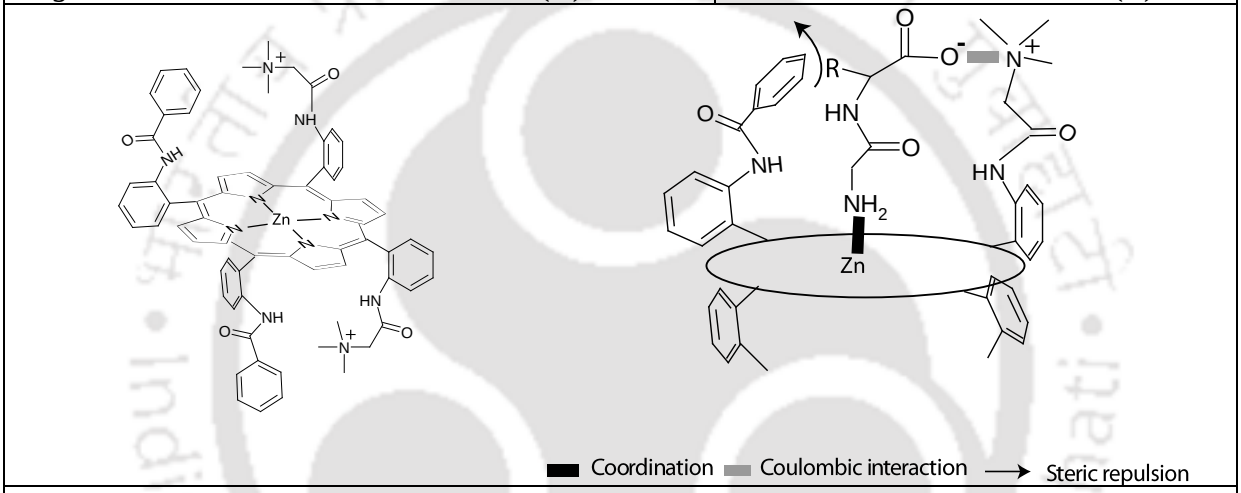	
Inorg. Chem. **2004**, *43*, 1211. (**C**)	
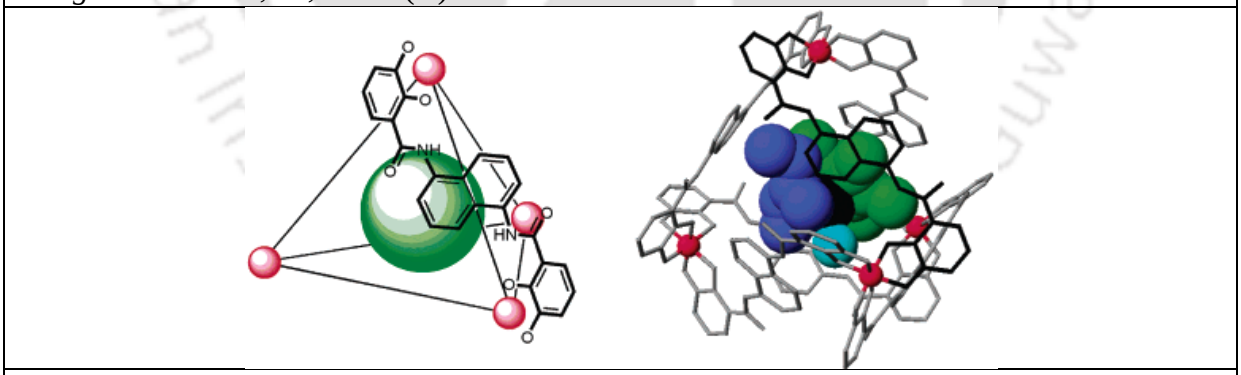	
J. Am. Chem. Soc. **2004**, *126*, 3674. (**D**)	
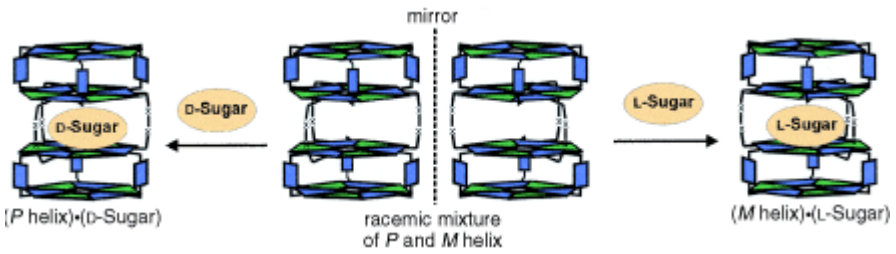	
Angew. Chem. Int. Ed. **2003**, *42*, 2300. (**E**)	

Table 1.5. Selected examples of chiral recognition.

<table>
<tr><td> 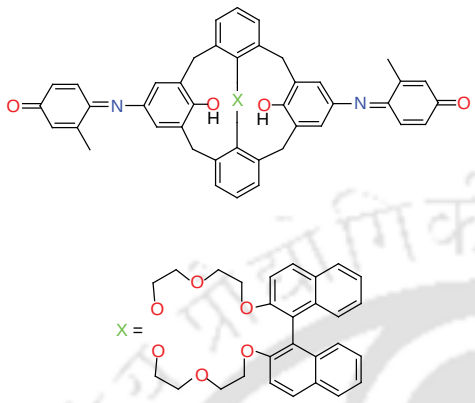

</td><td> 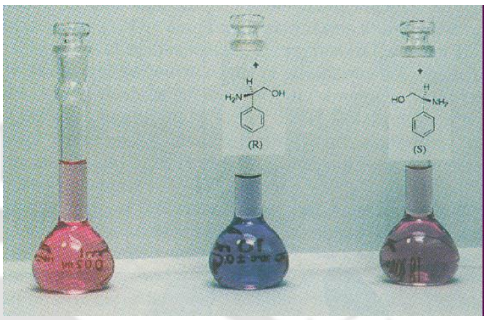 </td></tr>
<tr><td colspan="2">Nature, 1996, 382. (A)</td></tr>
<tr><td colspan="2"> 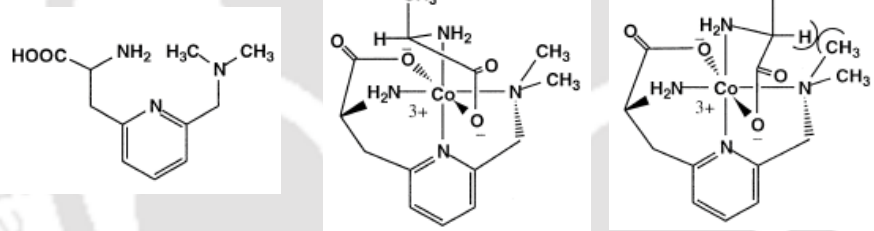 </td></tr>
<tr><td colspan="2">Nature, 1996, 401, 254.(B)</td></tr>
<tr><td colspan="2"> 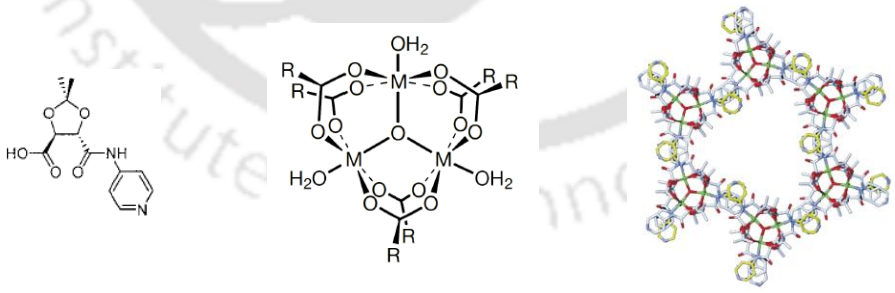 </td></tr>
<tr><td colspan="2">Nature, 2000, 404, 982. (C)</td></tr>
</table>

The literature overview showed that recognition of enantiomers by laboratory synthesized receptors are relatively large flexible organic molecules synthesized through multiple steps. While there are number of chiral inorganic metal complexes or assemblies (inherently rigid) reported in recent times, only few are structurally characterized along with chiral guest. A rare report by Chin and co workers[12] was able to show the host guest interaction in structurally characterized complexes. Incidentally that lone set of complexes did not have enough steric interaction to bind one enantiomer exclusively. Thus opportunity in synthesizing small molecular weight chiral metallo organic receptor exists. Small molecular weight and rigidity of metal complexes might yield structurally characterized host guest adduct which in turn can contribute to the understanding of the chiral recognition mechanism.

In this thesis we have attempted to explore synthesis of small molecular weight complexes having guest binding site within a cavity, structurally characterizing host-guest interaction and finally understanding the mechanism of chiral recognition if observed. We have used amino acid derivatives as ligand as it is one of the easiest and cost effective ways to incorporate chirality in the host due to availability of the pure L-amino acids from the natural source. The role of metal ion is to rigidify the otherwise flexible organic ligand through coordination bond formation.

References:

1. (a) Sugawara, Y.; Hara, C.; Aoki, T.; Sugimoto, N.; Masujima, T. *Chem. Senses* **2000**, *25*, 77. (b) Schweri, M.; Skolnick, P.; Rafferty, M.; Rice, K.; Janowsky, A.; Paul, S. *J. Neurochem.***1985**, *45*, 1062. (c) Carvalho, C. C. C. R.; Fonseca, M. M. R. *Food Chemistry* **2006**, *95*, 413. (d) Czeisler, C. A.; Walsh, J. K.; Roth, T; Hughes, R. J.; Wright, K. P.; Kingsbury, L.; Arora, S.; Schwartz, J. R. L.; Niebler, G. E.; Dinges, D. F. *N. Engl. J. Med.* **2005**, *353*, 476. (e) Slywka, G. W.; Melikian, A. P.; Whyatt, P. L.; Meyer, M. C.;. *J. Clin. Pharmacol.* **1975**, *15*, 598. (f) Ando, Y.; Fuse, E.; Figg, W. D. *Clin. Cancer Res.*; *an Official Journal of the American Association for Cancer Researc* **2002**, *8*, 1964. (g) Dorell, K.; Cohen, M. A.; Huprikar, S. S.; Gorman, J. M. Jones, M. *Psychosomatics* **2005**, *46*, 91. (h) Moore, N.; Verdoux, H.; Fantino, B. *International Clinical Psychopharmacology* **2005,** *20*, 131. (i) Goldstein, D. S.; *Cardiovasc. Drug Rev.* **2006**, *24*,189. (j) Connolly, H. M.; Crary, J. L.; McGoon, M.

D. *N. Engl. J. Med.* **1997**, *337*, 581. (k) Weissman, N. J. *Am. J. Med. Sci*. **2001**, *321*, 285. (m) Peter, J. H.; Eric, L. *Org. Process Res. Dev.* **1997**, 1, 72. (n) Steele, M.; Weiss, M.; Swanson, J.; Wang, J.; Prinzo, R. S.; Binder, C. E. *Can J. Clin. Pharmacol.* **2006**, *13*, 50. (o) Simonsen, J. L. *The Terpenes*. **1** (2nd Ed.), Cambridge University Press. **1953**. pp. 394.

2. Xie, R.; Chu, L.; Deng, J. *Chem. Soc. Rev*. **2008**, *37*, 1243.
3. (a) Stinson, S. C. *Chem. Eng. News* **1995**, 44. (b) Stinson, S. C. *Chem & Eng. News* **1999**, *77*, 101. (c) Axten, J. M. I., R.; Krim, L. and winkler, J. D. *J. Am. Chem. Soc.* **1999**, *121*, 6511.
4. Davankov, V. A. *Angew Chem. Int., Ed.* **1996**, *35*, 2649.
5. (a) Kubik, S. *Chem. Soc. Rev.* **2009**, *38*, 585. (b) Zhang, X. X.; Bradshaw, J. S. Izatt, R. M. *Chem. Rev.* **1997**, *97*, 3313. (c) Wang, Q.; Chen, X.; Tao, L.; Wang, L.; Xiao, D.; Yu, X. Pu, L. *J. Org. Chem.* **2007**, *72*, 97. (d) Carrillo, R.; López-Rodríguez, M.; Martín, V. S.; Martín, T. *Angew Chem. Int., Ed.* **2009**, **48**, 7803. (e) Ozera, H.; Kocakaya, S. O.; Akgun, A.; Hosgören, H.; Togrul, M. *Tetrahedron Asymmetry* **2009**, *20*, 1541.
6. (a) Schrader, T. *Angew Chem., Int. Ed*. **1996**, *35*, 2649. (b) Strader, C. D.; Fong, T. M.; Tota, M. R.; Underwood, D. *Annu. Rev. Biochem*. **1994**, *63*, 101.
7. (a) Baldini, L.; Casnati, A.; Sansone, F.; Ungaro, R. *Chem. Soc. Rev.* **2007**, *36*, 254. (b) Ema, T.; Tanida, D.; Sugita, K.; Sakai, T.; Miyazawa, K.; Ohnishi, A. *Org. Lett.*, **2008**, 10, 2365. (c) Li, Z.; Lin, J.; Pu, L. *Angew Chem. Int., Ed.* **2005**, *44*, 1690. (d) Hembury, G.A.; Borovkov, V. V.; Inoue, Y. *Chem. Rev.* **2008**, *108*, 1. (e) Kuberski, B.; Szumna, A. *Chem. Commun*. **2009**, 1959. (f) Scarso, A.; Shivanyuk, A.; Hayashida, O.; Rebek, J. Jr. *J. Am. Chem. Soc.* **2003**, *125*, 6239. (g) Rekharsky, M. V.; Inoue, Y. *J. Am. Chem. Soc.* **2002**, *124*, 813. (h) Zhang, X. X.; Bradshaw, J. S.; Lzatt, R. M. *Chem. Rev*. **1997**, *97*, 3313. (i) Kano, K. *J. Phys. Org. Chem.* **1998**, *10*, 286. (j) Gubitz, G. M.; Schmid, G. *Biopharm. Drug Dispos.* **2001**, *22*, 291. (k) Maier, N. M.; Lindner, W. *Anal. Bioanal. Chem*. **2007**, *389*, 377.
8. (a) Xiong, R.; You, X.; Abrahams, B. F.; Xue, Z.; Che, C. *Angew Chem. Int. Ed.* **2001**, *113*, 4554. (b) Palmer, L. C.; Zhao, Y.; Houk, K. N.; Rebek, J. Jr. *Chem. Commun*. **2005**, 3667. (c) Reeve, T. B.; Cros, J. Gennari, C. Piarulli, U. Vries J. G. *Angew Chem. Int. Ed.* **2006**, *45*, 2449. (d) Imai, H.; Munakata, H.; Uemori, Y.; Sakura, N. *Inorg. Chem.* **2004**, *43*, 1211. (e) Fiedler, D.; Leung, D. H.; Bergman, R. G.; Raymond, K. N. *J. Am. Chem. Soc.* **2004**, *126*, 3674. (f) Ishi-i, T.; Mateos-

Timoneda, M. A.; Timmerman, P.; Crego-Calama, M.; Reinhoudt, D. N.; Shinkai, S. *Angew Chem. Int. Ed.* **2003**, *42*, 2300.

9. (a) Davis, M. E. *Nature* **2002**, *417*, 813. (b) Kitagawa, S.; Kitaura, R.; Noro, S. *Angew Chem., Int. Ed*. **2004**, *43*, 2334. (c) Xiong, R.; You, X.; Abrahams, B. F.; Xue, Z.; Che, C. M. *Angew Chem., Int. Ed*. **2001**, *40*, 4422.
10. (a) Berthod, A. *Anal. Chem*. **2006**, *81*, 2093. (b) Seo, J. S.; Whang, D.; Lee, H.; Jun, S. I.; Oh, J.; Jeon, Y. J.; Kim, K. *Nature* **2000**, *404*, 982. (c) Alexander, J. M.; Clark, J. L.; Brett, T. J.; Stezowski, J. J. *PNAS* **2002**, *99*, 5115.
11. (a) Kubo, Y.; Maeda, S.; Tokita, S.; Kubo, M. *Nature* **1996**, *382*, 522. (b) Seo, J. S.; Whang, D.; Lee, H.; Jun, S. I.; Oh, J.; Jeon, Y. J.; Kim, K. *Nature* **2000**, *404*, 982.
12. Chin, J.; Lee, S. S.; Lee, K. J.; Park, S.; Kim, D. H. *Nature* **1999**, *401*, 254.
13. Alam, Md. A.; Nethaji, M.; Ray, M. *Angew. Chem., Int. Ed.* **2003**, *42*, 1940. (b) Alam, Md. A.; Nethaji, M.; Ray, M. *Inorg. Chem.* **2005**, *44*, 1302.

Chapter 2

In this chapter we have explored the coordination chemistry of ferrocenylmethyl amino acids (Scheme 2.1) with Cu(II) ion. While *bis*-complexes of amino acids with Cu(II) are well studied[1] due to their relevance to biological metal-protein interactions[2] and more recently because of their involvement in the copper transport process[3] in humans, metal complexes with ferrocenylmethyl derivatives were never explored.

Various other ferrocenyl derivatives of amino acids or peptides have been synthesized for their potential use as redox sensors.[4,5] Synthesis of ferrocenylmethyl derivatives has been reported before starting with ester of histidine[4b] or solid state synthesis of Schiff base form[6]. Interaction of non redox active metal ion with ferrocene bound to glycine, aspartic and glutamic acid through amide linkage have been monitored using electrochemical studies.[7] However, redox active metal complexes with amino acid derivative of ferrocene has never been isolated and structurally characterized.

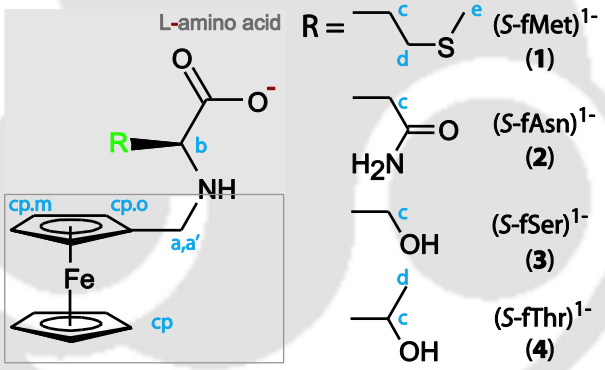

Scheme 2.1 The ferrocene derivatives with ^{1}H NMR labelling scheme.

Our interest in these amino acid derivatives stem from our group's earlier experience with salicylaldehyde derivative of amino acids where we[8] and others[9] have shown quite a few interesting structure utilizing versatile H-bonding capability of the amino acids. We had also noticed[8a,c] that, the formation of a wide range of complex network which sometimes make difficult to design network rationally.

While selecting this particular set of ferrocenylmethyl amino acids, we summarize that having both hydrophilic (amino acid) and hydrophobic (ferrocene) units within the same ligand might generate interesting structural diversity as well as more predictable structure. Our choice for this

particular set of amino acids (Scheme 2.1) was mainly due to the presence of H-bonding capable group in the side arm and which might interact with the lone axial donor in Cu(II), as it is usually prefers square pyramidal geometry. We choose methionine, as methionine thioether, unlike in biology[10], usually never bind to laboratory synthesized Cu(II) complexes. Thus we have a set of amino acid derivatives which can act as bidentate ligands (similar to amino acids), expected to form neutral *bis*-complexes with Cu(II) and have H-bond capable group in the side arm. We avoided histidine, aspartic acid and others which are either potentially tridentate ligand or can change the neutral character of the complex and thereby introducing complexity in the H-bonded network.

Thus in this chapter we are reporting synthesis and characterization of four ferrocenylmethyl derivative of amino acids and their respective Cu(II) complexes (Scheme 2.2). Structural characterization of the *bis*-Cu(II) complexes supported with their solution and electrochemical studies, revealed interesting effect of ferrocene substitution on axial coordination to Cu(II) and H-bonded network in the crystal lattice.

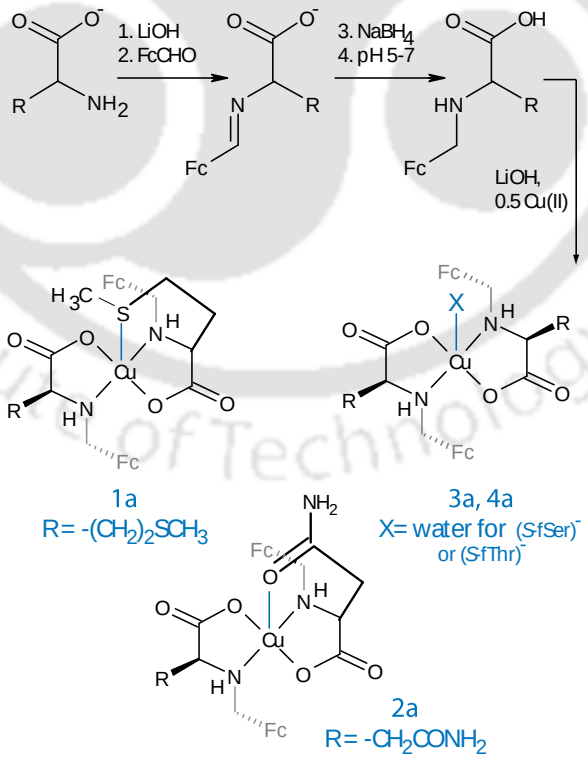

Scheme 2.2 Synthesis of the ligands and the Cu(II) complexes.

2.1 Experimental Section

2.1.1 Solvents and Reagents

Solvents and reagents were obtained from commercial sources and used without further purification unless otherwise stated. Ferrocene carboxaldehyde and anhydrous grade *N*,*N*-dimethylformamide (DMF) for electrochemical experiments was purchased from Aldrich Chemical Co. $NaBH_4$, amino acids and $Cu(NO_3)_2 \cdot 3H_2O$ were purchased from Merck limited and used as received. Methanol (MeOH) was distilled over magnesium methoxide [$Mg(OCH_3)_2$]. Ethanol (EtOH) was distilled over magnesium ethoxide [$Mg(OCH_2CH_3)_2$]. Diethyl ether (Et_2O) was dried first with anhydrous calcium chloride ($CaCl_2$) and then refluxed with metal sodium wire and finally distilled over sodium wire.

2.1.2 Measurements

The IR and UV-vis spectra were recorded on a Perkin-Elmer Spectrum One FT-IR spectrophotometer with KBr discs in the range 4000-400 cm^{-1} and electronic spectra on a Perkin-Elmer Lambda 25 UV-vis spectrophotometer respectively. The ^1H NMR spectra were recorded using a Varian Mercury plus 400 MHz instrument. The thermogravimetric analysis (TGA) of the compounds were performed using a Mettler Toledo SDTA 851e TGA thermal analyzer with heating rate of 5 ^oC per min under a N_2 atmosphere using 5-10 mg sample per run. Solid-state magnetic susceptibility of the complexes at room temperature was recorded using a Sherwood Scientific Magnetic balance MSB-1. Solution electrical conductivity measurements were made with a Eutech Instruments CON5/TDS 5 Conductivity Meter calibrated with 0.01 N KCl solution as calibrant. Elemental analyses were performed using a Carlo Erba 1108 elemental analyzer. ESI-MS for the ligands were recorded using a Micromass Quattro II mass spectrometer. Optical rotations were measured using a Perkin- Elmer 343 polarimeter. X-Band EPR spectra were recorded with a Jeol JES-FA series spectrometer fitted with a quartz dewar for measurements at liquid N_2 temperature. The spectra were calibrated with an internal manganese marker.

The crystals were mounted on glass fibers. All geometric and intensity data for the crystals were collected at room temperature using a Bruker SMART APEX. CCD diffractometer equipped with a fine focus 1.75 kW sealed tube Mo-K_α (λ = 0.71073 Å) X-ray source, with increasing ω (width of 0.3° per frame) at a scan speed of 10 s per frame. SMART software was

used for data acquisition and SAINT software for data extraction. Absorption corrections were not performed. The structures were solved and refined using SHELX-97.[11] All nonhydrogen atoms were refined anisotropically. The hydrogen atoms wherever possible were located from the difference fourier maps and were refined isotropically. Thus some of the C-H bonds will not be ideal and may vary. In some structures, hydrogen atoms attached to the lattice water molecules could not be located or fixed, thus calculated and reported formula differs. Selected crystallographic data and bond parameters are summarized in Table 2.1 and Table 2.2a,b respectively. Perspective views of the complexes were shown using ORTEP.[12]

2.2 Synthesis of ligands

Detailed synthetic procedures along with characterization data have been provided below. Representative ^{1}H NMR spectra shown in Figure 2.1.

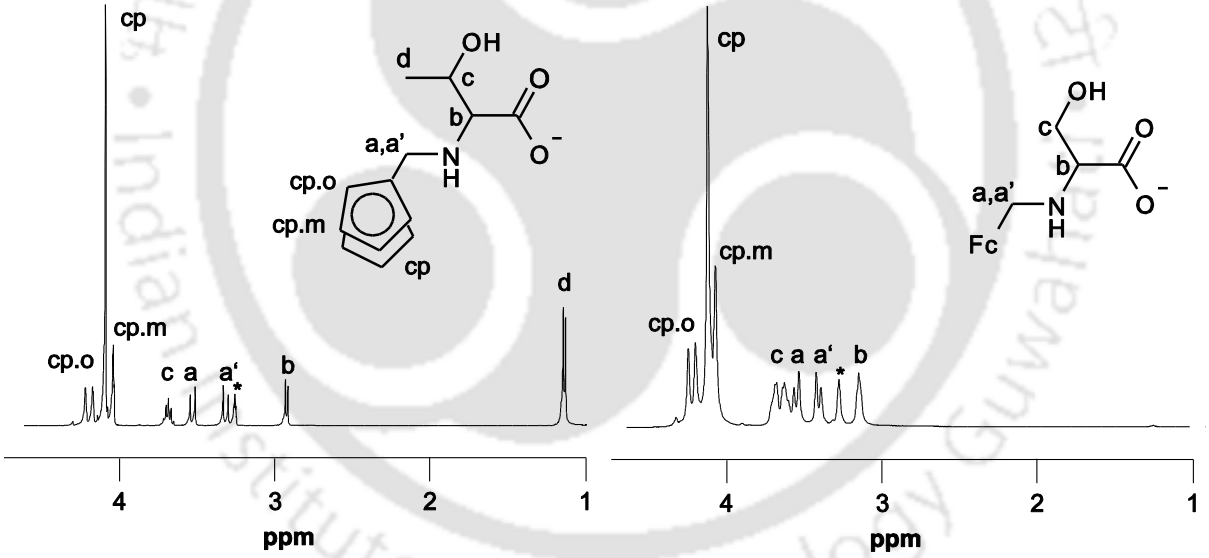

Figure 2.1 ^{1}H NMR spectra of the ligands **4** and **3** in CD_3OD with 1 equivalent of LiOH.

2.2.1 Ferrocenylmethyl derivative of methionine [H(*S*-fMeth)] (1)

L-methionine (1.00 g, 6.71 mmol) and $LiOH{\cdot}H_2O$ (0.284 g, 6.77 mmol) in methanol (30 mL) were stirred for 30 min to dissolve. A methanolic solution of ferrocenecarboxaldehyde (1.44 g, 6.72 mmol) was added drop wise to the above solution. The solution was stirred for 30 min and then treated with sodium borohydride (0.248 g, 6.71 mmol) with constant stirring. The

solvent was evaporated and the resulting sticky mass was dissolved in water. A cloudy solution was obtained, which was then acidified with dilute HCl and the solution pH was maintained between 5-7. The ligand precipitated out as yellow solid. The solid was filtered off, thoroughly washed with water and finally dried inside a vacuum desiccator. Yield 2.08 g (85%). Anal. calcd for $C_{16}H_{21}NO_2SFe$: C, 55.34; H, 6.09; N 4.03. Found: C, 54.68; H, 6.31; N, 3.92 %. $[\alpha]_D^{25}$ = -22^o in MeOH, *c* = 0.2 g/100 mL in the presence of 1 equivalent of $LiOH{\cdot}H_2O$. *m*/*z* (ESI-MS, [M-H^{-1}]) 346. UV/Vis: λ_{max} [nm] (ε/M^{-1} cm^{-1}): in MeOH with 1equivalent of $LiOH{\cdot}H_2O$: 211 (16100), 318 (180), 424 (160). IR (KBr, cm^{-1}), $\upsilon(COO)_{asym}$ 1588 s, $\upsilon(COO)_{sym}$ 1393 s. ^{1}H NMR (CD_3OD, ppm): $H^{cp.o}$ (4.27, s, 1H), $H^{cp.o}$ (4.22, s, 1H), H^{cp} (4.13, s, 5H), $H^{cp.m}$ (4.09, s, 2H), H^a (3.54, d, 1H, $J_{a,a'}$ = 12 Hz), $H^{a'}$ (3.36, d, 1H), H^b (3.14, t*, 1H), H^c (1.85, m, 2H), H^d (2.53, t*, 2H), H^e (2.06, s, 3H), * These are multiplets which appear as triplets.

2.2.2 Ferrocenylmethyl derivative of asparagine [H(*S*-fAsn)] (2)

This was prepared following the procedure described for **1** using L-asparagine (1.00 g, 6.66 mmol), $LiOH{\cdot}H_2O$ (0.27 g, 6.66 mmol), ferrocenecarboxaldehyde (1.43 g, 6.68 mmol) and sodium borohydride (0.25 g, 6.60 mmol). The pH was maintained between 6-7. Yield 1.64 g (75%). Anal. calcd for $C_{15}H_{18}N_2O_3Fe$: C, 54.57; H, 5.49; N 8.48. Found: C, 55.88; H, 5.47; N, 8.92 %. $[\alpha]_D^{25}$ = -26^o in MeOH, *c* = 0.2 g/100 mL in the presence of 1 equivalent of $LiOH{\cdot}H_2O$. *m*/*z* (ESI-MS, [M-H^{-1}]) 329. UV/Vis: λ_{max} [nm] (ε/M^{-1} cm^{-1}): in MeOH with 1equivalent of $LiOH{\cdot}H_2O$: 210 (22600), 316 (140), 420 (160). IR (KBr, cm^{-1}) $\upsilon(CO)_{amide}$ 1691 s; $\upsilon(COO)_{asym}$ 1621, $\upsilon(COO)_{sym}$ 1398. ^{1}H NMR (CD_3OD, ppm): $H^{cp.o}$ (4.31, s, 1H), $H^{cp.o}$ + H^{amine} (4.20, m, 3H), H^{cp} (4.10, s, 5H), $H^{cp.m}$ (4.05, s, 1H), H^a (3.50, d, 1H, $J_{a,a'}$ = 12 Hz), $H^{a'}$ + H^b (3.37, d, 2H), H^c (2.54, m, 1H), $H^{c'}$ (2.38, m, 1H). Due to geminal coupling H^c split into two non-equivalent H^c and $H^{c'}$.

2.2.3 Ferrocenylmethyl derivative of serine [H(*S*-fSer)] (3)

This was prepared following the method, stirring time and pH range as described for **1** using the following quantities of reagents: L-serine (1.00 g, 9.40 mmol), $LiOH{\cdot}H_2O$ (0.390 g, 9.39 mmol), ferrocenecarboxaldehyde (2.03 g, 9.48 mmol) and sodium borohydride (0.350 g, 9.72 mmol). Yield 2.49 g (88%). Anal. calcd for $C_{14}H_{17}NO_3Fe$: C, 55.47; H, 5.65; N 4.62.

Found: C, 55.30; H, 5.87; N, 4.33 %. $[\alpha]_D^{25}$ = -19° in MeOH, *c* = 0.2 g/ 100 mL in the presence of 1 equivalent of LiOH·H_2O. *m/z* (ESI-MS, [M-H^{-1}]) 302. UV/Vis: λ_{max} [nm] (ε/M^{-1} cm^{-1}): in MeOH with 1equivalent of LiOH·H_2O: 211 (16100), 318 (180), 424 (160). IR (KBr, cm^{-1}) υ(OH) 3413 sharp, $\upsilon(COO)_{asym}$ 1630 s, $\upsilon(COO)_{sym}$ 1380. ^{1}H NMR (CD_3OD, ppm): $H^{cp.o}$ (4.26, s, 1H), $H^{cp.o}$ (4.21, s, 1H), H^{cp} (4.14, s, 5H), $H^{cp.m}$ (4.09, s, 2H), H^a (3.57, d, 1H, $J_{a,a'}$ = 12 Hz), $H^{a'}$ (3.43, d, 1H), H^b (3.17, m, 1H), H^c (3.70, m, 1H), $H^{c'}$ (3.65, m, 1H). Due to geminal coupling H^c split into two non-equivalent H^c and $H^{c'}$

2.2.4 Ferrocenylmethyl derivative of threonine [H(*S*-fThr)] (4)

This was prepared following the method, stirring time and pH range described for **1** using the following quantities of reagents: L-threonine (1.00 g, 8.4 mmol), LiOH·H_2O (0.35 g, 8.40 mmol), ferrocenecarboxaldehyde (1.8 g, 8.4 mmol) and sodium borohydride (0.319 g, 8.45 mmol). Yield 2.23 g (84%). Anal. calcd for $C_{15}H_{19}NO_3Fe$: C, 56.80; H, 6.03; N 4.41. Found: C, 56.13; H, 6.08; N, 4.19 %. *m/z* (ESI-MS, [M-H^{-1}]) 316. $[\alpha]_D^{25}$ = -35° in MeOH, *c* = 0.2 g/100 mL in the presence of 1equivalent of LiOH·H_2O. UV/Vis: λ_{max} [nm] (ε/M^{-1} cm^{-1}): in MeOH with 1equivalent of LiOH·H_2O: 208 (33100), 321 (120), 431 (130). IR (KBr, cm^{-1}) $\upsilon(COO)_{asym}$ 1623 s, $\upsilon(COO)_{sym}$ 1415. ^{1}H NMR (CD_3OD, ppm): $H^{cp.o}$ (4.25, s, 1H), $H^{cp.o}$ (4.21, s, 1H), H^{cp} (4.13, s, 5H), $H^{cp.m}$ (4.08, s, 2H), H^a (3.57, d, 1H, *J*a,a′ = 12 Hz), $H^{a'}$ (3.36, d, 1H), H^b (2.96, d, 1H, $J_{b,c}$ = 6 Hz), H^c (3.72, m, 1H), $H^{c'}$ (1.18, d, 3H).

2.3 Syntheses of Complexes

Detailed synthetic methodologies along with analytical data are given below. UV-vis, EPR, and room temperature data has been provided in Table 2.3.

2.3.1 [Cu(*S*-fMeth)$_2$] (1a)

Ligand H(*S*-fMet) (**1**) (0.500 g, 1.43 mmol) was deprotonated with LiOH·H_2O (0.060 g, 1.44 mmol) in 25 mL MeOH which resulted in a clear brown color solution after 30 min. A methanolic solution of $Cu(NO_3)_2$·$3H_2O$ (0.17 g, 0.71 mmol) was added drop wise to the ligand with stirring. The color of the solution changed to green immediately. The solution was stirred for 2 h and evaporated to dryness on a rotary evaporator. The green solid obtained by adding

acetonitrile was recrystallized as dark green plates by diffusing diethyl ether into a methanolic solution of the crude solid over 2-3 days. The crystals were filtered off and washed with ether. Yield 74%. Anal. calcd for $(C_{16}H_{20}NO_2SFe)_2Cu$: C, 50.83; H, 5.33; N, 3.70. Found: C, 51.20; H 5.31; N, 3.91 %. IR (KBr, cm^{-1}) $\upsilon(COO)_{asym}$ 1629 s, $\upsilon(COO)_{sym}$ 1369.

2.3.2 [Cu(*S*-fAsn)$_2$]·4H$_2$O (2a)

This was prepared following the method described for **1a** with the following quantities of reagents: H(*S*-fAsn)(**2**) (0.500 g, 1.58 mmol), $LiOH·H_2O$ (0.065 g, 1.55 mmol) and $Cu(NO_3)_2·3H_2O$ (0.19 g, 0.78 mmol). Dark green crystals of **2a** were grown by diffusing diethyl ether into a methanolic solution of the complex. Yield 60%. Anal. Calcd for $Cu(C_{15}H_{17}N_2O_3Fe)_2·4H_2O$: C, 45.38; H 5.33; N, 7.05. Found: C, 45.57; H, 5.06; N, 6.88 %. IR (KBr, cm^{-1}) $\upsilon(COO)_{asym}$ 1627br, $\upsilon(COO)_{sym}$ 1405.

2.3.3 [Cu(*S*-fSer)$_2$(H$_2$O)] (3a)

This was prepared following the method described for **1a** with the following quantities of reagents: H(*S*-fSer)(**3**) (0.500 g, 1.64 mmol), $LiOH·H_2O$ (0.070 g, 1.66 mmol) and $Cu(NO_3)_2·3H_2O$ (0.190 g, 0.78 mmol). Dark green rod shaped crystals were formed after 2-3 days. The crystals were filtered off and washed with ether. Yield 65%. Anal. Calcd for $Cu(C_{14}H_{16}NO_3Fe)_2·H_2O$: C, 49.03; H, 4.99; N, 4.08. Found C, 48.69; H 4.98; N, 3.72 %. IR (KBr, cm^{-1}) $\upsilon(COO)_{asym}$ 1602 s, $\upsilon(COO)_{sym}$ 1404.

2.3.4 [Cu(*S*-fThr)$_2$(H$_2$O)]·3H$_2$O (4a)

This was prepared following the method described for **1a** with the following quantities of reagents: H(*S*-fThr)(**4**) (0.500 g, 1.59 mmol), $LiOH·H_2O$ (0.170 g, 1.59 mmol) and $Cu(NO_3)_2·3H_2O$ (0.170 g, 0.700 mmol). Green rod shaped crystals were formed after 2-3 days. The crystals were filtered off and washed with ether. Yield 64%. Anal. calcd for $[Cu(C_{15}H_{18}NO_3Fe)_2(H_2O)]·3H_2O$: C, 46.93; H, 5.78; N, 3.65. Found C, 46.64; H 5.64; N, 3.79 %. IR (KBr, cm^{-1}) $\upsilon(COO)_{asym}$ 1618 s, $\upsilon(COO)_{sym}$ 1384.

Table 2.1 Selected crystallographic data for complexes.

Complexes	**1a**	**2a**	**3a**	**4a**
Empirical formula	$C_{32}H_{40}CuFe_2N_2O_4S_2$	$C_{30}H_{30}CuFe_2N_4O_{10}$	$C_{28}H_{34}CuFe_2N_2O_7$	$C_{30}H_{39}CuFe_2N_2O_{10}$
fw	756.02	781.83	685.82	762.88
Crystal system	Monoclinic	Monoclinic	Orthorhombic	Orthorhombic
Space group	$P2_1$	$P2_1$	$P2_12_12_1$	$P2_12_12_1$
a Å	12.0995(2)	11.7307(3)	7.8867(2)	7.4664(4)
b Å	9.8513(2)	9.5491(2)	11.1661(3)	14.7857(4)
c Å	13.4689(2)	17.4332(4)	32.3867(8)	30.211(17)
α deg				
β deg	β = 98.281(1)	β = 106.120(2)	α=β=γ= 90	α=β=γ= 90
γ deg				
V, $Å^3$	1588.70(5)	1876.05(8)	2852.09(13)	3335.2(3)
Z	2	2	4	4
ρ	1.58	1.384	1.597	1.519
μ	1.736	1.378	1.791	1.546
FLACK parameter	0.008(7)	0.00(2)	0.001(9)	-0.016(14)
Crystal size	0.3 × 0.2 × 0.1	0.4 × 0.3 × 0.2	0.4 × 0.3 × 0.3	0.5 × 0.4 × 0.3
Reflns collected	24394	18791	35054	28885
Indep reflns	10084	6417	7124	4706
GOF	0.909	0.967	0.960	1.125
Final R indices [I > 2σ(I)]	R1= 0.0295, wR2 = 0.0546	R1 = 0.0544, wR2 = 0.1375	R1 = 0.0244, wR2 = 0.0615	R1=0.0321, wR2= 0.0678
R indices (all data)	R1 = 0.0555, wR2 = 0.0587	R1 = 0.0841, wR2 = 0.1563	R1 = 0.0306, wR2 = 0.0699	R1=0.0468, wR2= 0.0720

Table 2.2a Selected bond lengths (Å) and bond angles (°) for the complexes.

Complexes	**1a**	$Cu(L\text{-}meth)_2$	**2a**	$Cu(L\text{-}asn)_2$
Cu-N1	2.0188(15)	1.97(1)	1.985(5)	2.004(28)
Cu-N1A	2.0288(16)	2.01(1)	2.003(5)	2.035(26)
Cu-O1	1.9406(15)	1.970(8)	1.927(5)	1.947(21)
Cu-O1A	1.9194(14)	1.944(8)	1.923(4)	1.954(22)
Cu-axial	2.7906(6)	2.751(7)	2.414(5)	2.529(20)
	Cu-S	$Cu\text{-}O_{carbo}$		
N1-Cu-O1A	94.22(6)	95.9(4)	96.8(2)	96.1(10)
O1A-Cu-N1A	85.05(6)	84.2(4)	83.94(19)	82.4(9)
N1A-Cu-O1	95.02(6)	96.3(4)	97.2(2)	94.5(10)
O1-Cu-N1	84.28(6)	83.7(4)	83.4(2)	86.9(10)
N1-Cu-axial	86.34(4)	89.3(3)	82.76(19)	94.6(9)
axial-Cu-O1	91.70(5)	85.0(3)	86.92(19)	93.5(8)
O1-Cu-O1A	174.48(6)	179.6(4)	174.6(2)	176.2(10)
N1-Cu-N1A	164.99(6)	175.0(3)	166.7(2)	175.3(10)
		Ref. 1(d)		Ref. 1(c)

Table 2.2b Selected bond lengths (Å) and bond angles (°) for the complexes.

Complexes	**3a**	$Cu(L\text{-}ser)_2$	**4a**	$Cu(L\text{-}thr)_2$
Cu-N1	2.0172(16)	1.988(6)	2.014(3)	1.968(8)
Cu-N1A	2.0172(16)	1.975(6)	2.009(3)	1.982(8)
Cu-O1	1.9206(15)	1.970(6)	1.946(3)	1.941(7)
Cu-O1A	1.9275(15)	1.952(6)	1.937(3)	1.957(7
Cu-axial	2.3876(17)	2.359(6)	2.258(4)	2.478(8)
			$Cu\text{-}O_{water}$	$Cu\text{-}O_{carbo}$
N1-Cu-O1A	92.14(6)	82.4(2)	96.47(13)	96.4(3)
O1A-Cu-N1A	85.61(7)	88.3(2)	85.00(12)	83.4(3)
N1A-Cu-O1	95.62(7)	83.9(2)	92.46(12)	96.2(3)
O1-Cu-N1	85.40(7)	105.0(2)	84.37(12)	83.6(3)
N1-Cu-axial	99.56(7)		99.50(13)	93.2(3)
axial-Cu-O1	87.57(6)		91.67(14)	89.7(3)
O1-Cu-O1A	173.83(7)	170.7(2)	174.49(13)	177.5(3)
N1-Cu-N1A	167.93(7)	172.2(2)	161.30(13)	172.1(3)
		Ref.1(b)		Ref. 1(f)

Table 2.3 Solution UV-vis, EPR and solid state magnetic moment data of the complexes.

Complex	λ/nm (ε/$cm^{-1}M^{-1}$)	EPR, g	A_{II}/ G	μ_{eff}
1a	237 (13,000), 418 (320), 580sh	2.241, 2.047	184	2.10
2a	235sh, 414(590), 580(140)	2.243, 2.047	181	2.11
3a	234sh, 412(343), 580sh	2.244, 2.048	182	1.94
4a	236(12,800), 414(360), 580sh	2.239, 2.047	186	2.13

2.4 Result and discussion

2.4.1 Synthesis and characterization of ligands and complexes

The general route for the synthesis of ferrocenylmethyl derivatives of amino acid ligands, is to hydrolyze the reduced Schiff base of ferrocenecarboxaldehyde and the amino acid ester.[3b,c] Our attempts to reproduce the one pot solid state synthesis for Schiff bases with free amino acids reported by the Hassan *et al.* resulted in either poor yield or no product at all.[4] Problems in forming the Schiff base with certain amino acid esters has also been reported by Metzler- Nolte *et al.*[3b] We used LiOH to deprotonate the zwitterionic amino acid in order to form the initial Schiff base (Scheme 2.2). *In situ* reduction of the Schiff bases and subsequent pH adjustment resulted in the ferrocenylmethyl derivatives in good yield (70-85%). These ferrocenyl derivatives are insoluble either in water or any common organic solvent in protonated form. Because of this, the ^{1}H NMR, ESI-MS, UV-vis and optical rotation measurements were carried out in the presence of one equivalent of base (LiOH) as they are completely soluble in alkaline medium. The characterization data given in the experimental section are consistent with their formulation.

All the complexes were prepared by directly $Cu(NO_3)_2.3H_2O$, $LiOH.H_2O$ as base and corresponding ligands in M:L ratio 1:2 in methanol at room temperature. All the Cu(II) complexes are non conducting supporting the non-electrolytic nature of the complexes. The presence of water of crystallization in **2a**-**4a** was confirmed by thermogravimetric analysis (TGA) (Figure 2.2). The TGA of **2a**, **3a** and **4a** shows loss of 9.7, 2.7 and 8.4 % weight loss respectively between 40 -120ºC against calculated weight loss of 9.0 (for $4H_2O$), 2.6 (for 1 H_2O) and 9.4 (for 4 H_2O). The room temperature magnetic moments lies between 1.94-2.13 B.M. are within expected range for monomeric Cu(II) complex (Table 2.3).[13]

The IR spectra of the ligands and the complexes show strong and sharp asymmetric carboxylate stretches between 1580-1630 cm^{-1}.[8] Ligands **2** and **3** show sharp υ(amide) and υ(OH) at 1691 and 3413 cm^{-1} respectively. The peaks around 1100, 1005, 810 and 500 have been observed for all the ligand and complexes probably originated from ferrocene CH/CC/ring stretches.

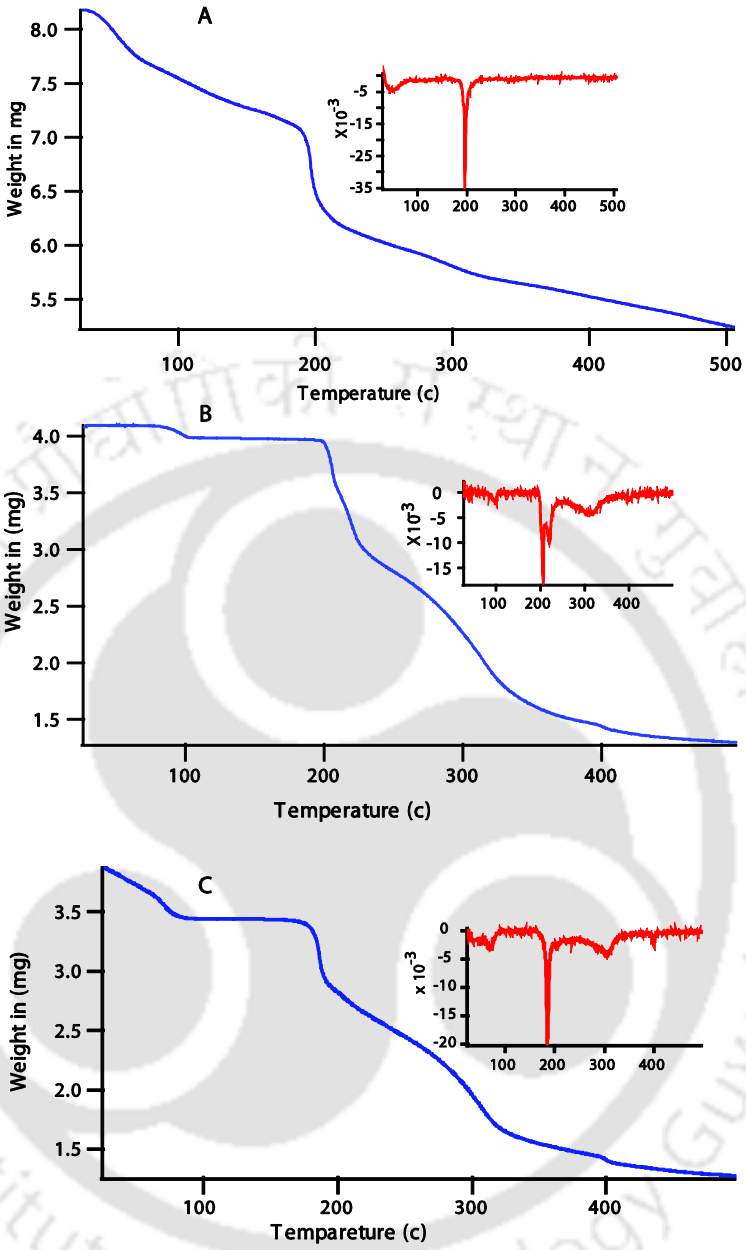

Figure 2.2 TGA plot of the complexes **2a** (A), **3a** (B) and **4a** (C) with respective derivative (DTA) plot as inset.

2.4.2 Molecular structures

The single crystals of **1a** to **4a** were isolated by diffusing ether to methanolic solutions of the complexes. All the complexes are monomeric in nature with slightly distorted (τ 0.1-0.2) square pyramidal geometry around the Cu(II). The amount of distortion parameter τ was calculated

from the structural data where the value of τ should be 0.0 for perfect square-pyramidal geometry and 1.0 for perfect trigonal bipyramidal (TBP) structure.[14] The conformation at the chiral carbon is *S* as the amino acid used in synthesis was *S* isomer. The in-plane bond lengths for $Cu–O_{carboxylate}$ are within the range 1.92-1.94 Å observed for other amino acid or amino acid derived ligand Cu(II) complexes.[1] The in-plane bond lengths for $Cu–N_{amine}$ are longer at ~2.01 except for **2a** compared to corresponding amino acid complexes (1.96-1.98 Å).[1]

The interesting feature of **1a** is the axial coordination by the methionine thioether (Figure 2.3). The axial bond in square-pyramidal Cu(II) is usually long and varies between 2.12 to 2.6 Å for O or N coordination, due to Jahn-Teller distortion.[15] In the few examples of reported Cu(II) complexes with bound thioether, the Cu–S(thioether) bond length varies between 2.85 to 2.94 Å longer than in **1a** (Cu–S1, 2.7906 (6)Å).[15b,c] We have not come across any Cu(II) complex coordinated thioether originated from methionine. Methionine is known to coordinate to Cu(II) in active site of plastocyanin (Cu–S, 2.9 Å) and azurin (Cu–S, 3.1 Å).[16] In $[Cu(methionine)_2]$ complex, Cu(II) is six coordinated with two long (2.676 and 2.751 Å) axial coordinations, coming from carboxyl oxygen of neighboring molecules, thus leaving methionine sulphur uncoordinated.[1d]

In **2a**, the amide carbonyl oxygen is coordinated to Cu(II) in lieu of methionine sulphur (Figure 2.4). The bent in axial bond as revealed by the angle between centroid of N1,O1–Cu–O3 at 83.0° is higher than in **1a** (**1a**: centroid of N1,O1–Cu–S1 angle is 88.6°). This bent shows the axial coordination is somewhat strained in **2a**. Comparing **1a** and **2a**, the thioether and carbonyl oxygen coordinate to Cu(II) axially despite being weak donor and geometrically constrained. In $[Cu(L\text{-asparagine})_2]$ structure, the axial coordination due to neighboring carbonyl oxygen is considerably higher at 2.529(20) and 2.774(25) Å.[1c]

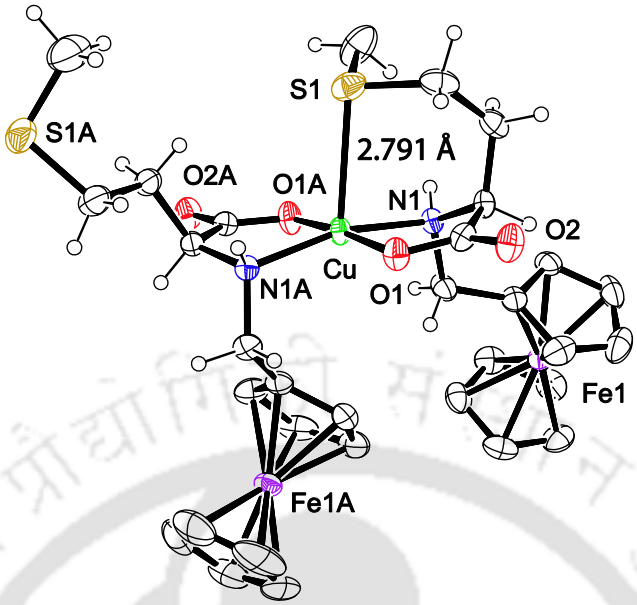

Figure 2.3 ORTEP diagram of **1a** with 50 % probability. Hydrogens are removed from ferrocene for clarity.

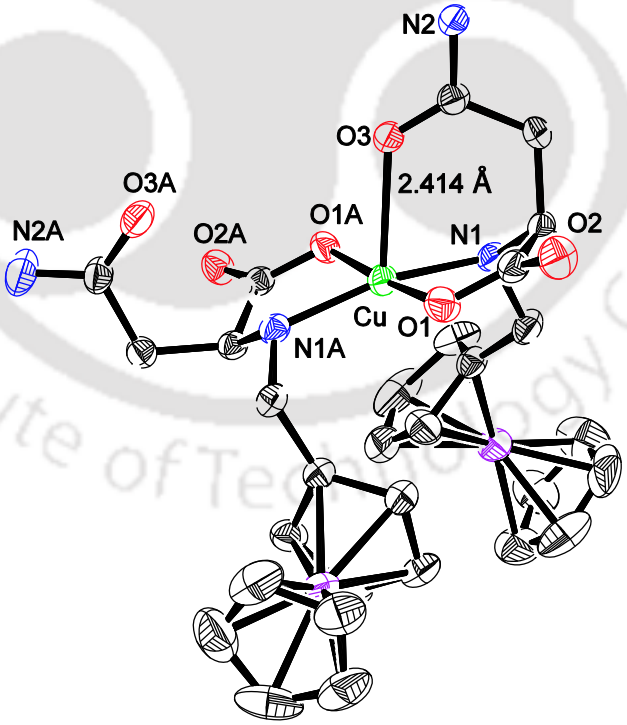

Figure 2.4 ORTEP diagram of **2a** with 50 % probability. Hydrogens are removed for clarity.

In **3a**, axial coordination is provided by a water molecule with short Cu–O distance of 2.3876(17) Å (Figure 2.5). The corresponding [Cu(L-serine)$_2$] have a short Cu–O axial distance of 2.359(6) where axial coordination originated from carboxylate oxygen of neighbouring molecule.[1b] One prominent feature of this structure is the H-bond between axially bound oxygen and serine hydroxyl group with a O…O bond distance of 3.04 Å (Figure 2.5). The usual O…O H-bond distances lies between 2.74 to 3.004.16 Å.

In **4a**, axial coordination is even shorter at 2.258(4) Å (Figure 2.6) compared to the axial Cu–O distance in [Cu(L-threonine)$_2$] at 2.478(8)Å.[1f] The prominent feature of this structure is the reversal of axial coordination on the ferrocene side compared to all the other structures presented in this chapter. Presence of two bulky isopropyl groups of threonine must have influenced the coordination of axial water on the other side. This in turn must have influenced the hydrophobic ferrocene units to rotate apart, a feature which is also unique to this molecule.

Overall, all the four amino acid derivatives form *bis* chelates with Cu(II) in *trans* configuration similar to their amino acid analogue. The polar *R* (Scheme I) groups and hydrophobic ferrocene units align on the different side of the chelate plane. The axial bond lengths in the present complexes are considerably shorter than corresponding Cu(II) complexes of the amino acids. The ferrocene derivatives are acting as weaker in-plane donor to Cu(II) as reflected in longer Cu–N_{amine} lengths at ~2.01 compared to < 2 Å in corresponding amino acid complexes.[1] Ferrocene substitution probably crowded the neighbourhood of secondary amine enough to weaken the amine coordination (longer amine-Cu(II) bond) which in turn helped shortening the axial bond.

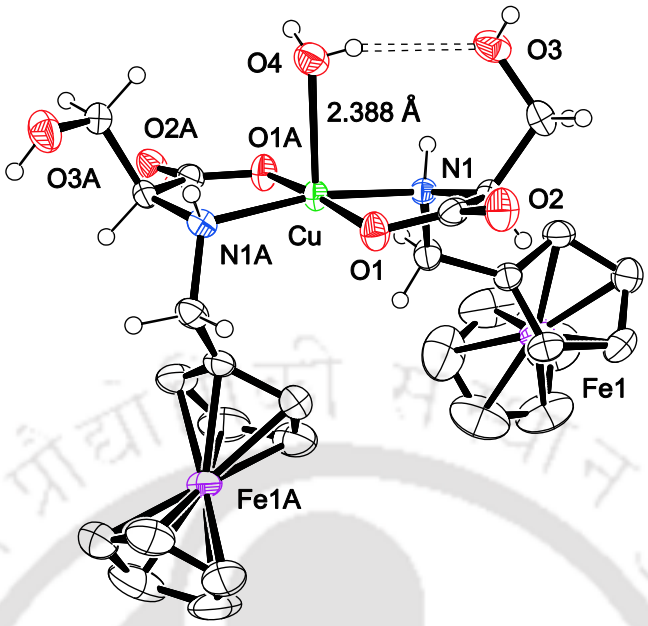

Figure 2.5 ORTEP diagram of **3a** with 50 % probability. Hydrogens are removed form ferrocene for clarity.

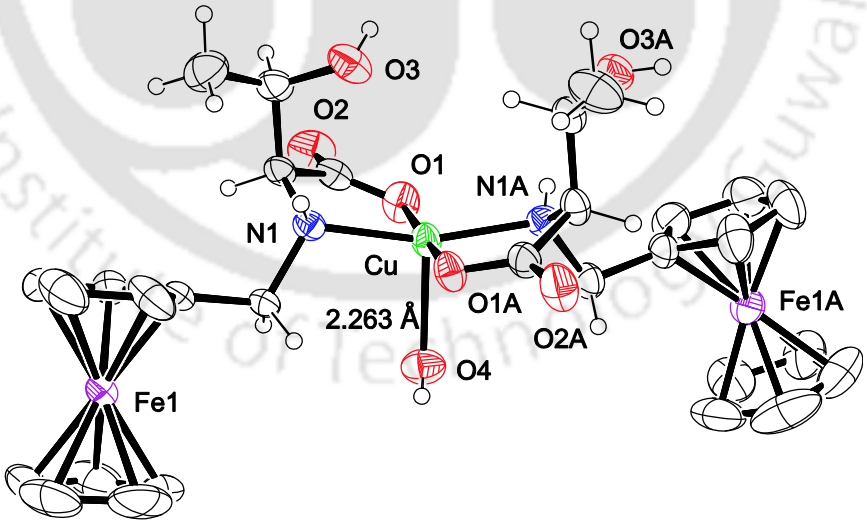

Figure 2.6 ORTEP diagram of **4a** with 50 % probability. Hydrogens are removed from ferrocene for clarity.

2.4.3 H-Bonded Networks

All the crystals have H-bonded network involving amino acid and coordinated waters. The polar faces of two different molecule form 2D network leaving ferrocene units to form a hydrophobic region. This leads to alternate layers of hydrophobic and hydrophilic regions (Figure 2.7 and 2.8). Earlier, with salicylaldehyde substituted amino acid, we[8] and others[9] found formation of great variety of H-bonded network but type of network formed was difficult to predict. In the present complexes, the alignment of hydrophilic groups on one side and ferrocene units on the other side made predictable layered structure.

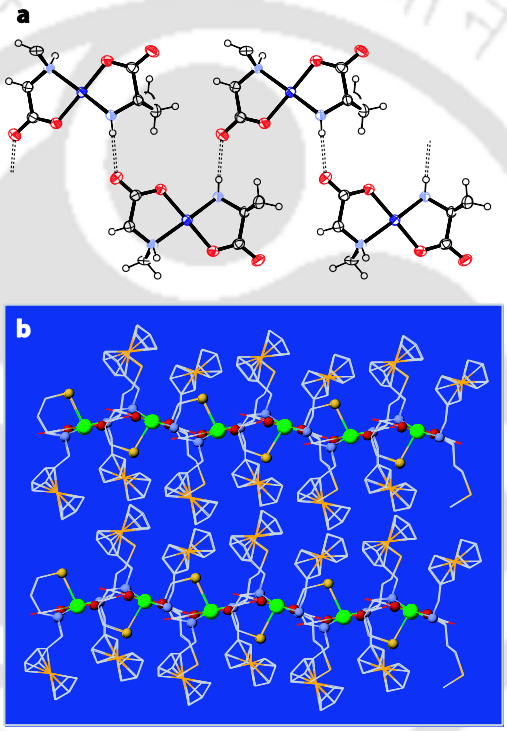

Figure 2.7 (a) In-plane H-bonded networks responsible for the layered structure (b) the lattice arrangement of **1a**.

In **4a** (Figure 2.6), the presence of polar water influenced the ferrocene units to move away from each other and methyl groups on the top which forced it to adopt a different arrangement containing channels (Figure 2.9). It however retains the separation of hydrophobic and hydrophilic regions like the other crystals. The importance of channels in crystal lattices has been highlighted by us[8b] and others[17,18] before. One major difference between these set of complexes with corresponding amino acid complexes are the absence of bridging mode of carboxylate coordination in the present complexes.

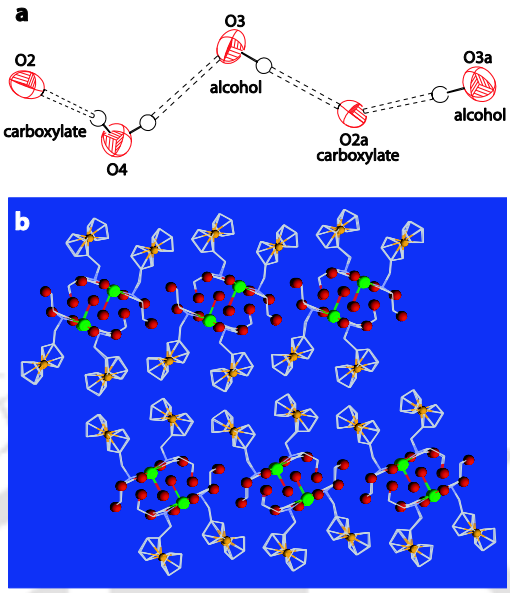

Figure 2.8 (a) H-bonding between water, alcohol group and carboxylate responsible for the layered structure in (b) the lattice arrangement of **3a**.

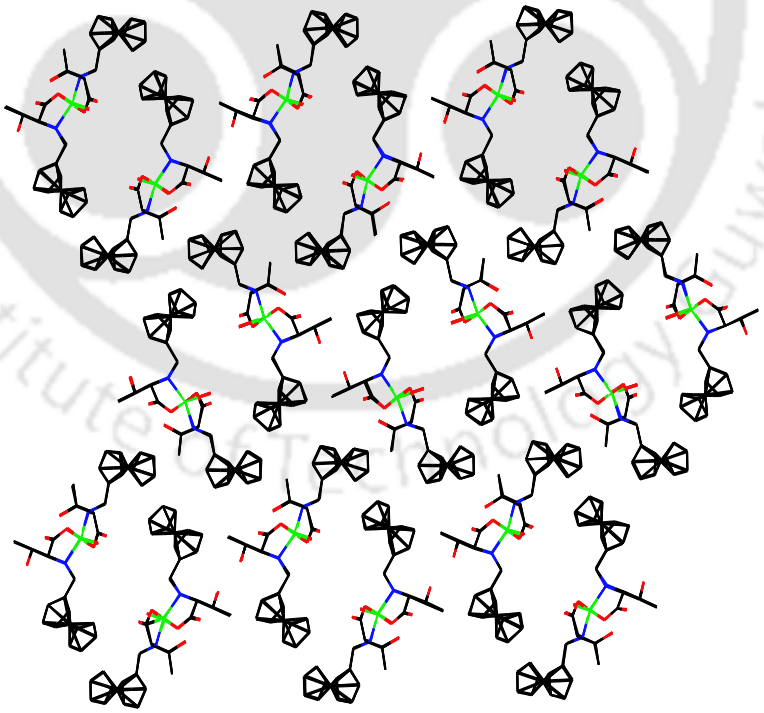

Figure 2.9 The channels in the network in **4a**. H-bonded water molecules inside the channels removed to improve clarity.

2.4.4 UV-visible absorption and EPR spectroscopy

The tendency to form coordination polymer leads to poor solubility of the complexes with underivatized amino acids. Thus most UV-vis and EPR studies were reported for solid state.[1e, 19]

The solution UV-vis and EPR spectroscopic data for the present complexes in MeOH have been presented in Table 2.3 and representative figures in Figure 2.10 and 2.11 respectively. The data for the ligands have been given in the experimental section. In addition to the transition at ~418 nm due to ferrocene unit, the complexes exhibit broad ligand field transitions at ~580 nm which was absent in the ligand spectra. This is similar to the bis amino acid Cu(II) complexes which show transitions between 580-610 nm.[1e,19] The solution EPR spectroscopic data for the complexes at 77 K (Table 2. 3) are consistent with the square-pyramidal structures of the complexes and comparable to corresponding L-Ala and L-Val complexes in solution showing g_{II} values ~ 2.26, $g_{\perp}$ ~ 2.06 and A_{II} values of between 175-179 G.[19a, 20, 21a]

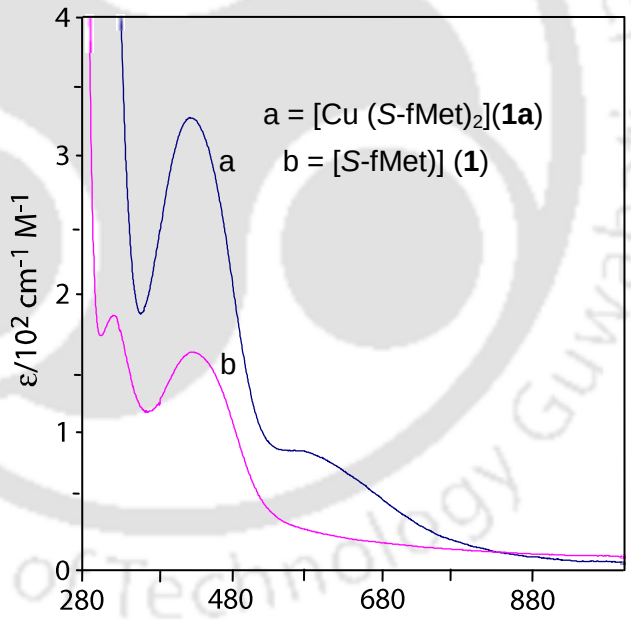

Figure 2.10 The UV-vis spectra of complex **1a** in MeOH and ligand **1** in MeOH with LiOH.

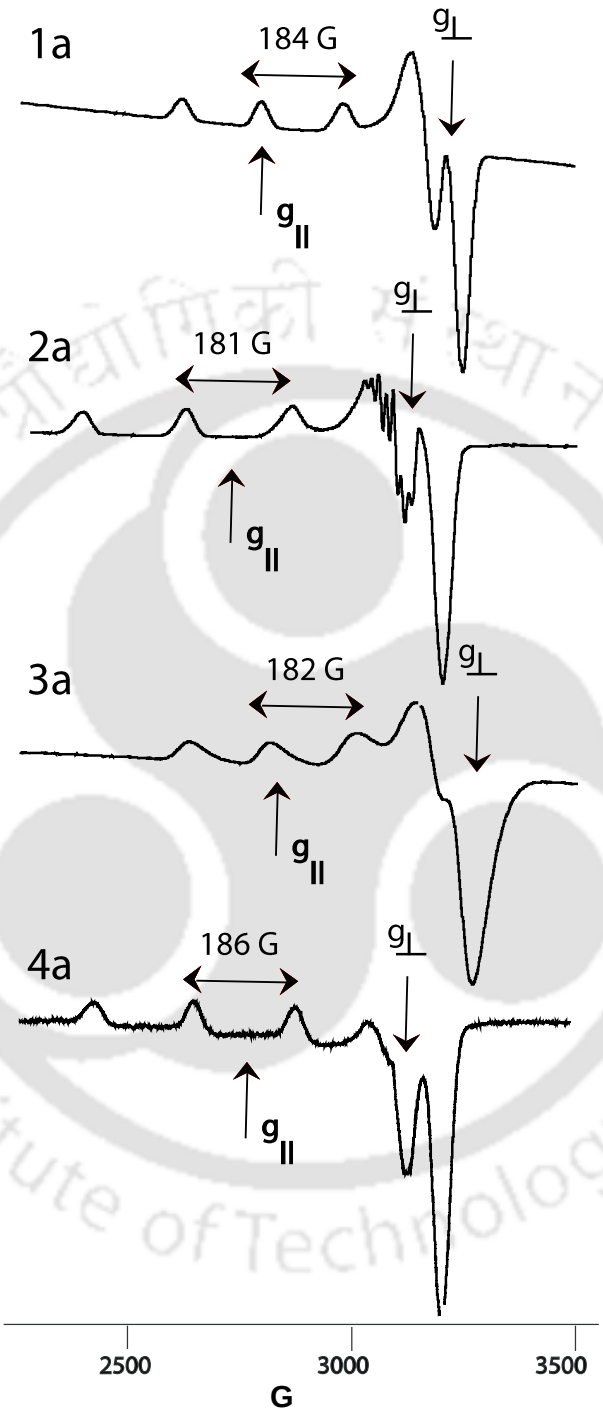

Figure 2.11 EPR of the complexes **1a** (A), **2a** (B), **3a** (C) and **4a** (D) in MeOH at 77 K.

2.4.5 Electrochemistry

The cyclic voltammetry of the complexes were performed in DMF as methanol/ethanol has a limited accessible potential range. The complexes are not soluble either in acetonitrile or dichloromethane. The cyclic voltammetry of the complexes at 50 mV/s show reversible oxidation due to both the ferrocene units at ~ 40 mV vs. Fc^+/Fc (Table 2.4, Figure 2.12). The complexes **1a** and **3a** in ethanol show the oxidation at 90 (ΔE_p, 105 mV) and 80 mV (ΔE_p, 123 mV) respectively. Thus neither solvent nor amino acid has a pronounced effect on the ferrocene couple. The Fc^+/Fc oxidation of ligands **1** and **3** in presence of LiOH shows negligible shift of <10 mV (for **3**, $E_{1/2}$ 7 mV, ΔE_p 140 mV) in Ethanol. An irreversible reduction with E_{pc} values between -1.5 to -1.7 V presumably for Cu(II)/Cu(I) was observed for all the four complexes. which upon reoxidation shows adsorbtion at the electrode surface possibly due to the disproportioniation of the Cu(I) complex.[21] The Cu(II) complex of *bis*-glutamic acid derivative (N_2O_2 coordination) in DMF shows irreversible Cu(II)/Cu(I) reduction at -0.9 V vs. Ag/AgCl (-1.34 V *vs*. Fc^+/Fc).[21] The Cu(II)/Cu(I) reduction in *bis*-amino acid Cu(II) complexes occurs at ~-0.7 V *vs* Fc^+/Fc.[21b] The considerable shift of the reductions in **2a-4a** in the negative direction indicates the Cu(II) is better stabilized in the present complexes. Complex **2a** to **4a** have N_2O_3 coordination instead of N_2O_2 in amino acid complexes. This might be one of the reason for better stability for Cu(II) over amino acid analogue.

Table 2.4 Electrochemical data of the complexes.

Complex	$E_{1/2}$/V (ΔEp/mV)	Epc / V
1a	0.06(100)	-1.52
2a	0.04(81)	-1.66
3a	0.04(88)	-1.58
4a	0.04(88)	-1.63

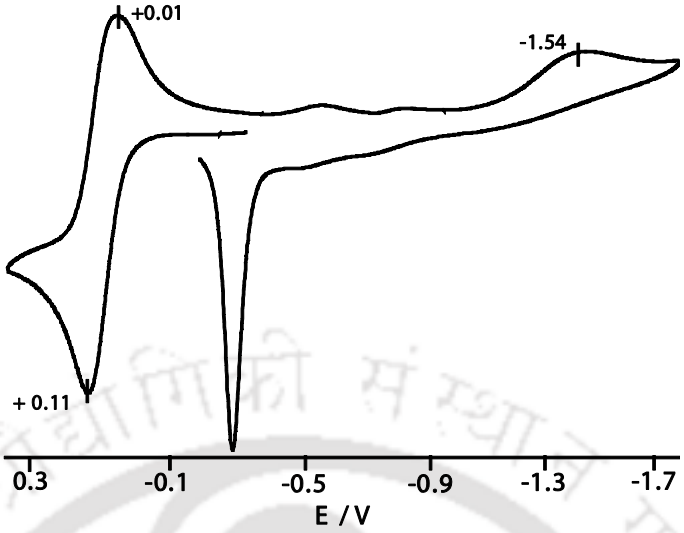

Figure 2.12 Cyclic Voltammogram of **1a** in DMF; Condition: Scan rate 50 mV S^{-1}, glassy carbon as working electrode, tetrabutylammonium perchlorate as supporting electrolyte. Potentials shown are *vs* Fc+/Fc.

2.4.6 Conclusion

The Cu(II) complexes of amino acid attract attention from diverse field of biology as well as coordination chemistry. The ferrocenyl methyl amino acids on the other hand get attention from bioorganometallic chemistry as well as electrochemical sensor design. In our group's continued interest to use flexible chiral ligands organizing around metal ion forming rigid chiral cavity or channels to facilitate chiral recognition and seperation, we explored the metal binding capability of ferrocenyl methyl amino acids with Cu(II).[8]

Results presented in this chapter showed that the properties of the *bis* complexes closely matched with their amino acid counterpart except an observable strengthening of the axial binding in the solid state structure. The strenthening in axial bond resulted in the coordination of weak methionine thioether (**1a**) or carbonyl oxygen (**2a**) to Cu(II). Coordination of methionine observed in proteins such as plastocyanin or azurin[16] but never in a structurally characterized synthetic Cu(II) complex.

Except **4a**, all the complexes showed both the chiral arms organizing around the axial coordination site. The structure of **3a** showed ligands involvement in forming H-bond with the axial ligand. Thus increasing the chance of chiral interaction with the axial ligand.

The complexes with amino acid or amino acid derivative ligands usually form wide range of H-bonded complex networks making it difficult to design networks rationally. Due to the hydrophobic and hydrophilic region separation, the present complexes retains layered structure even when the amino acid changes. Additionally, **4a** shows formation of channels with removable solvent.

While the electrochemical results did not show appreciable change in Fc^{+}/Fc couple from one amino acid to the other, the reduction E_{pc} found to be sensitive to axial coordination (Table 2.4).

Overall, in Cu(II) complexes of ferrocenylmethyl amino acids (a) ligands organizes around Cu(II) in a C_2 symmetric fashion, (b) enhances the axial coordination, (c) Cu(II)/Cu(I) reduction is sensitive to axial coordination and (d) preferentially forms alternately hydrophobic and hydrophilic layered structures.

References

1. Structures of Cu(II) complexes with pure amino acids used in this work:(a) McAuliffe, C. A.; Quagliano, J. V.; Vallarino, L. M. *Inorg. Chem.* **1966**, *5*, 1996. (b) Helm, D. V. D.; Franks, W. A. *Acta. Crystallogr., Sect. B* **1969**, *25*, 451. (c) Stephens, F. S.; Vagg R. S.; Willams, P. A. *Acta. Crystallogr., Sect. B* **1975**, *31*, 841. (d) Ou, C.; Powers, D. A.; Thich, J. A.; Felthouse, T. R.; Hendrickson, D. N.; Potenza, J. A.; Schugar, H. J. *Inorg. Chem*. **1978**, *17*, 34. (e) Hitchman, M. A.; Kwan, L. *J. Chem. Soc., Dalton Trans*. **1987**, 457 (f) Rizzi, A. C.; Piro, O. E.; Castellano, E. E.; Nascimento, O. R.; Brondino, C. D. *Inorg. Chim. Acta* **2000**, *305*, 19.

2. (a) Freeman, H. C. *Inorganic Biochemistry*, ed. Eichhorn, G. L. Elsevier, Amsterdam, **1973**, ch. 3 and references cited therein; (b) Brill, A. S. *Transition Metals in Biochemistry*, Springer Verlag, Berlin, **1977**.

3. (a) Sarkar, B. *Chem. Rev.* **1999**, *99*, 2535. (b) Deschamps, P.; Kulkarni, P. P.; Gautam-Basak, M.; Sarkar, B. *Coord. Chem. Rev.* **2005**, *249*, 895.

4. (a) Kraatz, H.; Lusztyk, J. Enright, G. D. *Inorg. Chem.* **1997**, *36*, 2400. (b) Hess, A.; Sehnert, J.; Weyhermiiller, T.; Metzler-Nolte, N. *Inorg. Chem.* **2000**, *39*, 5437. (c) Staveren, D. R. V.; Metzler-Nolte, N. *Chem. Rev.* **2004**, *104*, 5931. (d) Coutouli- Argyropoulou, E.; Sideris, C. Kokkinidis, G. *J. Organomet. Chem.* **2006**, *691*, 3909. (*e*) Kirin, S. I.; Kraatz, H. Metzler-Nolte, N. *Chem. Soc. Rev.* **2006**, *35*, 348. (f) Kraatz, H. *J. Inorg. Organomet. Polym. Mater.* **2005**, *15*, 83. (g) Nomoto, A.; Moriuchi, T.; Yamazaki, S.; Ogawa, A.; Hirao, T. *Chem. Commun.* **1998**, 1963. (h) Moriuchi, T.; Nagai, T.; Hirao, T. *Org. Lett.* **2006**, *8*, 31.

5. (a) Cui, X.; Delgado, R.; Carapuc¸ H. M.; Drew, M. G. B.; F´elix, V. *Dalton Trans.* **2005**, 3297. (b) Miyaji, H.; Gasser, G.; Green, S. J.; Molard, Y.; Strawbridge, S. M.; Tucker, J. H. R. *Chem. Commun.* **2005**, 5355. (c) Zhang, B.; Xu, J.; Zhao, Y.; Duan, C.; Cao, X.; Meng, Q. *Dalton Trans.* **2006**, 1271. (d) Beer, P. D.; Cadman, J. *Coord. Chem. Rev.* **2000**, *205*, 131. (e) Debroy, P.; Roy, S. *Coord. Chem. Rev.* **2007**, *251*, 203.

6. Osman, A. M.; El-Maghraby, M. A.; Hassan K. M. *Bull. Chem. Soc. Jpn.* **1975**, *48*, 2226.

7. Appoh, F. E.; Sutherland, T. C.; Kraatz, H., *J. Organomet. Chem.***2005**, *690*, 1209.

8. (a) Alam, Md. A.; Nethaji, M.; Ray, M. *Angew. Chem., Int. Ed.* **2003**, *42*, 1940. (b) Alam, Md. A.; Nethaji, M.; Ray, M. *Inorg. Chem.* **2005**, *44*, 1302.

9. (a) Ranford, J. D.; Vittal, J. J.; Wu, D. *Angew. Chem., Int. Ed.* **1998**, *37*, 1114. (b) Ranford, J. D.; Vittal, J. J.; Wu, D.; Yang, X. *Angew. Chem., Int. Ed.* **1999**, *38*, 3498. (c) Sreenivasulu, B.; Vittal, J. J. *Angew. Chem., Int. Ed.* **2004**, *43*, 5769. (d) Vittal, J. J.; Yang, X. *Cryst. Growth Des.*, **2002**, *2*, 259. (e) Yang, X.; Ranford J. D.; Vittal, J. J. *Cryst. Growth Des.* **2004**, *4*, 781. (f) Yang, C.-T.; Vetrichelvan, M.; Yang, X.; Moubaraki, B.; Murray, K. S.; Vittal, J. J. *Dalton Trans.* **2004**, 113.

10. Holm, R. H.; Kennepohl, P.; Solomon, E. I., *Chem. Rev.* **1996**, *96*, 2239.

11. Sheldrick, G. M. SHELXL-97, Program for the Solution of Crystal Structures; University of Göttingen: Göttingen, Germany.

12. Johnson, C. K. *ORTEP, Report ORNL-3794*, Oak Ridge National Laboratory, Oak Ridge, TN, **1976**.

13. (a) Earnshaw, A. *Introduction to Magnetochemistry*, Academic Press, London, 1968. (b) Figgis, B. N.; Lewis, J. *Prog. Inorg. Chem.* **1964**, ***6***, 37.

14. Addision, A.W.; Rao, T. N. Reedijk, J.; Rijn, J. V.; Verschoor, G. C. *J. Chem. Soc. Dalton Trans.* **1984**, 1349.

15. (*a*) Hathaway, B. J. in *Comprehensive Coordination Chemistry*, ed Wilkinson, G.; Gillard, R. D.; McCleverty, J. A. Pergamon Press, London, **1987**, vol. 5, p. 533. (*b*) Addison, A. W.; Sinn, E. *Inorg. Chem.* **1983**, *22*, 1225. (*c*) Bonamico, M.; Dessy, G.; Mugnoli, A.; Vaeiago, A.; Zambonelli, L. *Acta Crystallogr.* **1965**, *19*, 886. (*d*) Agus, Y.; Louis, R.; Weiss, R. *J. Am. Chem. Soc.* **1979**, *101*, 3381.

16. Holm, R. H.; Kennepohl, P.; Solomon, E. I. *Chem. Rev.* **1996**, *96*, 2239.

17. (*a*) Yaghi, M. O.; Li, H.; Davis, C.; Richardson, D.; Groy, T. L. *Acc. Chem. Res.* **1998**, *3*, 1474. (*b*) Ikegame, M.; Tajima, K.; Aida, T. *Angew. Chem., Int. Ed.* **2003**, *42*, 2154. (*c*) Kitaura, R.; Kitagawa, S.; Kubota, Y.; Kobayashi, T. C.; Kindo, K.; Mita, Y.; Matsuo, A.; Kobayashi, M.; Chang, H. C.; Ozawa, T. C.; Suzuki, M.; Sakata, M.; Takata, M. *Science* **2002**, *298*, 2358. (*d*) Kitagawa, S.; Kitaura, R.; Noro, S. *Angew. Chem., Int. Ed.* **2004**, *43*, 2334.

18. Langley, P. J.; Hulliger, J. *Chem. Soc. Rev.* **1999**, *28*, 279.

19. (*a*) Yokoi, H.; Sai, M.; Isobe, T.; Ohsawa, S. *Bull. Chem. Soc. Jpn.* **1972**, *45*, 2189. (*b*) Stanila, A.; Marcu, A.; Rusu, D.; David, L. *J. Mol. Str.* **2007**, *364*, 834.

20. Sakaguchi, U.; Addison, A. W. *J. Chem. Soc., Dalton Trans.* **1979**, 600.

21. (*a*) Stone, D. L.; Smith, D. K.; Whitwood, A. C. *Polyhedron* **2004**, *23*, 1709. (*b*) Thomas, G.; Zacharlas, P. S. *Polyhedron* **1985**, *4*, 811.

Chapter 3

In the previous chapter we have explored the coordination chemistry of the ferrocenylmethyl derivatives of four amino acids with Cu(II) ion. We observed that two ligands organize around Cu(II) in a C_2 symmetry such that both amino acid residues stay on the same side of the Cu(II) coordination plane (Scheme 3.1). As our primary target in this thesis was to create a chiral cavity around binding site of the metal centre for guest recognition, in this chapter we have used L-tyrosine derivative to form a chiral pocket around the fifth coordination site of Cu(II) (axial) and studied the guest binding preference with three monodentate heterocycles and water.

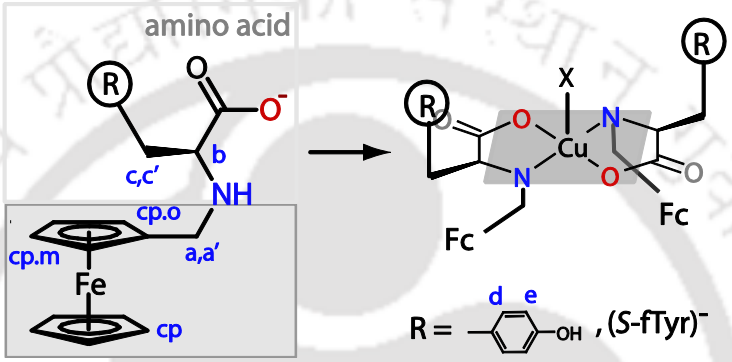

Scheme 3.1 The orientation of amino acid residues around Cu(II) along with ^{1}H NMR labelling scheme.

3.1 Experimental Section

3.1.1 Solvents and Reagents

Details of the solvent purification and analytical measurements have already discussed in chapter 2. The ligand *S*-fTyr(**HL**) and its Cu(II) complexes were synthesized and characterized as below.

3.2 Synthesis

3.2.1 [H(*S*-fTyr)] (HL)

A methanolic solution of ferrocenealdehyde (1.18 g, 5.51 mmol) was added dropwise to a stirring solution of L-tyrosine (1.00 g, 5.52 mmol) and $LiOH{\cdot}H_2O$ (0.23 g, 5.50 mmol) in methanol (25 mL). The stirring was continued for 2 h, followed by addition of sodium borohydride (0.21 g, 5.55 mmol) with further stirring of 1 h. The solvent was evaporated and the resulting sticky mass was dissolved in water and acidified with dilute HCl. The pH of the solution was maintained between 5-7. The ligand precipitated as a brown solid. It was thoroughly washed with water and MeOH after filtration and dried in a vacuum desiccator. Yield 1.60 g

(76%). Anal. Calcd for $C_{20}H_{21}NO_3Fe$: C, 63.30; H, 5.58; N, 3.69. Found: C, 63.10; H, 6.29; N, 3.66. $[\alpha]_D^{25}$ = -26° in MeOH, *c* = 0.2 in the presence of 1 equivalent $LiOH{\cdot}H_2O$. *m*/*z* (ESI-MS, $[M-H^{-1}]$) 379.087 (calcd 379.084). IR (KBr, cm^{-1}), $\upsilon(COO)_{asym}$ 1579 (s), $\upsilon(COO)_{sym}$ 1394 (s). ^1H NMR (CD_3OD, ppm): $H^{cp.o}$ (4.10, d, 1H), $H^{cp.o}$ (4.13, d, 1H), H^{cp} (3.99, s, 5H), H^{cp} (4.03, s, 2H), H^a (3.51, d, 1H, $J_{a,a'}$ = 12.8 Hz), $H^{a'}$ (3.22, d, 1H), H^b (3.31, m, 1H), H^c (2.94, dd, 1H), $H^{c'}$ (2.67, dd, 1H), $H^{d,d'}$ (6.96, d, 2H), $H^{e,e'}$ (6.59, d, 2H). Due to geminal coupling H^c split into two non-equivalent H^c and $H^{c'}$.

3.2.2 [Cu(*S*-fTyr)$_2$(MeCN)$_2$] (1). The ligand H(*S*-fTyr) (0.500 g, 1.32 mmol) and $Cu(acetate)_2{\cdot}H_2O$ (0.13 g, 0.66 mmol) in 25 mL MeOH were stirred for 2 h. The solvent was evaporated to dryness followed by washing the residue with acetonitrile. The green solid thus obtained was recrystallized from a mixture of acetonitrile and methanol (1:3) affording dark green crystals of **1** after 4-5 h. Crystals were washed with diethyl ether and dried under vacuo. Yield 0.40 g (64%). Anal. Calcd for $Cu(C_{44}H_{46}N_4O_6Fe_2)$: C, 58.58; H, 5.13; N, 6.21. Found: C, 57.19; H, 5.10; N, 6.34. IR (KBr, cm^{-1}) $\upsilon(COO)_{asym}$ 1619 (s). $\upsilon(COO)_{sym}$ 1377 (s), (CN) 1698 (s). μ_{eff} (solid, 298 K): 2.21 B.M; EPR: MeOH, 77 K, $g_\perp$ = 2.230, g_{II} = 2.035, A_{II} = 183 G.
Alternatively, **1** can also be prepared by substituting $Cu(acetate)_2{\cdot}H_2O$ in the above procedure with $Cu(NO_3)_2{\cdot}3H_2O$ and LiOH in metal : ligand : base ratio of 0.5 : 1 : 1 respectively.

3.2.3 [Cu(*S*-fTyr)$_2$(pyrazine)] (2). The ligand H(*S*-fTyr) (0.500 g, 1.32 mmol) and $Cu(acetate)_2{\cdot}H_2O$ (0.13 g, 0.66 mmol) in 25 mL MeOH were stirred for 2 h. The solvent was evaporated to dryness, residue was redissolved in MeOH and filtered. Pyrazine (0.10 g, 1.25 mmol) was added to the filtrate and stirred for another 2 h. The green precipitate was filtered and dried. Recrystallization from MeOH by slow evaporation afforded dark green rod shaped crystals after three days. Crystals were washed with diethyl ether and dried in vacuo. Yield 0.38 g (64%). Anal. Calcd for $Cu(C_{44}H_{44}N_4O_6Fe_2)(H_2O)$: C, 57.56; H, 5.05; N, 6.10. Found: C, 57.03; H, 5.17; N, 5.65. IR (KBr, cm^{-1}) $\upsilon(COO)_{asym}$ 1625 (s), $\upsilon(COO)_{sym}$ 1377 (s). μ_{eff} (solid, 298 K): 2.16 B. M.; EPR: MeOH, 77 K, $g_\perp$ = 2.235, g_{II} = 2.040, A_{II} = 181 G.
Alternatively, **2** can also be prepared by dissolving **1** and pyrazine in 1:1 ratio in minimum volume of MeOH followed by 30 min stirring. Crystals of **2** were obtained by slow evaporation of the resulting mixture after four days.

3.2.4 [Cu(*S*-fTyr)$_2$(Py)] (3). The ligand H(*S*-fTyr) (0.500 g, 1.32 mmol) and Cu(acetate)$_2$·H$_2$O (0.13 g, 0.66 mmol) in 25 mL MeOH were stirred for 2 h and evaporated to dryness. The solid residue thus obtained was redissolved in MeOH and filtered to remove undissolved materials. Pyridine (2 mL) was added to the filtrate and stirred for 1 h. The complex precipitated as a light green solid, was filtered and dried in vacuo. The complex was recrystallized by slow evaporation of the methanolic solution and block shaped crystals were obtained after four days. Yield 0.37 g (62%). Anal. Calcd for Cu ($C_{45}H_{45}N_3O_6Fe_2$)(H_2O): C, 58.93; H, 5.16; N, 4.58. Found: C, 59.43; H, 5.34; N, 4.59. IR (KBr, cm^{-1}) $\upsilon(COO)_{asym}$ 1621 (s). $\upsilon(COO)_{sym}$ 1378 (s), (py) 697 (s). μ_{eff} (solid, 298 K): 1.96 B. M.; EPR: MeOH, 77 K, $g_{\perp}$ = 2.235, g_{II} = 2.040, A_{II} = 182

Alternatively, **1** and pyridine in 1:1 ratio was stirred for 30 min in MeOH. Slow evaporation of the solution yielded crystals of **3** after two days.

3.2.5 [Cu(*S*-fTyr)$_2$(bpy)] (4). Solid 4, 4′ -bipyridine was added to a stirred methanolic solution of complex **1** in ratio (1:1) and stirring was continued for 4 h. Green plate like crystals of **4** were obtained upon slow evaporation of the resulting solution after a week. Crystals were washed with ether and dried in vacuo. Yield 0.37 g (60%). Anal. Calcd for Cu ($C_{50}H_{50}N_4O_7Fe_2$): C, 60.40; H, 5.06; N, 5.63. Found: C, 60.51; H, 5.04; N, 5.59. IR (KBr, cm^{-1}) $\upsilon(COO)_{asym}$ 1614 (s), $\upsilon(COO)_{sym}$ 1379 (s). μ_{eff} (solid, 298 K): 2.08 B. M.; EPR: MeOH, 77 K, $g_{\perp}$ = 2.237, g_{II} = 2.040, A_{II} = 182 G.

3.2.6 [Cu(*S*-fTyr)$_2$(H$_2$O)] (5). The ligand H(*S*-fTyr) (0.500 g, 1.32 mmol) and Cu(acetate)$_2$·H$_2$O (0.13 g, 0.66 mmol) in 25 mL methanol were stirred for 2 h and evaporated to dryness. The resulting sticky mass was redissolved in MeOH and filtered. Slow evaporation of the filtrate offered green plate like crystals of **5** after four days. Crystals were washed with ether and dried in vacuo. Yield 0.382 g (68%). Anal. Calcd for Cu($C_{40}H_{40}N_2O_6Fe_2$)(H_2O)$_2$(CH_3OH)$_{0.5}$: C, 55.78; H, 5.31; N, 3.21. Found: C, 55.44; H, 5.34; N, 3.55. IR (KBr, cm^{-1}) $\upsilon(COO)_{asym}$ 1604 (s), $\upsilon(COO)_{asym}$ 1376 (s). μ_{eff} (solid, 298 K): 1.99 B. M.; EPR: MeOH, 77 K, $g_{\perp}$ = 2.236, g_{II} = 2.040, A_{II} = 181 G.

This complex can also be prepared using Cu(NO_3)$_2$·3H$_2$O and LiOH as base in place of Cu(acetate)$_2$·H$_2$O with M : L : base ratio of 0.5 : 1 : 1 respectively.

Table 3.1 Selected crystallographic data of the complexes

Complexes	**1**	**2**	**3**	**4**	**5**
Empirical formula	$C_{48}H_{52}CuFe_2N_6O_6$	$C_{44}H_{44}CuFe_2N_4O_6$	$C_{45}H_{45}CuFe_2N_3O_6$	$C_{50}H_{50}CuFe_2N_4O_7$	$C_{41}H_{48}CuFe_2N_2O_9$
Formula weight(fw)	983.18	900.07	899.11	994.19	887.05
Crystal system	Teragonal	Orthorhombic	Orthorhombic	Monoclinic	Monoclinic
Space group	P43 21 2	$P2_12_12$	$P2_12_12$	$P2_1$	$P2_1$
a Å	10.7303(1)	10.971(1)	11.0240(2)	12.3132(4)	13.2115(3)
b Å	10.7303(1)	11.7405(1)	11.7776(2)	10.4178(3)	11.5925(3)
c Å	41.1772(7)	15.2578(2)	15.3338(3)	17.2315(5)	13.9124(3)
α deg					
β deg	α=β=γ= 90	α=β=γ= 90	α=β=γ= 90	β=98.306(2)	β=110.072(1)
γ deg					
V, Å^3	4741.12(10)	1965.39(4)	1990.88(6)	2187.21(11)	2001.33(8)
Z	4	2	2	2	2
Calculated density(ρ)	1.375	1.521	1.5	1.507	1.472
Absorption coefficient(μ)	1.101	1.320	1.310	1.195	1.298
FLACK parameter	-0.019(14)	0.014(15)	0.017(10)	-0.016(7)	0.003(6)
F(000)	2032	930	930	1026	920
Reflns collected	53882	16568	29385	25354	23979
Indep reflns	5162	4515	7965	9323	9596
Goodness-of-fit on F^2	1.012	1.035	1.074	1.069	0.976
R indices	R1= 0.0573,	R1 = 0.0279,	R1 = 0.0336,	R1=0.0370,	R1=0.0249,
[I > 2σ(I)]	wR2 = 0.0702	wR2 = 0.0809	wR2 = 0.0879	wR2= 0.0485	wR2= 0.0553
R indices	R1 = 0.0511,	R1 = 0.0317,	R1 = 0.0491,	R1= 0.0759,	R1= 0.0313,
(all data)	wR2 = 0.0766	wR2 = 0.0822	wR2 = 0.0922	wR2= 0.0526	wR2= 0.0569

Refinment method full-matrix least-squares on F^2

Table 3.2 Selected bond lengths (Å) and angles (º) for complexes.

	1	**2**	**3**	**4**	**5**
Cu–O1	1.9342(18)	1.926(2)	1.9329(14)	1.136(2)	`1.9217(12)
Cu–O1A	1.9342(18)	1.926(2)	1.9329(14)	1.92192)	1.9544(12)
Cu–N1	2.017(2)	2.035(2)	2.0443(14)	2.051(3)	2.0051(13)
Cu–N1A	2.017(2)	2.035(2)	2.0443(14)	2.049(3)	2.0137(14)
Cu–axial	2.535(3)	2.316(4)	2.253(2)	2.210(2)	2.453(2)
Cu–axial	2.663(3)	_	_	_	_
O1–Cu–O1A	173.67(13)	176.18(14)	173.50(10)	175.93(9)	177.03(5)
N1–Cu–N1A	175.21(13)	159.38(13)	159.16(8)	147.03(11)	167.27(6)
O1–Cu–N1A	95.85(7)	84.88(9)	84.55(6)	96.09(10)	94.66(6)
O1A–Cu–N1	95.85(7)	94.43(8)	94.27(6)	94.82(10)	97.26(5)
N1–Cu–La1[a]	92.39(6)	100.31(6)	100.42(4)	103.49(10)	90.24(6)
O1–Cu–La2[a]	86.83(9)	91.91(7)	93.25(5)	93.12(9)	85.24(6)
τ	0.0256	0.28	0.239	0.481	0.162
H-bonding					
O_{tyr}.....O_{caroxy}	2.641(3)	2.674(4)	2.678(3)	2.639(3)	2.628(2)
O_{tyr}....O_{tyr}					2.829(3)
O_{caroxy}....O_{water}				2.767(4)	2.700(3)
O_{tyr}.....O_{water}				2.705(4), 2.883(4)	

[1]La is axial ligands.

3.3 Result and discussion

3.3.1 Syntheses and Selected Properties

All the Cu(II) complexes were synthesized directly by reacting Cu(II), H_2S-fTyr, base (LiOH or acetate anion) and guest molecule. Alternatively, **2-5** can be prepared from **1** by addition of guest donor molecules (Scheme 3.2). All the complexes were characterized using FT-IR, elemental analysis and room temperature magnetic moments (experimental section). The IR spectra of the ligand and the complexes show strong and sharp asymmetric carboxylate stretches between 1580-1630 cm,$^{-1}$ symmetric stretches ~1377 cm^{-1}.[1-2] The complexes are non conducting supporting the non-electrolytic nature of the complexes. The elemental analyses support the formulation of the complexes. However, because of tendency to lose lattice solvent and tendency of acquiring moisture, amount of solvent in the structure and the bulk differ. The room temperature solid state magnetic moments lies between 1.94-2.13 B.M. are within expected range for monomeric Cu(II) complex (experimental section).[3] All the complexes were further characterized using X-ray crystallography.

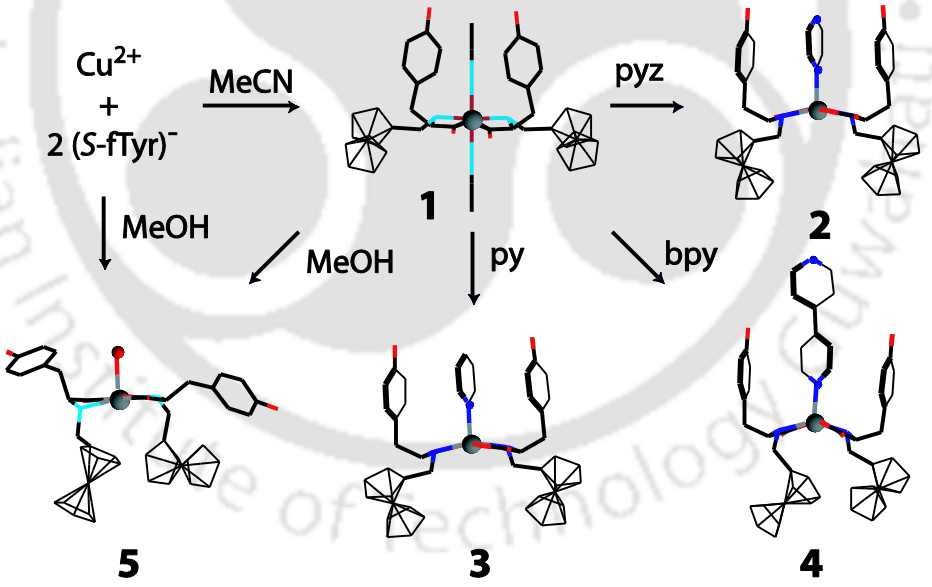

Scheme 3.2 Synthesis of Cu(II) complexes.

3.3.2 Molecular structures

Structural parameters and selected bond lengths and angles for all the complexes have been provided in Table 3.1 and Table 3.2 respectively. All the complexes are monomeric in nature

with a various amount of distortion (τ, 0.0-0.5) towards square planar geometry around Cu(II). The distortion parameter τ was calculated from the structural data where the value of τ should be 0.0 for perfect square-pyramidal geometry and 1.0 for a perfect trigonal bipyramidal (TBP) structure.[4]

In **1**, Cu(II) is octahedrally coordinated by two bidentate $(S\text{-fTyr})^{-1}$ ligands and two acetonitriles (Figure 3.1). Orientation of the two $(S\text{-fTyr})^{-1}$ ligand around Cu(II) in a *C*2 symmetry resulted in the parallel alignment of both the phenol arms forming a narrow cavity around the axial coordination site of Cu(II). There are four molecules of acetonitrile per one molecule of **1** in the crystal. Two of which are axially bound to Cu(II) and the other two are solvent of crystallization. One of the two axially coordinated acetonitrile is inside the cavity with a longer Cu–N (2.662(3) Å, Table 2) bond. The other acetonitrile molecule is bound to copper with relatively shorter Cu–N bond (2.537(3) Å, Table 2) between the two ferrocene units. The observed $Cu–N_{MeCN}$ length in **1** is longer than observed for few structurally characterized axially bound acetonitriles (2.06-2.57 Å)[5] The binding of acetonitrile inside the cavity which is a weak donor, leave options open to replace it easily with other guest molecules.

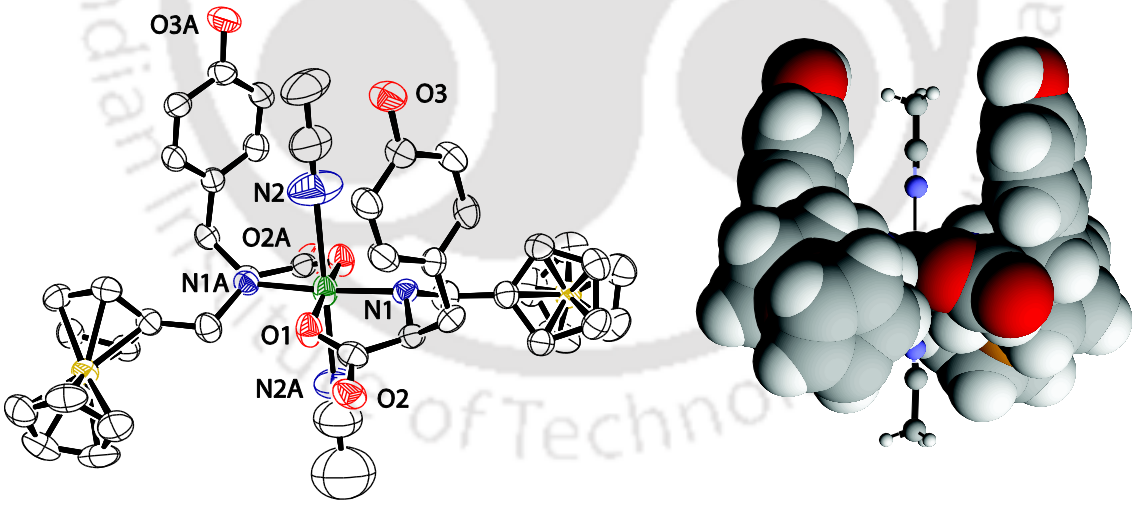

Figure 3.1 ORTEP diagram of **1** with 50 %.probability. Hydrogens are removed for clarity.

Considering the narrowness of the cavity, we have synthesized the pyrazine adduct (**2**) (Figure 3.2). Pyrazine usually act as in-plane bridging ligand towards Cu(II) rather than a monodentate ligand.[6] However, in **2**, pyrazine has coordinated as monodentate axial ligand. The

Cu–$N_{pyrazine}$ distance of 2.316(4) Å is well within the range of 1.95-2.42 Å observed for bridging pyrazines.[6] The plane of pyrazine molecule is almost parallel (4.7°, Figure 3.2) with both the phenol rings. The aromatic ring to ring distance of 3.994 Å is longer than usual π....π interaction distance range of 3.4-3.8 Å.[7]

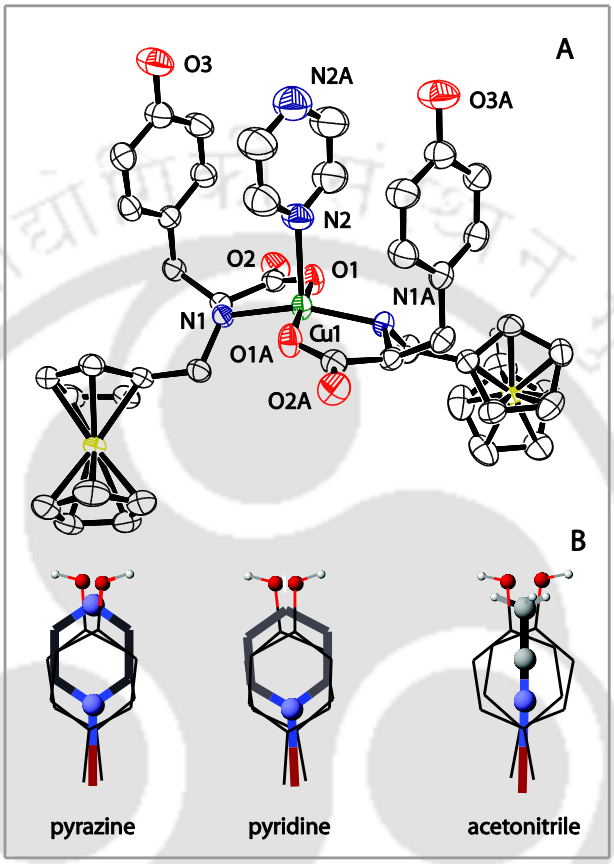

Figure 3.2 ORTEP diagram of **2** with 50 %.probability. Hydrogens are removed for clarity. Insert sketch figures showing the π…..π interactions.

We chose pyridine as the guest to form adduct due to similarity in shape and size with pyrazine but with a stronger binding ability (pK_a of pyridine 6.01 > pK_a of pyrazine 0.78). The structure of **3** (Figure 3.3) is identical with that of **2.** The Cu–$N_{pyridine}$ distance at 2.253(2) Å is shorter than Cu–$N_{pyrazine}$, reflecting pyridine's stronger binding ability. Pyridine ring to phenol ring distance of 3.948 Å is slightly shorter than the distance in **2**.

We chose 4, 4′-bipyridine (bpy) as the guest to test the rigidity of the cavity. Bpy is taller than pyridine or pyrazine and the two pyridine rings usually are non planar. The angle between the two plane varies between 0-90° depending on the steric interactions present within a

molecule.[8] Bidentate nature of bpy also introduce the possibility of a bridged dinuclear complex. The structure of **4** shows the cavity is resilient enough to allow 4, 4′-bipyridine to act as monodentate ligand without destroying the cavity (Figure 3.4). However, the parallality of bpy ring with the phenols are lost with tilting of bpy ring by ~60° with respect to phenol rings. This tilting brought C–H hydrogens pointing towards the π cloud of phenols (C–H…ring, ~2.7 Å) generating C–H...π interactions. The two rings of bpy are at an angle of ~52° with respect to each other.

We have also characterized [Cu(*S*-fTyr)$_2$(H_2O)](**5**)(Figure 3.5) which was isolated from MeOH without adding acetonitrile. The structure of **5** showed axial coordination of water resulted in rotation of tyrosine arms destroying the cavity. Comparison between **5** and **1**-**4** shows that the cavity is stable in presence of aromatic or unsaturated guest, presumably due to the weak π–π or C–H...π interaction but repelled by polar water molecule. Presence of either water or acetonitrile coordinated to Cu(II) between the ferrocene units results in a rotation of ferrocene arms away from each other observed in **1** and L-threonine analogue[1] as well.

The conformation at the chiral carbon is *S* as the amino acid used in the synthesis was the *S* isomer. The in-plane Cu–$O_{carboxylate}$ and Cu–N_{amine} bond lengths are comparable to what was observed for similar type of ligands as well as in amino acid complexes of Cu(II)[9a,c,1]

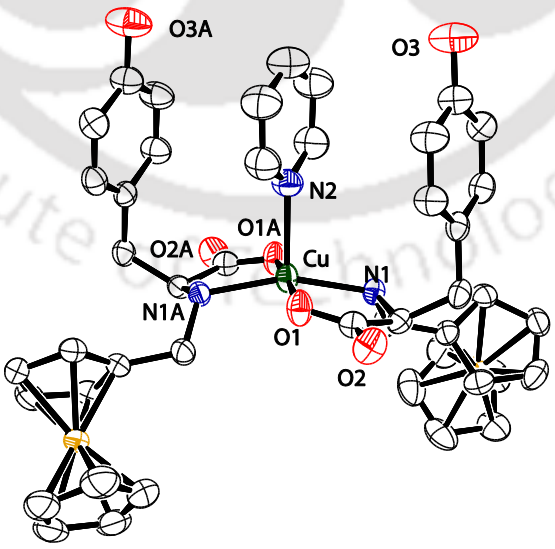

Figure 3.3 ORTEP diagram of **3** with 50 %.probability. Hydrogens are removed for clarity.

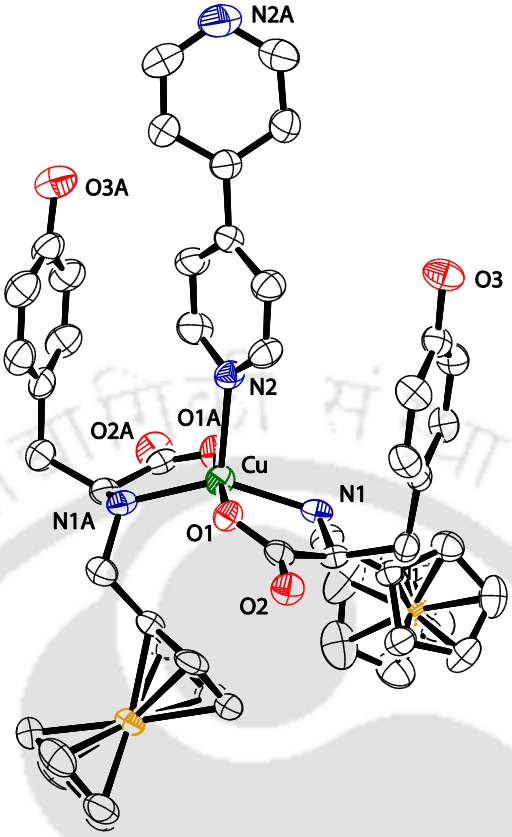

Figure 3.4 ORTEP diagram of **4** with 50 %.probability. Hydrogens are removed for clarity.

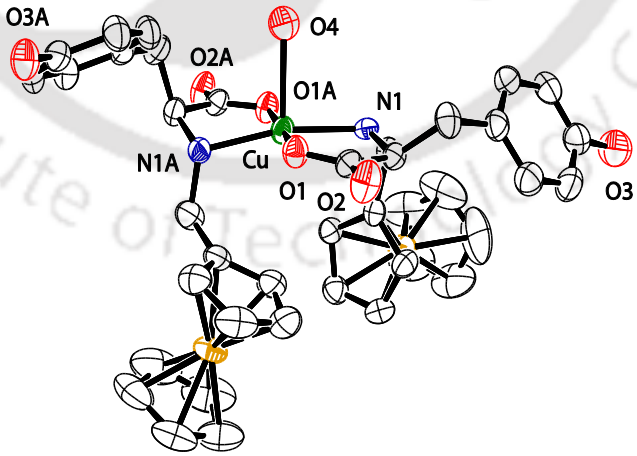

Figure 3.5 ORTEP diagram of **5** with 50 %.probability. Hydrogens are removed for clarity.

3.3.3 H-bonded networks

The latices of all the structures reported here and those reported earlier[1] with different amino acids have one thing common. The H-bonding ability of amino acid side chains and coordinated carboxylate groups form extensive H-bonded network, leaving relatively hydrophobic ferrocene units clustered together. This culminates in alternating hydrophobic and hydrophilic layered structure in all (Figure 3.6).

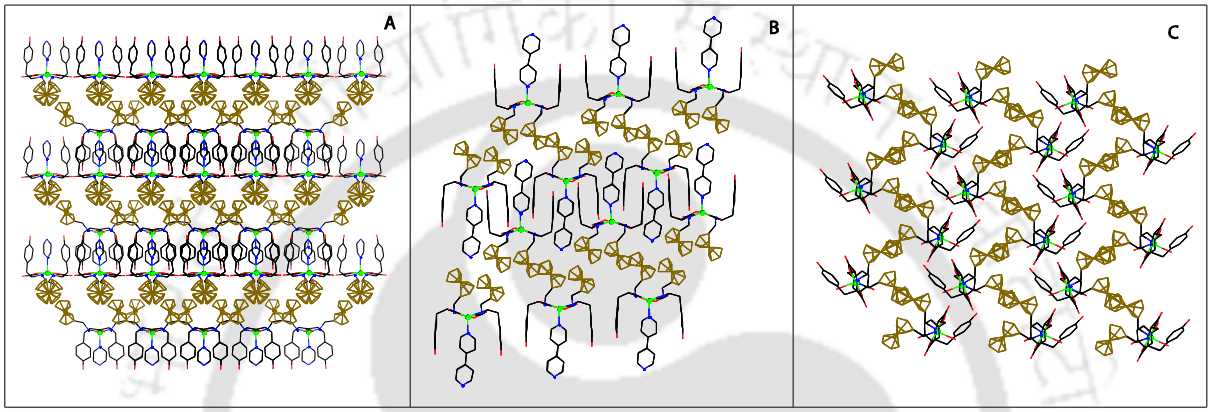

Figure 3.6 Alternative hydrophobic and hydrophilic layered structure of **2**(a), **4**(B) and **1**(C).

Usually crystallization of metal complexes with amino acid derivatives are highly dependent on external conditions such as solvent, moisture etc. and can be quite unpredictable.[9c, 10] The *bis*-Cu(II) complexes of ferrocenylmethyl amino acids on the other hand are well behaved due to the orientation of polar groups and non polar groups on different side of the molecular plane (Scheme 3.1).

3.4 UV-visible absorption and EPR spectroscopy

The electronic spectral characteristic of the complexes are almost identical to the analogu Cu(II) complexes reported with other amino acids (Figure 3.7).[1] The complexes show essentially three transitions in MeOH at 255, 425 and 560 nm. The transition at ~255 nm and 425 nm are of ligand and ferrocene origin respectively. The broad transition at ~560 nm is due to the *d-d* transitions of Cu(II). The axial coordination does not have any significant effect on any of these transitions. The solution EPR spectra (Figure 3.8) for the complexes are consistent with the square-pyramidal structure of the complexes and values (Table 3.3) are comparable to analogue

complexes with other amino acid complexes.[1,11] Axial coordination does not have any significant effect on the EPR parameters.

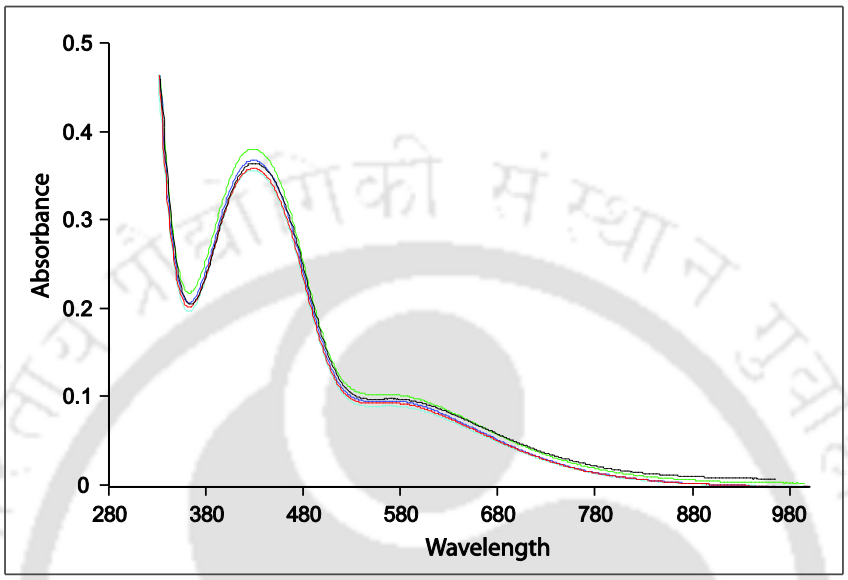

Figure 3.7 The UV-vis spectra of complexes **1-5** in MeOH.

Table 3.3 Solution UV-vis, EPR[b] and solid state magnetic moment[c] data of the complexes.

Complex	λ/nm (ε/cm^{-1}M^{-1})	EPR, g	A_{II}/G	μ_{eff}
1	256 (12,000), 425 (380), 565sh	2.230, 2.035	183	2.21
2	256(15,000) 425(350), 560sh	2.235, 2.040	181	2.16
3	255(13,000) 425(360), 565sh	2.235, 2.040	182	1.96
4	232(15,000), 280 sh, 336 sh, 420(365), 564sh	2.237, 2.040	182	2.08
5	257(13,000),423(350) 556 sh	2.236, 2.040	181	1.99

[a] In MeOH. [b] At 77K. [c] 298 K.

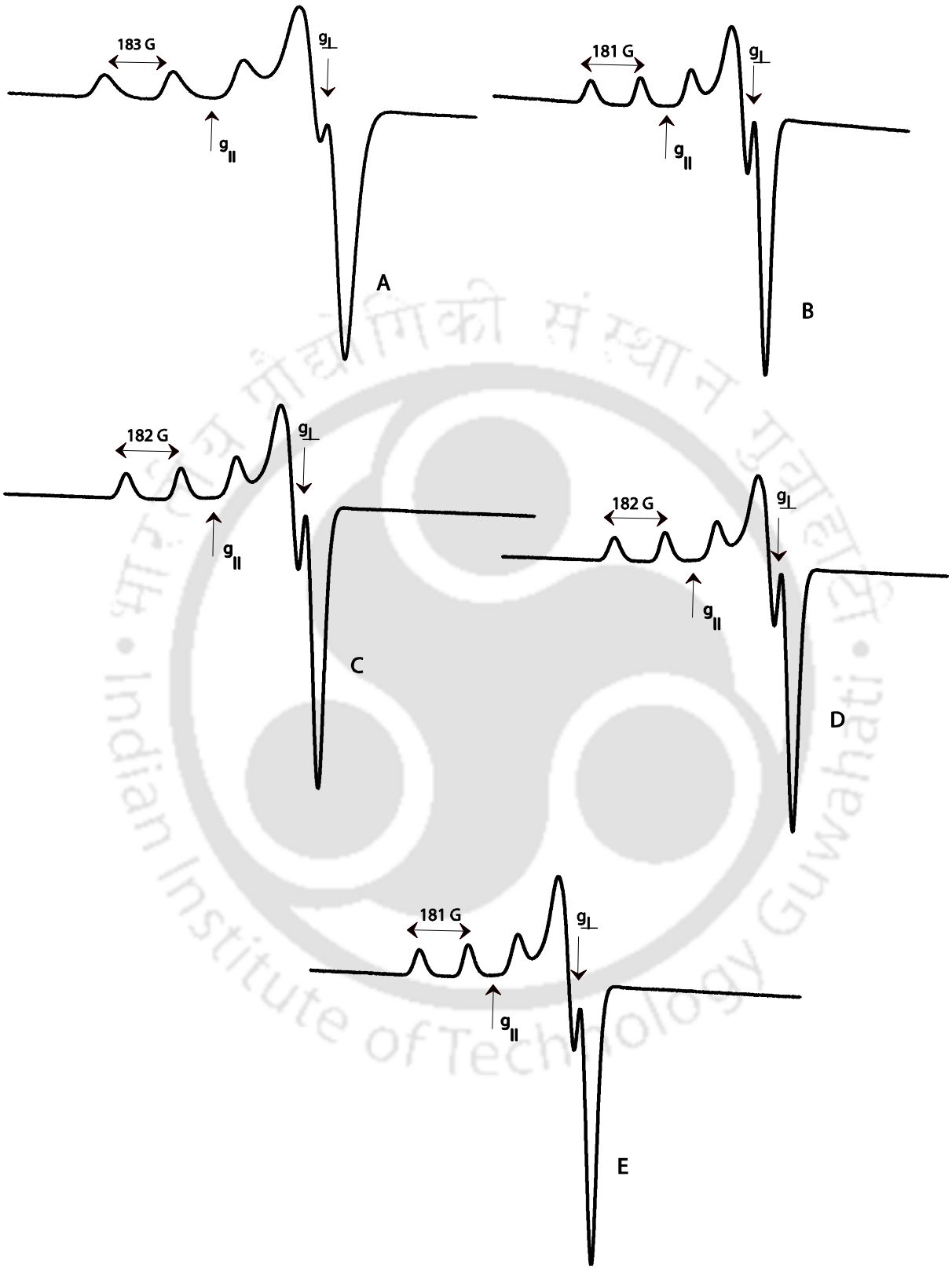

Figure 3.8 EPR spectra of the complexes **1-5** in MeOH at 77 K

3.5 Electrochemistry

Cyclic voltammetry of the complexes were performed in DMF as the complexes were not soluble in solvents with better accessible potential range. The cyclicvoltammograms of the complexes at 50 mVs^{-1} showed reversible oxidation of the ferrocene unit at ~40 mV *vs* Fc^{+}/Fc (Table 3.4, Figure 3.9) unaffected by the axial ligation or amino acid residue[1] at the copper(II) center. The complexes **1**-**5** show a irreversible reduction, presumably for the Cu(II)/Cu(I), with E_{pc} between 1.60-1.69 V *vs* Fc^{+}/Fc. Unlike the analogu complexes with other amino acid[1], the current set of complexes do not show adsorption on the electrode during Cu(I)/Cu(II) oxidation. Effect of axial coordination on the Cu(II)/Cu(I) couple is observable and the E_{pc} value shifted to more negative potential with shorter axial bond length. In fact in the case of **2**-**4** where the five coordinated complexes have axial N donor, the E_{pc} shift is linear with respect to axial bond length (Figure 3.9). This is significant because cyclic voltammetry can be used to monitor guest binding inside the cavity in solution.

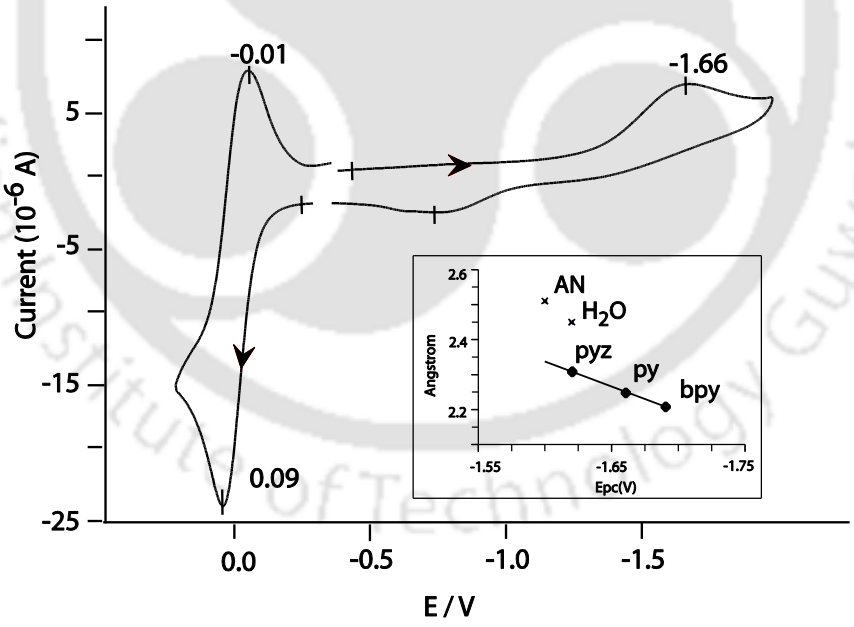

Figure 3.9 Cyclic Voltammogram of **3** in DMF; Condition: Scan rate, 50 mV S^{-1}; glassy carbon as working electrode; tetrabutylammonium perchlorate as supporting electrolyte. Potentials shown are *vs* Fc^{+}/Fc. Linear plot of potentials *vs* axial bond lengths is shown as insert.

Table 3.4 Electrochemical data of the complexes.

Complex	$E_{1/2}$/V (ΔE_p/mV)	E_{pc}[b] / V	E_{pa} / V
1	0.03 (125)	-1.60	-0.73
2	0.03(100)	-1.62	-0.73
3	0.04 (100)	-1.66	-0.65
4	0.04 (90)	-1.69	-0.72
5	0.04(90)	-1.62	-0.73

[b]Data in DMF at 50 mVs^{-1} rate. All potentials are *vs* Fc^+/Fc.

3.6 Conclusions

Thus we are able to form a narrow cavity around Cu(II). Subsequently, easily replaceable bound acetonitrile inside the cavity in **1** was substituted with three N-donor guests of various size and donor strengths. For monodentate planar N-donors as guests (**2**-**4**), the cavity enforces parallel alignment of aromatic guest with aromatic rings from the ligands (Figure 3.3). The cavity is resilient enough to accommodate non planar 4, 4′-bpy in **4**. The depth of the cavity prevents the pyrazine and 4,4′-bpy forming bridges. In fact there are only handful complexes where these two ligands do not form bridges. The cavity is however getting destroyed in the presence of water (**5**). Thus the stability of the cavity depends on the type of guest. While the cavity is stable in presence of aromatic or unsaturated small molecule (MeCN), polar water destroys the cavity by presumably repelling the hydrophobic aromatic ring of the tyrosine. Further, the Cu^{II}/Cu^{I} couple is found to be sensitive to the strength of the guest ligand.

References

1. Sahoo, S. C.; Ray, M. *Dalton Trans.* **2007**, *44*, 5148.

2. Nakamoto, K. *Infrared and Raman Spectra of Inorganic and Coordination Compounds*, Part B, John Wiley & Sons, New York.

3. (a) Earnshaw, A. *Introduction to Magnetochemistry*, Academic Press, London, 1968. (b) Figgis, B. N.; lewis, J. *Prog. Inorg. Chem.*, Ed. F. A. Cotton, **1964**, *6*, 37.

4. Addision, A. W.; Rao, T. N.; Reedijk, Jr., J.; Rijn, V.; Verschoor, G. C. *J. Chem. Soc., Dalton Trans.* **1984**, 1349.

5. Ye, L. J.; You, Z. *Acta crystallogr. Sect. E*, **2007**, *63*, M1837. (b) Lang, J.; Kawaguchi, H.; Tatsumi, K. *Chem. Commun.* **1999**, 2315. (c) Sangeetha, N. R.; Pal, S. *J. Chem. Crystallogr.* **1999**, *29*, 287.

6. (a) Jensen, P.; Batten, S. R.; Fallon, G. D.; Hockless, D. C. R.; Moubaraki, B.; Murray, K. S. Robson, R. *J. Solid State Chem.* **1999**, *145*, 387. (b) Chen, Y.; Zhao, X. J.; Gan X.; Fu, W. F. *Inorg. Chim. Acta.* **2008**, *361*, 2335. (c) Das, A.; Todorov, I.; Dey, S. K.; Mitra, S. *Inorg. Chim. Acta* **2008**, *359*, 2041. (d) Chesnut, D. J.; Kusnetzow, A.; Birge, R. R.; Zubieta, J. *Inorg. Chem.* **1999**, *38*, 2663. (e) Jimbo-Kobayashi, A.; Kobayashi, A.; Tamura, I.; Kawada, N.; Miyamoto, T. *Bull. Chem. Soc. Jpn.* **2005**, *78*, 445. (f) Persky, N. S.; Chow, J. M.; Poschmann, K. A.; Lacuesta, N. N.; Stoll, S. L.; Bott, S. G.; Obrey, S. *Inorg. Chem.* **2001**, *40*, 29.

7. (a) Liu, Q. X.; Zhao, X. J.; Wu, X. M.; Yin, L. N.; Guo, J. H.; Wang, X. G.; Feng, J. C. *Inorg. Chim. Acta* **2008**, *361*, 2616. (b) Chen, Y.; Zhao, X. J.; Gan, X.; Fu, W. F. *Inorg. Chim. Acta.* **2008**, *361*, 2335. (c) Zhang, J.; Wang, Y.; Huang, X.; Lin, Y.; Chen, X. *Chem. Eur. J.* **2005**, *11*, 552. (d) Mutasem, O. S.; Edward, V. F.; David, S. C. *J. Am. Chem. Soc.* **2002**, *124*, 10887. (e) Janiak, C. *J. Chem. Soc., Dalton Trans.* **2000**, 3885.

8. Smith, A. S.; Fraser, C. L. In *Comprehensive Cordination Chemistry II*, 1st Ed. A. B. P. Lever, vol. 1, p. 1

9. (a) Alam, Md. A.; Nethaji, M.; Ray, M. *Angew. Chem., Int. Ed.* **2003**, *42*, 1940. (b) Alam, Md. A.; Koner, R. R.; Das, A.; Nethaji, M.; Ray, M. *Cryst. Growth Des.* **2007**, *7*, 1818.

10.(a) Gangulya, R.; Sreenivasulua, B.; Vittal, J. J. *Coord. Chem. Rev.* **2008**, *252*, 1028. (b) Yang, X.; Ranford, J. D.; Vittal, J. J. *Cryst. Growth Des.* **2004**, *4*, 781. (c) Yang, C. T.; Vetrichelvan, M.; Yang, X.; Moubaraki, B.; Murray, K. S.; Vittal, J. J. *Dalton Trans.* **2004**, 113.

11. Sakaguchi, U.; Addison, A. W. *J. Chem. Soc., Dalton Trans.* **1979**, 600.

Chapter 4

In the previous two chapters, first we have explored the coordination chemistry of ferrocenylmethyl amino acid as a ligand towards Cu(II) using four different amino acids and followed by formation of a cavity with L-tyrosine derivative. Throughout, we have restricted our studies to L-amino acid only. In this chapter we intend to study the effect of chirality as well as the effect of co-ligand on the geometry and electronic properties of the complexes. If the chirality of the two ligands in the complexe is different then there are two possible isomers may form. Upon changing one of the ligand to a bidentate ligand, we might gain some insight of their property, as we will lose the cavity after changing the ligand ratio and recently one similar complex has been found useful in DNA cleavage[1], In this chapter we have synthesized the ferocenylmethyl derivative of L-leucine ligand as a new entry to compare the results with similar set of previous complexes and prepared different types of Cu(II) complexes using pure and recemic form of the ligand and finally explored their coordination properties.

4.1 Experimental Section

4.1.1 Solvents and Reagents

Solvents and reagents were obtained from commercial sources and used without further purification unless otherwise stated. Ferrocene carboxaldehyde and anhydrous grade *N*,*N*-dimethylformamide (DMF) for electrochemical experiments was purchased from Aldrich Chemical Co. $NaBH_4$, amino acids, Cu(acetate).H_2O and $Cu(NO_3)_2 \cdot 3H_2O$ were purchased from Merck limited and used as received. Methanol (MeOH) was distilled over magnesium methoxide [$Mg(OCH_3)_2$]. Ethanol (EtOH) was distilled over magnesium ethoxide [$Mg(OCH_2CH_3)_2$]. Diethyl ether (Et_2O) was dried first with anhydrous calcium chloride ($CaCl_2$) and then refluxed with metal sodium wire and finally distilled and kept over sodium wire.

4.1.2 Measurements

The IR and UV-vis spectra were recorded on a Perkin-Elmer Spectrum One FT-IR spectrophotometer with KBr discs in the range 4000-400 cm^{-1} and electronic spectra on a Perkin- Elmer Lambda 25 UV-vis spectrophotometer respectively. The ^1H NMR spectra were recorded using a Varian Mercury plus 400 MHz instrument. The thermogravimetric analysis (TGA) of the compounds was performed using a Mettler Toledo SDTA 851e TGA thermal analyzer with heating rate of 5 ^oC per min under a N_2 atmosphere using 5-10 mg sample per run.

Solid-state magnetic susceptibility of the complexes at room temperature was recorded using a Sherwood Scientific Magnetic balance MSB-1. Solution electrical conductivity measurements were made with a Eutech Instruments CON5/TDS 5 Conductivity Meter calibrated with 0.01 N KCl solutions as calibrant. Elemental analyses were performed using a Carlo Erba 1108 elemental analyzer. ESI-MS for the ligands were recorded using a Micromass Quattro II mass spectrometer. Optical rotations were measured using a Perkin- Elmer 343 polarimeter. X-Band EPR spectra were recorded with a Jeol JES-FA series spectrometer fitted with a quartz dewar for measurements at liquid nitrogen temperature. The spectra were calibrated with an internal manganese marker.

4.2 Synthesis of ligands

4.2.1 H(*S*-fLeu).

A methanolic solution of ferrocenealdehyde (1.63 g, 7.62 mmol) was added drop wise to a stirring solution of L-leucine (1.00 g, 7.62 mmol) and $LiOH{\cdot}H_2O$ (0.32 g, 7.62 mmol) in methanol (25 mL). The stirring was continued for 2 h, followed by addition of sodium borohydride (0.57 g, 15 mmol) with further stirring for 1 h. The solvent was evaporated and the resulting mixture was dissolved in water and acidified with dil. HCl. The pH of the solution was maintained between 5-7. The ligand was precipitated as yellow solid. It was thoroughly washed with water and MeOH after filtration and dried in vaccum desiccators over silica. Yield 1.63 g (65%). Anal. Calcd for $C_{17}H_{23}NO_2Fe$: C, 61.98; H, 7.04; N, 4.25. Found: C, 60.12; H, 7.19; N, 3.25. $[\alpha]_D^{25^\circ} = -26^\circ$ in MeOH, c = 0.2 in presence of 1 equivalent $LiOH{\cdot}H_2O$. *m/z* (ESI-MS, $[M\text{-}H^{-1}]$ 330. UV/Vis: λ_{max} [nm] (ε, $M^{-1}cm^{-1}$): in MeOH with 1equivalent of $LiOH{\cdot}H_2O$: 328(211), 435(167). IR (KBr, cm^{-1}), $\upsilon(COO)_{asym}$ 1610(s), $\upsilon(COO)_{sym}$ 1393(s). ^1H NMR (CD_3OD, ppm): $H^{cp.o}$ (3.97, d, 2H), $H^{cp.m}$ (3.78, d, 2H), H^{cp} (3.85, s, 5H), H^a (3.27, d, 1H, $J_{a,a'}$ = 12.4 Hz), $H^{a'}$ (3.07, d, 1H), H^b (2.83,m, 1H), H^c (1.2, m, 1H), $H^{c'}$ (1.08, m 1H), H^d (1.41, m, 1H), H^e (0.66, d, 3H), $H^{e'}$ (0.60, d, 3H). ^1H NMR spectrum was shown in Fig 4.1. Due to geminal coupling of H^c splitted into two non equivalent H^c and $H^{c'}$.

4.2.2 [H(*R*-fLeu)]

This was synthesized following the procedure outlined above for H(*S*-fLeu) using D-Leucine instead of L-Leucine. Yield (60%). Anal. Calcd for $C_{17}H_{23}NO_2Fe$: C, 61.98; H, 7.04; N, 4.25. Found: C, 60.12; H, 7.19; N, 3.25. $[\alpha]_D^{25^o} = +26^o$ in MeOH, c = 0.2 in presence of 1 equivalent $LiOH{\cdot}H_2O$. *m/z* (ESI-MS, $[M\text{-}H^{-1}]$ 330. UV/Vis: λ_{max} [nm] (ε, $M^{-1}cm^{-1}$): in MeOH with 1 equivalent of $LiOH{\cdot}H_2O$: 328(211), 435(167). IR (KBr, cm^{-1}), $\upsilon(COO)_{asym}$ 1610(s), $\upsilon(COO)_{sym}$ 1393(s). ^1H NMR (CD_3OD, ppm): $H^{cp.o}$ (4.12, d, 2H), $H^{cp.m}$ (3.96, d, 2H), H^{cp} (4.00, s, 5H), H^a (3.42, d, 1H, $J_{a,a'}$ = 12.4 Hz), $H^{a'}$ (3.21, d, 1H), H^b (2.99,m, 1H), H^c (1.34, m, 1H), $H^{c'}$(1.23, m 1H), H^d (1.58, m, 1H), H^e (0.81, d, 3H), $H^{e'}$ (0.75, d, 3H). Due to geminal coupling of H^c splitted into two non equivalent H^c and $H^{c'}$.

4.2.3 H(*rac*-fLeu). This was prepared by equimolar mixture of H(*R*-fLeu) and H(*S*-fLeu) synthesized above. Optical rotation was checked to ensure equimolar mixture.

4.2.4 [H(*rac*-fMeth)]

A methanolic solution of ferrocenealdehyde (1.43 g, 6.7 mmol) was added dropwise to a stirring solution of *dl*-methionine (1.00 g, 6.7 mmol) and $LiOH{\cdot}H_2O$ (0.28 g, 6.69 mmol) in methanol (25 mL). The stirring was continued for 2 h, followed by addition of sodium borohydride (0.50 g, 13 mmol) with further stirring of 1 h. The solvent was evaporated and the resulting sticky mass was dissolved in water and acidified with dil. CH_3COOH. The pH of the solution was maintained between 5-7. The ligand was precipitated as yellow solid. It was thoroughly washed with water and MeOH after filtration and dried in vaccum desiccator. Yield 1.74 g (75%). Anal. Calcd for $C_{16}H_{21}NO_2SFe$: C, 55.03; H, 6.09; N, 4.03. Found: C, 54.85; H, 6.16; N, 4.15. $[\alpha]_D^{25^o} = 0.0^o$ in MeOH, c = 0.2 in presence of 1 equivalent $LiOH{\cdot}H_2O$. *m/z* (ESI-MS, $[M–H]^{-1}$) 346. UV/Vis: λ_{max} [nm] (ε, $M^{-1}cm^{-1}$): in MeOH with 1equivalent of $LiOH{\cdot}H_2O$: 330(95), 440(133). IR (KBr, cm^{-1}), $\upsilon(COO)_{asym}$ 1582(s), $\upsilon(COO)_{sym}$ 1368(s). ^1H NMR (CD_3OD, ppm): $H^{cp.o}$ (4.10, s, 1H), $H^{cp.o}$ (4.05, s, 1H), H^{cp} (3.96, s, 5H), $H^{cp.m}$ (3.92, s, 2H), H^a (3.37, d, 1H, $J_{a,a'}$ = 12.8 Hz), $H^{a'}$ (3.18, d, 1H), H^b (2.97,t, 1H), H^c (1.67, m, 2H), H^d (2.35, t, 2H), H^e (2.02, s, 3H). Due to geminal coupling H^c splitted into two non equivalent H^c and $H^{c'}$.

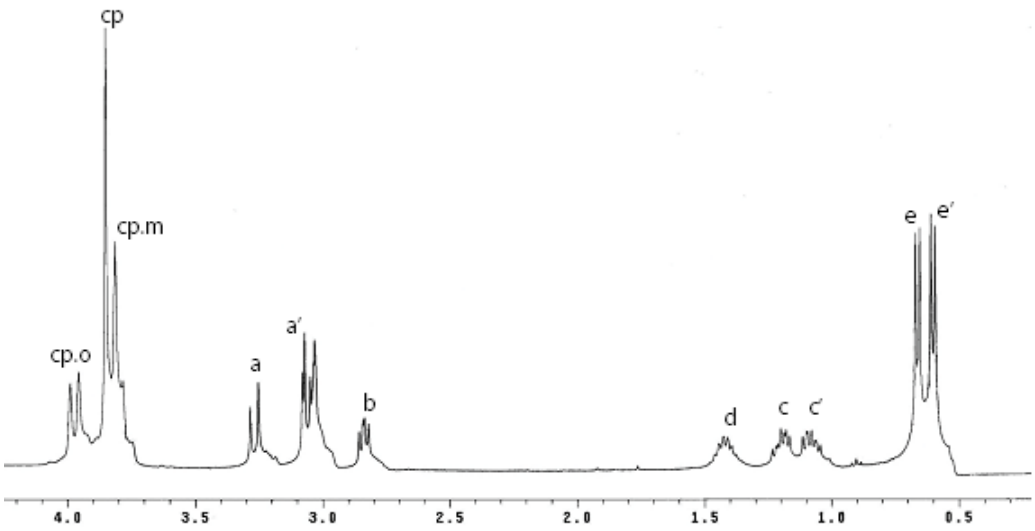

Figure 4.1 ^{1}H NMR specta of the ligand (S-fLeu) with labeling scheme.

4.3 Syntheses of Complexes

Detailed synthetic methodologies are given below.

4.3.1 [Cu(*S*-fLeu)$_2$(H$_2$O)] (1)

The ligand H(*S*-fLeu) (0.500 g, 1.51 mmol) and Cu(acetate)$_2$.H$_2$O (0.15 g, 0.75 mmol) in 25 mL MeOH were stirred for 2 h. The solvent was evaporated to 10 ml and kept undisturbed for slow evaporation. After 4-5 days green rod shape crystals of **1** were formed. Crystals were washed with diethyl ether and dried under vaccuo. Yield 0.32 g (63%). Anal. Calcd for Cu ($C_{34}H_{45}Fe_2N_2O_7$): C, 51.89; H, 6.02; N, 3.50. Found: C, 51.69; H, 6.22; N, 2.97. UV/Vis: λ_{max} [nm] (ε, $M^{-1}cm^{-1}$), in MeOH, 267(sh), 433(353), 608(sh). IR (KBr, cm^{-1}) $\upsilon(COO)_{asym}$ 1630(s). $\upsilon(COO)_{sym}$ 1369(s), μ_{eff} (solid, 298 K): 1.9 μ_B.

4.3.2 [Cu(*R*-fLeu)$_2$(H$_2$O)] (1a)

The ligand H(*R*-fLeu) (0.500 g, 1.51 mmol) and Cu(acetate)$_2$.H$_2$O (0.15 g, 0.75 mmol) in 25 mL MeOH were stirred for 2 h. The solvent was evaporated to 10 ml and kept undisturbed for slow evaporation. After a week green rod shape crystals of **1a** were formed. Crystals were washed with diethyl ether and dried under vaccuo over silica. Yield 0.32g (63%). Anal. Calcd for Cu ($C_{34}H_{45}Fe_2N_2O_7$): C, 51.89; H, 6.02; N, 3.50. Found: C, 51.62; H, 6.20; N, 3.47. UV/Vis: λ_{max}

[nm] (ε, $M^{-1}cm^{-1}$), in MeOH, 269(sh), 433(353), 610(sh). IR (KBr, cm^{-1}) $\upsilon(COO)_{asym}$ 1633(s). $\upsilon(COO)_{sym}$ 1380(m), μ_{eff} (solid, 298 K): 1.9 μ_B.

4.3.3 [Cu(*rac*-fLeu)$_2$(H_2O)] (2).

$Cu(acetate)_2$. H_2O (0.15 g, 0.75 mmol) in methanol was mixed to the solution mixture of H(S-fLeu) (0.25 g, 0.75 mmol), H(R-fLeu)(0.25 g, 0.75 mmol), and $LiOH.H_2O$ (0.06 g, 1.5 mmol) in 10 ml MeOH and stirred for 30 min. Immediately a yellow-brown precipitate was formed. The mixture was filtered after stirring for 2 h, washed with cold MeOH and dried in vaccuo. Yield 0.54 g (60%). Anal. Calcd for $Cu(C_{34}H_{45}FeN_2O_7)(H_2O)$: C, 51.89; H, 6.02; N, 3.50. Found: C, 51.58; H, 5.85; N, 3.47. UV/Vis: λ_{max} [nm] (ε, $M^{-1}cm^{-1}$): in DMF, 267(sh), 425(sh), 600(sh). IR (KBr, cm^{-1}) $\upsilon(COO)_{asym}$ 1639(s), $\upsilon(COO)_{sym}$ 1369(s). μ_{eff} (solid, 298 K): 1.8 μ_B.

4.3.4 [Cu(*S*-fLeu)(bpy)(NO_3)] (3)

$Cu(NO_3)_2.3H_2O$ (0.36 g, 1.5 mmol) and 2,2'-bipyridine (0.23 g, 1.5mmol) were mixed in 20 ml MeOH and stirred for 30 min. The solution became deep blue. To that, solution of ligand H(*S*-fLeu) (0.500 g, 1.51 mmol) and $LiOH.H_2O$ (0.06 g, 1.5mmol) in 10 mL MeOH was added and stirred for 2h. The mixture was filtered and kept for undisturbed for slow evaporation. Dark green rod shaped crystals were appeared after one week. Crystals were washed with diethyl ether and dried in vaccuo. Yield 0.54 g (60%). Anal. Calcd for $Cu(C_{27}H_{30}FeN_4O_5)(H_2O)$: C, 51.66; H, 5.14; N, 8.93. Found: C, 50.03; H, 5.15; N, 9.40. UV/Vis: λ_{max} [nm] (ε, $M^{-1}cm^{-1}$): in MeOH, 427(353), 605(sh). IR (KBr, cm^{-1}) $\upsilon(COO)_{asym}$ 1637(s), $\upsilon(COO)_{sym}$ 1369(s), $\upsilon(NO_3)_{sym}$ 1384(s). μ_{eff} (solid, 298 K): 1.5 μ_B.

4.3.5 [Cu(*S*-fLeu)(phen)(NO_3)] (4)

$Cu(NO_3)_2.3H_2O$ (0.36 g, 1.5 mmol) and 1,10-phenanthroline (0.3 g, 1.5mmol) were mixed in 20ml MeOH and stirred for 30 min. The solution became deep blue. To that solution of ligand H(*S*-fLeu) (0.500 g, 1.51 mmol) and $LiOH.H_2O$ (0.06 g, 1.5mmol) in 10 mL MeOH was added and stirred for 2h. The mixture was filtered and kept for undisturbed for slow evaporation. Dark green rod shaped crystals were appeared after one week. Crystals were washed with ether

and dried in vaccuo. Crystal suitable for X-ray data collection was grown by slow diffusing diethyl ether into DMF solution. Yield 0.54 g (60%). Anal. Calcd. for $Cu(C_{27}H_{30}FeN_4O_5)(H_2O)$: C, 51.66; H, 5.14; N, 8.93. Found: C, 50.03; H, 5.15; N, 9.40. UV/Vis: λ_{max} [nm] (ε, $M^{-1}cm^{-1}$): in MeOH, 267(sh), 441(453), 610(sh). IR (KBr, cm^{-1}) $\upsilon(COO)_{asym}$ 1628(s), $\upsilon(COO)_{sym}$ 1379(s), $\upsilon(NO_3)_{sym}$ 1384(s). μ_{eff} (solid, 298 K): 1.7 μ_B.

4.3.6 [Cu(*rac*-fMeth)$_2$(H_2O)] (5).

The ligand H(*rac*-fMeth) (0.500 g, 1.43 mmol) and $Cu(acetate)_2.H_2O$ (0.14 g, 0.71 mmol) in 100 mL MeOH were mixed slowly without stirring. The mixture was kept undisturbed for slow evaporation. Within a day complex precipitated as light brown-green microcrystaline solid, was filtered and dried in vaccuo. The complex was not soluble in any common organic solvents once it was crystalizing from mother solution. Yield 0.37 g (70%). Anal. Calcd for Cu $(C_{32}H_{40}Fe_2N_2O_4S)(H_2O)$: C, 58.54; H, 5.60; N, 3.54. Found: C, 49.24; H, 6.01; N, 2.18. IR (KBr, cm^{-1}) $\upsilon(COO)_{asym}$ 1633(s), $\upsilon(COO)_{sym}$ 1374(s), μ_{eff} (solid, 298 K): 2.13 μ_B.

X-ray Crystallography: Single crystal of **1, 1a** and **3** were grown by air evaporation from methanol solution and **4** by diffusing diethyl ether into a DMF solution. Single crystals of **2** were grown by slow evaporation of a DMF-methanol solution of the corresponding complexes in open air over several days. The crystals were mounted on glass fibers. All geometric and intensity data for the crystals were collected at room temperature using a Bruker SMART APEX. CCD diffractometer equipped with a fine focus 1.75 kW sealed tube Mo-Kα (λ = 0.71073 Å) X-ray source, with increasing ω (width of 0.3° per frame) at a scan speed of 10 s per frame. SMART software was used for the data acquisition and SAINT software for data extraction. Absorption corrections were not performed. The structures were solved and refined using SHELX-97.[7] All nonhydrogen atoms were refined anisotropically. The hydrogen atoms wherever possible were located from the difference Fourier maps and were refined isotropically. Crystal structure of **2** couldn't solve completely due to poor quality crystal. A partially solved structure was discussed in the proceeding section.

Table 4.1 Selected crystallographic data for the complexes[a]

Complexes	**1**	**2**	**3**	**4**
Empirical formula	$C_{34}H_{48}CuFe_2N_2O_7$	$C_{35}H_{44}CuFe_2N_2O_6$	$C_{27}H_{30}CuFeN_4O_5$	$C_{62}H_{70}Cu_2Fe_2N_8O_{11}$
Formula weight (fw)	784.00	763.968	609.94	1342.06
Wavelength (Å)	0.71073	0.71073	0.71073	0.71073
Crystal system	Orthorhombic	Triclinic	Monoclinic	Monoclinic
Space group	$P2_12_12_1$	P_1	$P2_1$	$P2_1$
a, Å	8.481(2)	5.9633(16)	11.5745(7)	14.1714(9)
b, Å	15.044(4)	11.666(3)	13.0477(8)	10.4385(6)
c, Å	30.906(8)	14.801(4)	18.7712(10)	21.5509(13)
α, deg	90.00	86.187(4)	90.00	90
β, deg	90.00	82.181(19)	102.935(3)	108.345(4)
γ, deg	90.00	75.193(17)	90.00	90
Volume, $Å^3$	3943.3(18)	985.79(4)	2762.9(3)	3026.0(3)
Z	4	1	4	2
ρ, Mg/m^3	1.321	1.212	1.466	1.473
μ, mm^{-1}	1.304	1.298	1.338	1.230
Reflections collected	26147	5534	36786	18798
Reflections indep	9503	2857	12975	5671
Flack parameter	-0.02(3)	0.40(15)	0.01(3)	0.05(2)
F(000)	1636	353	1260	1392
GOF	1.031	1.509	1.029	1.013
R(int)	0.0875	0.0775	0.0422	0.0266
Final R indices [*I*>2sigma(*I*)]	R_1= 0.0715, WR_2= 0.1564	R_1= 0.1419 WR_2= 0.3875	R_1=0.0467, WR_2=0.1006	R_1=0.0493 WR_2=0.1067
R indices (all data)	R_1= 0.1398, WR_2= 0.1943	R_1= 0.1922, WR_2= 0.4305	R_1=0.0921, WR_2=0.1176	R_1=0.0727, WR_2=0.1190

Table 4.2 Selected bond distances and angles of complex **1** and **3**.

Complex **1**		Complex **3a**		Complex **3b**	
Cu1-O1	1.927(5)	Cu1-O1	1.950(3)	Cu2-O6	1.934(3)
Cu1-O3	1.948(5)	Cu1-N1	2.008(4)	Cu2-O8	2.345(5)
Cu1-N1	2.016(5)	Cu1-N2	1.982(4)	Cu2-N5	2.051(3)
Cu1-N2	2.024(5)	Cu1-N3	2.009(4)	Cu2-N6	2.010(4)
Cu1-O5	2.279(4)	Cu1-O3	2.619(8)	Cu2-N7	1.996(4)
O1-Cu1-O3	176.09(18)	Cu1-O4	2.610(1)	O6-Cu2-N7	174.56(17)
O1-Cu1-N1	92.1(2)	O1-Cu1-N1	81.64(14)	O6-Cu2-N6	94.52(15)
O3-Cu1-N1	84.38(19)	O1-Cu1-N2	174.36(17)	O6-Cu2-O8	99.08(18)
O1-Cu1-N2	84.2(2)	N2-Cu1-N1	99.57(16)	N7-Cu2-N6	81.17(17)
O3-Cu1-N2	99.7(2)	O1-Cu1-N3	95.12(16)	O6-Cu2-N5	82.15(13)
N1-Cu1-N2	156.41(19)	N2-Cu1-N3	81.35(18)	N6-Cu2-O8	115.77(17)
O1-Cu1-O5	86.35(19)	N1-Cu1-N3	153.72(16)	N7-Cu2-N5	99.69(16)
O3-Cu1-O5	92.85(18)	O1-Cu1-O3	87.75(2)	N6-Cu2-N5	147.51(15)

Table 4.3 Selected bond distances and angles of complex **4.**

Complex **4a**		Complex **4b**	
Cu1-O1	1.893(6)	Cu2-O6	1.915(6)
Cu1-N2	2.006(7)	Cu2-O8	2.418(8)
Cu1-N3	2.019(8)	Cu2-N7	1.995(8)
Cu1-N1	2.025(8)	Cu2-N5	2.005(7)
Cu1-O3	2.368(8)	Cu2-N6	2.050(8)
O1-Cu1-N2	172.4(3)	N7-Cu2-N5	174.56(3)
O1-Cu1-N3	91.1(3)	O6-Cu2-N6	170.9(3)
O1-Cu1-O3	94.6(3)	N5-Cu2-O8	89.7(3)
N2-Cu1-O3	87.9(3)	N6- Cu2- O8	81.9(3)
N2-Cu1-N3	81.7(4)	N5-Cu2-N6	102.5(3)
O1-Cu1-N1	83.0(3)	O6-Cu2-N7	99.09(3)
N3-Cu1-O3	90.4(3)	O6-Cu2-N5	84.80(3)
N1-Cu1-O3	101.8(3)	O6-Cu2-O8	103.8(3)
N2-Cu1-N1	103.5(3)	N7-Cu2-O8	94.8(3)
N3-Cu1-N1	166.8(3)	N7-Cu2-N6	81.4(3)

4.4 Result and discussion

4.4.1 Synthesis and selected properties

All the Cu(II) complexes were synthesized directly by reacting Cu(II), ligands, and base (LiOH or acetate anion). (Scheme 4.1) and characterized using FTIR, elemental analysis and room temperature magnetic moments (experimental section). The IR spectra of the ligand and the complexes show strong and sharp asymmetric carboxylate stretches between 1580-1630 cm^{-1} symmetric stretches ~1377 cm^{-1}.[6] The complexes **1, 1a, 2 and 5** are non conducting while **3** and **4** behave as 1:1 electrolyte supporting the formulation of the complexes. The room temperature solid state magnetic moments lies between 1.94-2.13 B.M. are within expected range for monomeric Cu(II) complex (experimental section).[10] The elemental analyses support the formulation of the complexes. However, because of tendency to lose lattice solvent and tendency of acquiring moisture, amount of solvent in the structure and the bulk differs.

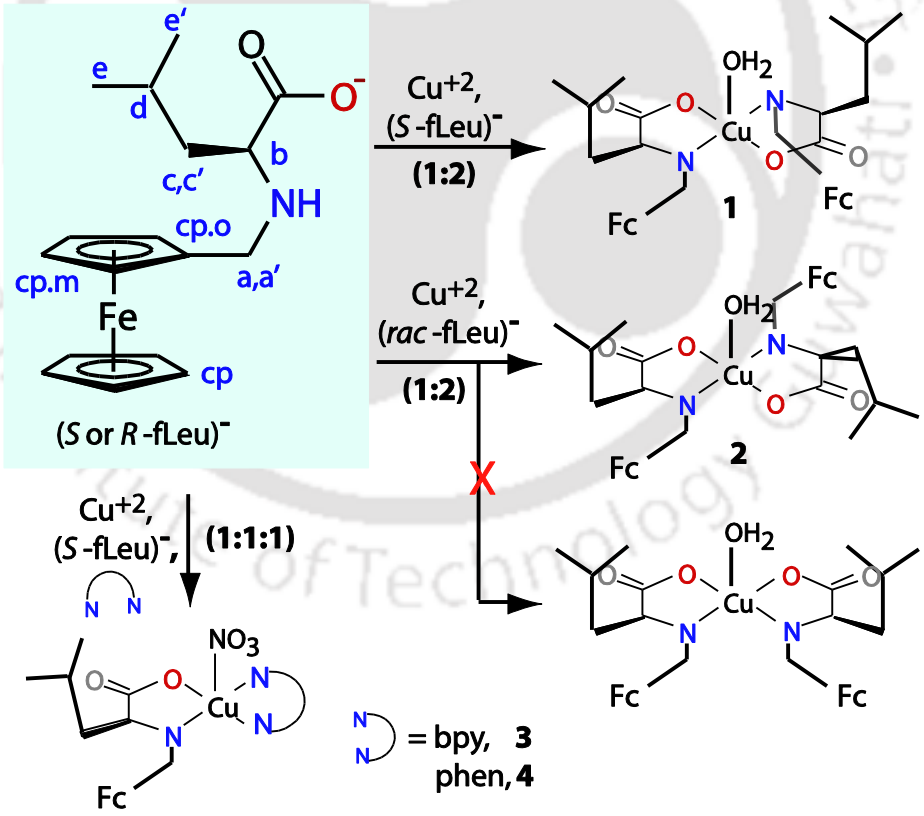

Scheme 4.1. The ligand (*S*-fLeu) with ^{1}H NMR labeling and synthesis of complexes.

4.4.2 Crystal structures. Structures of four complexes, [Cu(*S*-fLeu)$_2$(H$_2$O)](**1**), [Cu(*rac*-fLeu)$_2$(H$_2$O)](**2**), [Cu(*S*-fLeu)(bipyridine)(NO$_3$)](**3**) and [Cu(*S*-fLeu)(phen)(NO$_3$)](**4**) were solved. *Bis* complexes with racemic ligands tend to form thin needles. After several attempts we were able to solve **2** but due to poor quality of data we will discuss only about the geometry but not bond parameters. Crystallographic parameters and bond parameters of the crystals are in Table 4.1, 4.2 and 4.3 respectively. Figure 4.2 shows the ORTEP diagrams of the molecules.

4.4.2.1 Structures of the *bis*-complexes

Complex **1** was crystallized in the space group $P2_12_12_1$ and the asymmetric unit contained one molecule of [Cu(*S*-fLue)$_2$(H$_2$O)]. Bivalent copper is penta coordinated by N$_2$O$_3$ chromophore with a distorted square-pyramidal geometry, as inferred from the τ value of 0.33. The N$_2$O$_2$ unit forms the basal plane from the ligand side with O5 from a water molecule, occupying the axial position. The perspective view of **1** is shown in Fig.4.2. The in-plane Cu-O$_{carboxylate}$ bond lengths of 1.93, 1.94 Å are within the range observed for previous set of complexes.[2,3] The axial Cu-O bond length (2.283Å) is comparably shorter than previous set of complexes but close to L-threonine analogue (Chapter 2). Isopropyl groups of the leucine ligand rotated away from the water molecule without formation of a cavity.

Reaction between racemic ligand and Cu(II) produced **2** as fine needles unsuitable for single crystal X-ray analysis. Similar reaction with racemic methionine produced **5**. Both **2** and **5** are soluble only in DMF unlike other homochiral analogues reported in this thesis. Crystals of **2** suitable for data collection were grown by slow evaporation of DMF/Methanol over several days. Diffraction quality was poor and data could not be solved with a reasonable R value. The partially solved structure of **2** is in Figure 4.2. The two ligands are of opposite chirality. The SEM pictures and EDX analysis (Figure 4.3 and 4.4) of both **2** and **5** isolated from methanol shows similar needle formation. Their dramatically different solubility (soluble in DMF) compared to homochiral analogues (soluble in methanol) suggests, formation of racemic complexes instead of self resolved chiral crystals. Layer structure (Figure 4.5) again retained in the lattice of both the complexes, even after changing the ligand chirality. In complex **2** there is a solvent accessible void was observed. (Figure 4.5)

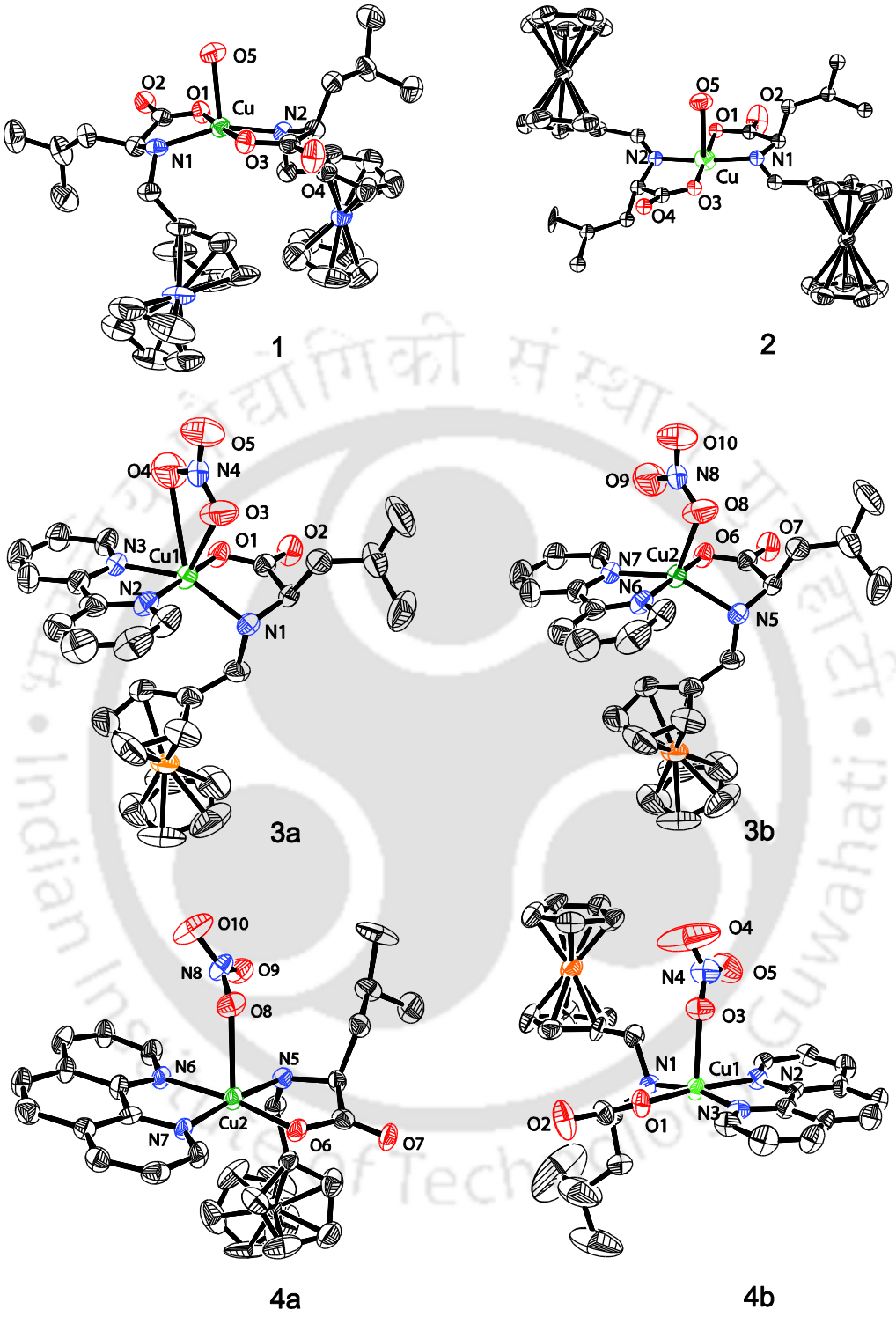

Figure 4.2 ORTEP diagram of complexes of **1, 2, 3** and **4** (probability set to 50 %). Solvents and hydrogens are omitted for clarity.

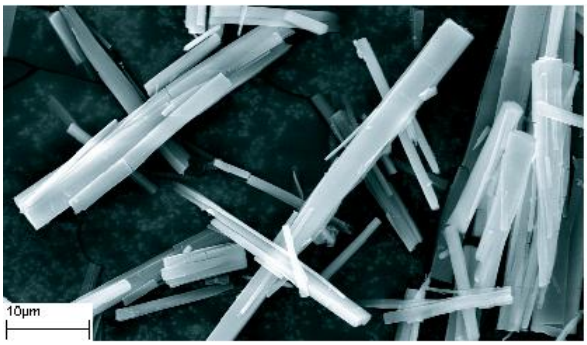

EDX data for Cu(*rac*-fMeth)2		
Element	Weight %	Atomic %
C	55.37	77.57
O	9.59	10.09
S	9.53	5.00
Fe	16.17	4.87
Cu	9.35	2.47
Total	100.00	

Figure 4.3 SEM pictures of complex **5.**

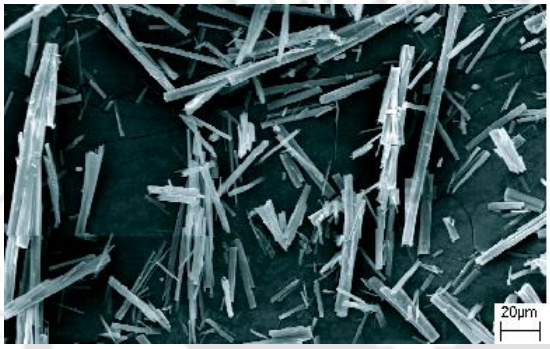

EDX data for Cu(*rac*-fLeu)2		
Element	Weight %	Atomic %
C	55.62	80.85
O	7.45	8.13
Fe	23.05	7.20
Cu	13.88	3.82
Total	100.00	

Figure 4.4 SEM pictures of complexes 2.

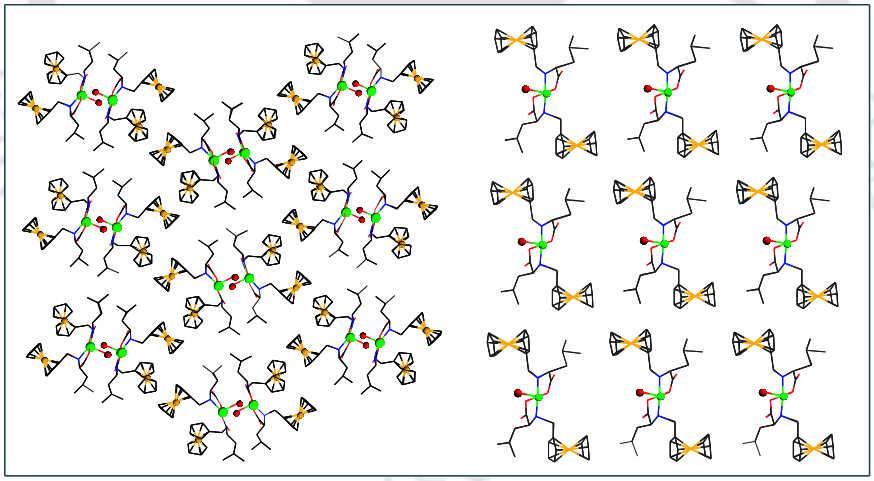

Figure 4.5 Lattice diagrams of complexes **1** and **2.**

Comparing these data with that of previous chapters, we can conclude that (a) homochirality is a requirement for cavity formation, (b) polar water molecule in the axial position tends to destroy the cavity and (c) tyrosine derivative provide the best cavity due to its flatness.

4.4.2.2 Structures of crystal 3 and 4

Complex **3** crystallized in the space group *P2₁* and the asymmetric unit contains two molecules with formula [Cu(*S*-fLeu)(bpy)(NO_3)]. The Cu(II) is pentacoordinated in one unit by monodentate NO_3^- while in other it is hexa coordinated by bidentate NO_3^-. The presence of NO_3^- was confirmed by the peak at 1384 cm^{-1}. Due to different mode of binding of the NO_3^- ion, τ value differes at 0.34 and 0.44 respectively. The perspective view of **3** is shown in Figure 4.2. Both units are facing to each other in their less crowded side keeping the bulky ferrocene unit apart. Layering of hydrophobic and hydrophilic part occurs even after changing the environment from pure ligand to mix-ligand system. Due to introduction of bpy ligand, the number of possible H-bonding decreased between the molecules except the type $O_{carboxylate}\cdots H\text{-}N_{amine,}$ which provides a chain like arrangement in direction of *a*-axis (Figure 4.6).

Complex **4** crystallized in the space group *P2₁* and the asymmetric unit contained two molecules of [Cu(*S*-fLeu)(phen)(NO_3)]. The presence of NO_3^- was confirmed by the peak at 1384 cm^{-1}.Molecular structure is similar to **3b** (Figure 4.2). What is notable between **4a** and **4b** molecules is that the relative position of the isopropyl group with respect to ferrocene unit is reversed. Molar conductance values in methanol support 1:1 electrolyte[6] behavior in solution which indicates that nitrates are not bound to Cu(II) in solution. From structure **4** & **5** it is found that both the molecules of the asymmetric unit of **5** are close w. r. t to mode of NO_3^- ion binding but it is different for **4**. Similarly both the molecules of the asymmetric unit of **4** are close w. r. t molecular arrangement but it is reverse for **5**.

4.4.3 Electrochemical behavior of the complexes.

The electrochemical behavior of the complexes was studied in DMF as before. The data presented in Table 4.4. Complexes **1** and **1a** behave similar to those reported in earlier chapters. Measurements were not performed on **2** due to its poor solubility. Comparing electrochemical data with earlier complexes, it is found that there is very little effect of amino acid arm on the ferrocene redox potential. The main difference between *bis* complexes of same ligand and mixed ligand complexes, where the large positive shift in Cu(II)/Cu(I) potential (E_{pc}) in mixed ligand complexes (Figure 4.7). Presence of bidentate pyridine type of ligand supplied two intermediately soft N donor, which is expected to stabilize Cu(I) state. Further, total charge of the molecule is now positive. This should also make reduction easier. Thus substitution of one amino acid derivative with a neutral bidentate N donor stabilizes the Cu(I) state over Cu(II).

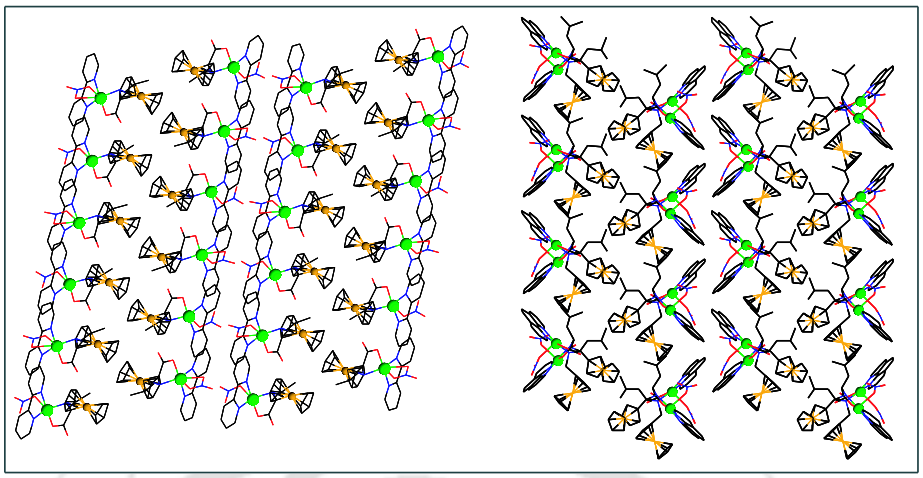

Figure 4.6 Lattice diagrams of complexes **3** and **4**.

Table 4.4 Electrochemical data for the complexes.

	Fc^+/Fc[a]	Cu(II)/Cu(I)[b]		
	$E_{1/2}$ /V			
$[Cu(L)_2(H_2O)]$, L =	(ΔE_p/mV)	E_{pc}/V	E_{pa}/V	
L-leu, **1**	0.06 (85)	-1.70	-0.65	This chapter
L-tyr	0.04 (90)	-1.62	-0.72	Chapter 3
L-ser	0.04 (88)	-1.58	a	Chapter 2
L-thr	0.04 (88)	-1.63	a	Chapter 2
$[Cu(L)(L')]NO_3$, L'=				
Bipyridine, **3**	0.05 (100)	-0.81	-0.37	This chapter
Phenanthroline, **4**	0.06 (90)	-0.75	-0.39	This chapter

[a] Data in DMF at 50 mV s^{-1} san rate. All potentials are vs Fc^+/Fc. Other conditions are given in the experimental section. [b] Reduction of Cu(II). [c] At 298 K.

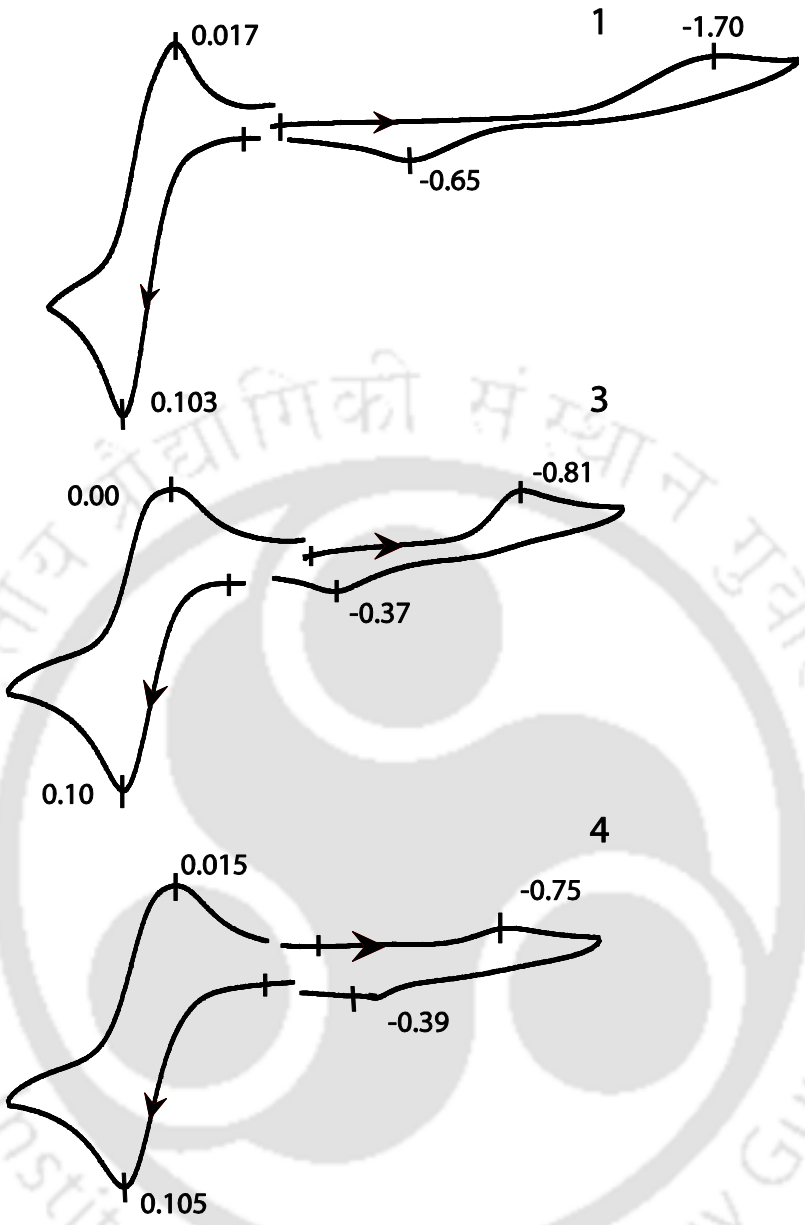

Figure 4.7 Cyclic voltametry diagrams of the Cu(II) complexes.

4.4.5 Conclusion

Combining the results presented in the present and the previous two chapters we found that (a) ferrocenylmethyl amino acids (methionine, serine, threonine, asparagines, tyrosine and leucine) forms bis complexes with Cu(II) in the same way (axially C_2 symmetric), provided the amino acid is chirally pure, (b) if the ligand is racemic it forms a racemic complex and the C_2 symmetry is lost (Figure 4.2), (c) axial C_2 symmetric arrangement in the case of enantiomerically pure

ligand could be used to form cavity with one binding site in the case of tyrosine derivative, (d) cavity formed gets destroyed if water is bound when there is no other axial ligand present, and (e) electrochemical data indicated that bidentate neutral co-ligand with N donor stabilizes Cu(I) better than ferrocenyl derivative of amino acid. This last point might be one of the reason why this type of complex was used in the DNA cleavage as Cu(II)/Cu(I) transformation is one of the requirement for cleavage. Finally, as a chiral receptor these sets of molecule suffer two disadvantages: (i) only one binding site for the guest excludes option for three point recognition, (ii) narrow nature of the cavity limits on choosing suitable chiral guests for the cavity. In the next chapters we will explore a different type of cavity.

References:

1. Goswami, T. K.; Roy, M.; Nethaji M.; Chakravarty A. R.; *Organometallics*, **2009**, *28*, 1992.

2. Sahoo, S. C.; Ray, M. *Dalton Trans.* **2007**, 5148.

3. Sahoo, S. C.; Ray, M. *Dalton Trans.* **2009**, 3230.

4. (*a*) McAuliffe, C. A.; Quagliano, J. V.; Vallarino, L. M. *Inorg. Chem.***1966**, *5*, 1996. (b) Helm, D. V. D.; Franks, W. A. *Acta. Crystallogr.,Sect. B*, **1969**, *25*, 451. (c) Stephens, F. S.; Vagg, R. S.; Willams, P. A. *Acta. Crystallogr., Sect. B*, **1975**, **31**, 841. (d) Ou, C.-C.; Powers, D. A.; Thich, J. A.; Felthouse,T. R.; Hendrickson, D. N.; Potenza, J. A.; Schugar, H. J. *Inorg. Chem.* **1978**, *17*, 34. (e) Hitchman, M. A.; Kwan, L. *J. Chem. Soc., Dalton Trans.* **1987**, 457. (f) Rizzi, A. C.; Piro, O. E.; Castellano, E. E.; Nascimento, O. R.; Brondino, C. D. *Inorg. Chim. Acta*, **2000**, *305*, 19.

5. (a) Yokoi, H.; Sai, M.; Isobe, T.; Ohsawa, S. *Bull. Chem. Soc. Jpn.* **1972**, *45*, 2189. (b) Stanila, A.; Marcu, A.; Rusu, D.; David, L. *J. Mol. Struct.* **2007**, *364***,** 834.

6. Geary, W. J. *J. Coord. Chem. Rev.* **1971**, *7*, 81.

Chapter 5

The results presented in the earlier chapters showed that the cavity with ferrocenylmethyl amino acid derivatives with Cu(II) form either narrow cavity or no cavity at all. The narrowness of the cavity formed with tyrosine derivative limits the choice of guest molecules and we were unable to find a chiral guest suitable to fit in the cavity. Because of this we looked at complexes of salicylaldehyde derivative of L-histidine reported earlier from our group.[1] The reported complex $[Fe^{III}_2(OH)(L^{L\text{-}his})_2(CH_3COO)]$ had a cavity around bridging acetate group on one side and two carboxylate and hydroxide aligned on the other side. The carboxylates were suitably positioned to form H-bond with a guest but did not have enough space inside the cavity so that guest can suitably stay with less constrain. We had synthesized a similar binuclear complexes with Ni(II)[2]. The idea was that Ni(II) would form a similar complex where by virtue of different metal and bridging situation, we might be able to form a cavity suitable for H-bonding with the guest. In this chapter we have synthesized and characterized a set of complexes with the general formula $M[Ni^{II}_2(L^{L\text{-}his})_2(CH_3COO)]$ where M^+ was varied with K^+, Cs^+, NH_4^+ and R-NH_3^+(where R= $Ph(CH_3)CH$-). The structure with Na^+ had showed the formation of a cavity around two aligned carboxylate[2]. Through variation of counter ions we have tried to understand the binding preference of the cavity. For comparison purpose we have used structural data of **1** in some of the tables and figures.

5.1 Experimental Section

5.1.1 Solvents and Reagents

Details of the solvent purification and analytical measurements have been already discussed in chapter 2. The ligand L-salhis ($H_2L^{L\text{-}his}$) was synthesized using the reported procedure[1]. Data of $Na[Ni^{II}_2(L^{L\text{-}his})_2(CH_3COO)].4MeOH$ (**1**) for comparison were taken from a previous thesis.[2] The complexes have tendency to lose solvent of crystallization and acquire moisture. Hence the number of MeOH/water in the crystal structure and in analysis differs.

5.2 Synthesis

5.2.1 $K[Ni^{II}_2(L^{L\text{-}his})_2(CH_3COO)]$ (2)

A methanolic solution of $Ni(NO_3)_2{\cdot}6H_2O$ (0.291 gm, 1.00 mmol) was added drop wise to a clear solution of $H_2L^{L\text{-}his}$ (0.261 gm, 1.00 mmol) and KOH (0.112 gm, 2 mmol) in 25 mL methanol. Color of the solution was changed from light blue to greenish-blue with gelatinous

precipitate. Excess potassium acetate (0.196 gm, 2 mmol) in methanol was added to this reaction mixture. The precipitate was dissolved and the color was changed to blue. The reaction mixture was stirred for 30 min. Volume of the reaction mixture was reduced by rotary evaporation to ~ 10 mL and kept in refrigerator. After 2-3 days, blue plate shaped crystals were formed which was filtered and washed with cold methanol. The crystals were dried under vacuum, yield 85 %. The crystals lost crystallinity after drying. Anal. Calcd for $K[Ni_2(L^{L\text{-}his})_2(OAc)]\cdot 2H_2O\cdot 2MeOH$ Cal: C, 43.26; H, 4.92; N, 10.09; Found: C, 43.87; H, 5.01; N, 10.14. μ_{eff} (powder, 298K): 3.13 B. M./Ni, Λ_M (ohm^{-1} cm^2 mol^{-1}): 58 (MeOH), 2.3 (DMF).

5.2.2 $Cs[Ni^{II}_2(L^{L\text{-}his})_2(CH_3COO)]$ (3)

A methanolic solution of $Ni(NO_3)_2\cdot 6H_2O$ (0.145 gm, 0.50 mmol) was added drop wise to a clear solution of $H_2L^{L\text{-}his}$ (0.130 gm, 0.50 mmol) and KOH (0.056 gm, 1 mmol) in 25 mL methanol. Color of the solution was changed from light blue to greenish-blue with gelatinous precipitate. Excess cesium acetate (0.191 gm, 1 mmol) in methanol was added to this reaction mixture. The precipitate was dissolved and the color was changed to blue. The reaction mixture was stirred for 30 min. Volume of the reaction mixture was reduced by rotary evaporation to ~10 mL and kept in the refrigerator. After 2-3 days, blue plate shaped crystals were formed which was filtered and washed with cold methanol. The crystals were dried under vacuum, yield 80 %. The crystals lost crystallinity after drying. Anal. Calcd for $Cs[Ni_2(L^{L\text{-}his})_2(OAc)]\cdot 5H_2O$. Cal: C, 36.67; H, 4.29; N, 9.17; Found: C, 36.54; H, 4.31, 9.03. μ_{eff} (powder, 298K): 3.21 B. M./Ni, Λ_M (ohm^{-1} cm^2 mol^{-1}): 50 (MeOH), 1.8 (DMF).

5.2.3 $NH_4[Ni^{II}_2(L^{L\text{-}his})_2(CH_3COO)]$ (4)

A methanolic solution of $Ni(NO_3)_2\cdot 6H_2O$ (0.291 gm, 1.00 mmol) was added drop wise to a clear solution of $H_2L^{L\text{-}his}$ (0.269 gm, 1.00 mmol) and KOH (0.112 gm, 2 mmol) in 25 mL methanol. Color of the solution was changed from light blue to greenish-blue with gelatinous precipitate. Excess ammonium acetate (0.154 gm, 2 mmol) in methanol was added to this reaction mixture. The precipitate was dissolved and the color was changed to blue. The reaction mixture was stirred for 30 min. Volume of the reaction mixture was reduced by rotary evaporation to ~10 mL and kept in the refrigerator. After 2-3 days, blue plate shaped crystals were formed which was filtered and washed with cold methanol. The crystals were dried under vacuum, yield 84 %. The

crystals lost crystallinity after drying. Anal. Calcd. for $NH_4[Ni_2(L^{L\text{-}his})_2(OAc)]\cdot 5H_2O$. Cal: C, 41.94; H, 5.37; N, 12.23; Found: C, 42.35; H, 5.40; N, 12.11. μ_{eff} (powder, 298K): 3.30, B. M./Ni, Λ_M (ohm^{-1} cm^2 mol^{-1}): 65 (MeOH), 8.6 (DMF).

5.2.4 Synthesis of [(*R*)-methylbenzylammonium)][$Ni_2(L^{L\text{-}his})_2(OAc)$] (5)

A methanolic solution of $Ni(acetate)_2\cdot 4H_2O$ (0.248 gm, 1.00 mmol) was mixed with $H_2L^{L\text{-}his}$ (0.261 gm, 1.00 mmol). The mixture was stirred with heating in a water bath. After 30 min of stirring greenish-blue precipitate were appeared. (*R*)-methylbenzylamine (0.060 gm, 0.5 mmol) in methanol was added to this reaction mixture. The precipitate was dissolved and the color was changed to blue. The reaction mixture was stirred for 30 min. Volume of the reaction mixture was reduced by rotary evaporation to ~10 mL and kept in refrigerator. After a day, blue rod shaped crystals were formed which was filtered and washed with cold methanol. The crystals were dried under vacuum, yield 80 %. The CHN analysis matched well with the formula [(*R*)-methylbenzylammonium][$Ni_2(L^{L\text{-}his})_2(OAc)$]$\cdot 6H_2O$. Cal: C, 46.89; H, 5.57; N, 10.64; Found: C, 47.27; H, 5.63; N, 10.31. μ_{eff} (powder, 298K); 3.23 B. M./Ni, Λ_M (ohm^{-1} cm^2 mol^{-1}): 60 (MeOH), 5.3 (DMF).

5.2.5 Synthesis of [(*S*)-methylbenzylammonium][$Ni_2(L^{L\text{-}his})_2(OAc)$] (6)

A methanolic solution of $Ni(acetate)_2\cdot 4H_2O$ (0.248 gm, 1.00 mmol) was mixed with *S*-$H_2L^{L\text{-}his}$ (0.261 gm, 1.00 mmol). The mixture was stirred with heating in a water bath. After 30 min of stirring greenish-blue precipitate were appeared. (*S*)-methylbenzylamine (0.060 gm, 0.5 mmol) in methanol was added to this reaction mixture. The precipitate was dissolved and the color was changed to blue. The reaction mixture was stirred for 30 min. Volume of the reaction mixture was reduced by rotary evaporation to ~10 mL and kept in the refrigerator. After a day, blue rod shaped crystals were formed which was filtered and washed with cold methanol. The crystals were dried under vacuum, yield 80 %. The CHN analysis matched with the formula [(*S*)-methylbenzylammonium][$Ni_2(L^{L\text{-}his})_2(OAc)$]$\cdot 5H_2O$. Cal: C, 47.82; H, 5.46; N, 10.85; Found: C, 47.99; H, 5.53; N, 11.16. μ_{eff} (powder, 298K): 3.18 B. M./Ni, Λ_M (ohm^{-1} cm^2 mol^{-1}): 62 (MeOH), 4.9 (DMF).

Crystallography: Crystals of the complexes obtained during synthesis were used for X-ray analysis. Except **1**, the crystals were mounted on glass fiber. The complex **4** was mounted with mother liquor in a sealed glass capillary. All geometric and intensity data for the crystals were collected at room temperature using a Bruker SMART APEX CCD diffractometer equipped with a fine focus 1.75 kW sealed tube Mo-Kα (λ = 0.71073 Å) X-ray source. The SMART software was used for data acquisition and the SAINT software for data extraction. After the initial solution and refinement with SHELXL, the final refinements were performed on WinGX environment using SHELX-97.[3a] All non-hydrogen atoms were refined anisotropically. Wherever possible, the hydrogen atoms were located from the difference Fourier maps and were refined isotropically. Thus some of the C–H bond will not be ideal and may vary. Perspective views of the complexes were shown using ORTEP. [3b]

5.3 Results and Discussion

5.3.1 Synthesis and Selected Properties

Complexes (except **4** & **5**) were synthesized by stirring $Ni(NO_3)_2{\cdot}6H_2O$, $H_2L^{L\text{-}his}$, KOH and MOAc (M= K^+, Cs^+, and NH_4^+), together in MeOH at 1:1:2:2 ratio (Scheme 5.1). Upon concentrating the solution followed by cooling in refrigerator yielded the block to plate shaped crystals in ~75-80 % yield. Comparing the IR spectra of complexes with that of deprotonated ligand and the complexes reported previously, two closely spaced peaks at 1610, 1593 $cm^{-1}$and a peak at 1348 cm^{-1} were identified as asymmetric and symmetric carboxylate stretches originated from the ligand respectively. The complexes showed broad stretches at 3469 cm^{-1} due to OH (water or H-bonded OH) stretch. Due to broadness of the OH peak N–H stretch could not be identified clearly. Further the complexes have two peaks at 1560 and 1452 cm^{-1} with $\Delta\nu \approx 108$ cm^{-1}, attributed to the ν_{asym} and ν_{sym} stretching modes of the acetate anion coordinated to the Ni(II) centers in the bridging form.[4,5] The stretches for NO_3^- from starting material was absent. The room temperature magnetic moment of the complexes was found to be ~ 3.00 per Ni atom. Similar values were reported for other bridged dinuclear Ni(II) complexes[4,5]

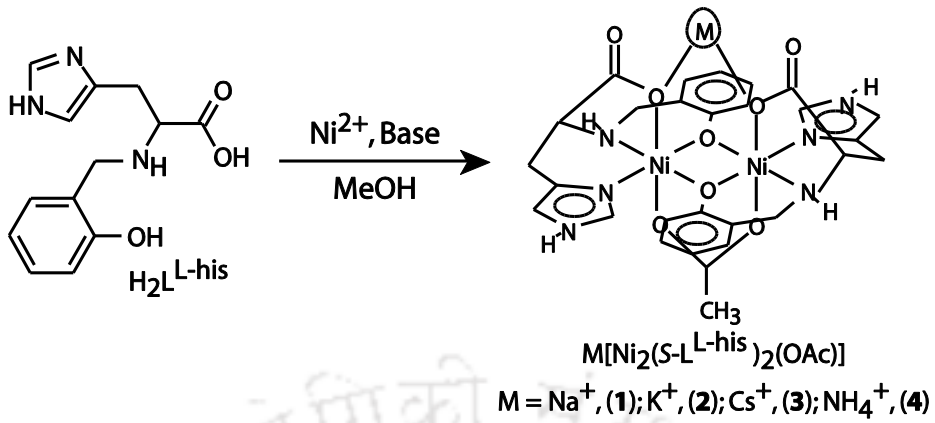

Scheme 5.1 Synthesis of the binuclear complexes.

5.3.2 Molecular structure and the cavity.

The anion, $[Ni_2(L^{l\text{-}his})_2(CH_3COO)]^-$, in **1**-**6** is a acetate bridged dinuclear Ni(II) complex and virtually identical across the structures. Structural parameters in Table 5.1 and selected bond lengths and angles have been provided in Table 5.2, 5.3. Below we have discussed the structure of the anion in **2** as a typical one.

Each octahedral Ni(II) is coordinated by a tetradentate $(L^{L\text{-}his})^{1-}$ ligand, bridging acetate and a bridging phenolate from the other Ni(II) essentially making the anion a tribridged dimer. The two $(L^{L\text{-}his})^{1-}$ with their aromatic phenolate rings forms a approximately C_2 symmetric bowl shaped cavity surrounding two metal bound carboxylates (Figure 5.1). The bond lengths around two Ni(II) centers are close but not identical (Table 5.2). The Ni…Ni separation between 3.004 to 3.0556(1) Å for **1**-**6** is comparable to similar dinuclear complexes[6,7] but shows lack of any metal metal interaction (Table 5.2). The conformation at the chiral carbon of the ligand is *S*. In addition to the asymmetric carbon centre in the ligand, the coordination of amine N to the Ni(II) gives rise to an asymmetric secondary nitrogen atom, which has the *R* configuration. This phenomenon of opposite conformation preference at chiral carbon and amine N has been observed in all the previously characterized and present complexes of this ligand. Assignment of the conformation is supported by low value of Flack parameter (Table 5.1).

Table 5.1 Selected crystallographic data for complexes.

Complexes	**2**	**3**	**4**	**5**
Empirical formula	$C_{29}H_{33}KN_6O_6Ni_2$	$C_{29}H_{32}N_6CsNi_2O_{14}$	$C_{57}H_{62}N_{14}Ni_4O_{22}$	$C_{38}H_{29}Ni_2N_7O_{12}$
Formula weight	830.09	938.90	1530.05	893.20
Wavelength (Å)	0.71073	0.71073	0.71073	0.71073
Crystal system	Orthorhombic	Orthorhombic	Monoclinic	Orthorhombic
Space group	$P2_12_12_1$	$P2_12_12_1$	$P2_1$	$P2_12_12_1$
a, Å	12.7079(5)	12.6003(12)	12.8346(7)	19.1388(9)
b, Å	15.6471(6)	16.0455(15)	19.3890(11)	19.4266(10)
c, Å	19.2646(6)	19.1600(17)	17.2036(10)	12.7626(6)
α, deg	90.00	90.00	90	90.00
β, deg	90.00	90.00	90.852(3)	90.00
γ, deg	90.00	90.00	90	90.00
Volume, $Å^3$	3830.6(2)	3873.7(6)	4280.6(4)	4745.2(4)
Z	4	4	2	2
ρ, Mg/m^3	1.439	1.610	1.187	1.184
μ, mm^{-1}	1.157	1.967	0.933	0.847
Reflections collected	26796	42396	35363	41473
Reflections indep	7858	7154	16420	4964
Flack parameter	-0.008(16)	0.05(4)	0.011(14)	0.02(4)
F(000)	1712	1884	1580	1848
GOF	0.960	1.066	1.016	1.009
Final R indices [*I*>2sigma(*I*)]	R1= 0.0481, wR2 = 0.1076	R1 = 0.0661, wR2 = 0.1367	R1 = 0.0671, wR2 = 0.1735	R1=0.0755, wR2= 0.2344
R indices (all data)	R1 = 0.0992, wR2 = 0.1247	R1 = 0.1676, wR2 = 0.1848	R1 = 0.1023, wR2 = 0.1948	R1=0.0902, wR2= 0.2497

Table 5.2 Selected bond lengths (Å) for the complexes.

	Complex 1	**Complex 2**	**Complex 3**
Ni...Ni	3.004	3.0556(1)	3.054(2)
Ni1-$O_{phenolate}$	2.060(3)	2.103(3)	2.059(9)
	2.037(3)	2.000(3)	2.057(8)
Ni2-$O_{phenolate}$	2.028(2)	2.078(3)	2.016(9)
	2.057(3)	2.051(3)	2.100(8)
Ni1-$O_{carboxylate}$	2.064(3)	2.090(3)	2.091(9)
Ni2-$O_{carboxylate}$	2.081(3)	2.113(3)	2.082(8)
Ni1-$O_{acetate}$	2.077(3)	2.049(3)	2.100(10)
Ni2-$O_{acetate}$	2.089(3)	2.112(3)	2.068(9)
Ni1-N_{amine}	2.088(4)	2.076(4)	2.065(11)
Ni2-N_{amine}	2.073(4)	2.065(4)	2.076(11)
Ni1-$N_{imidazole}$	2.070(3)	2.054(4)	2.115(10)
Ni2-$N_{imidazole}$	2.032(4)	2.096(4)	2.036(10)
Alkali-$O_{carboxy}$	2.386(3)	2.867(3)	3.017(8)
	2.334(3)	2.734(3)	3.103(8)
Alkali-$O_{acetate}$[1]		2.780(3)	3.087(9)
Alkali-$O_{solvent}$[2]	2.346(2)	2.842(5)	3.48(3)
	2.410(2)		3.203(13)
			3.571(12)

[2]Solvent: MeOH in **1** and water in **2** and **3**. Alkali is Na, K or Cs in **1-3** respectively. Data of complex **1** was taken from Ref. 2

Table 5.3 Selected bond angles (Å) for the complexes

	Complex 4a[1]	**Complex 4b**	**Complex 5**
Ni...Ni	3.034(1)	3.005(1)	3.032(2)
Ni1-$O_{phenolate}$	2.055(4)	2.071(5)	2.089(7)
	2.036(4)	2.067(5)	2.002(7)
Ni2-$O_{phenolate}$	2.009(4)	2.029(5)	2.042(7)
	2.070(4)	2.059(5)	2.047(7)

Ni1-$O_{carboxylate}$	2.124(4)	2.058(5)	2.093(9)
Ni2-$O_{carboxylate}$	2.110(4)	2.097(5)	2.125(8)
Ni1-$O_{acetate}$	2.107(5)	2.073(5)	2.089(7)
Ni2-$O_{acetate}$	2.087(5)	2.111(5)	2.101(9)
Ni1-N_{amine}	2.075(5)	2.086(7)	2.065(9)
Ni2-N_{amine}	2.061(5)	2.103(6)	2.090(9)
Ni1-$N_{imidazole}$	2.051(5)	2.054(6)	2.059(8)
Ni2-$N_{imidazole}$	2.049(6)	2.033(5)	2.063(10)

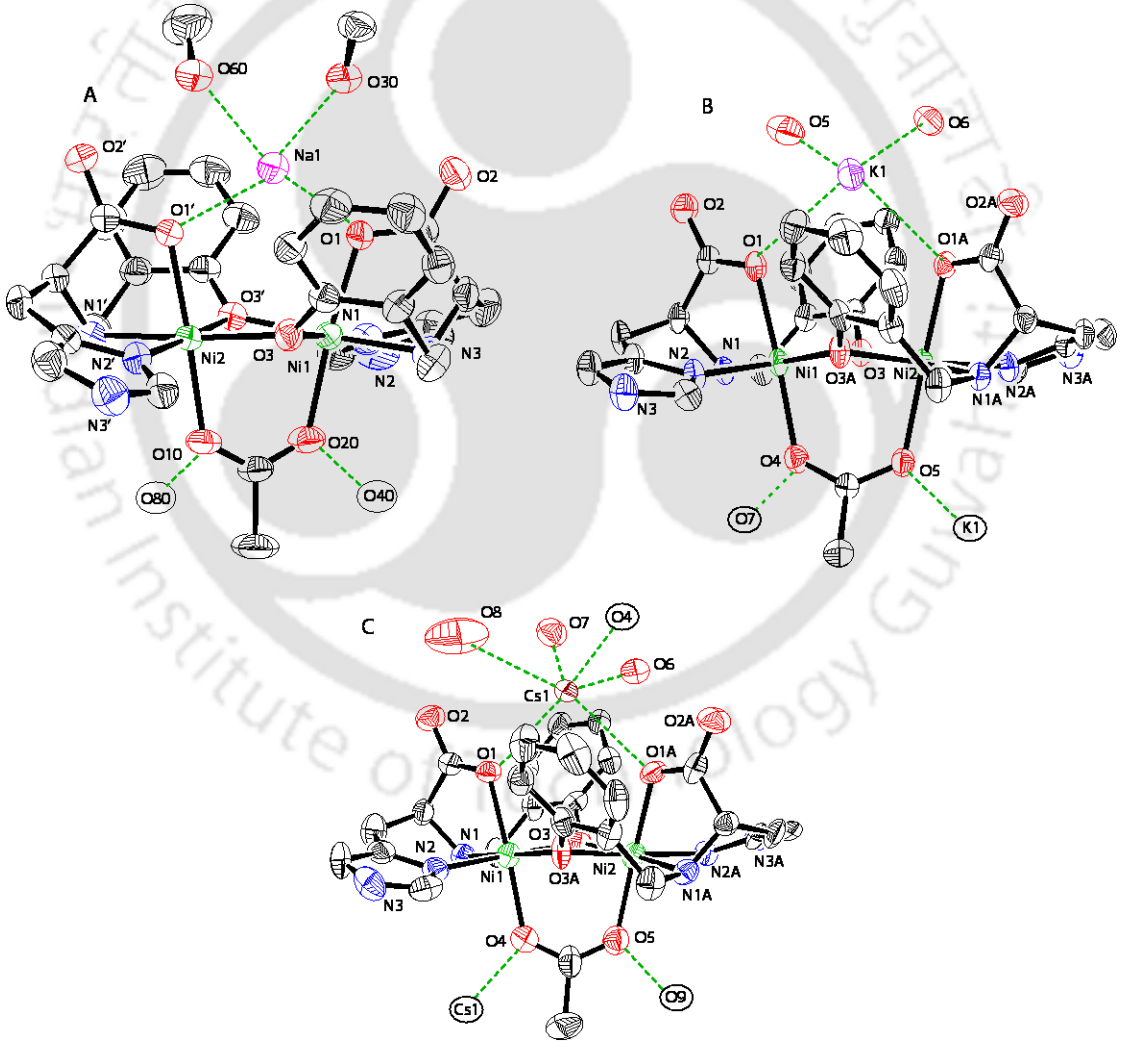

Figure 5.1 The ORTEP figures of complexes **1**, **2**, and **3** (probability set to 50 %). Hydrogens are omitted for clarity.

5.3.3 Alkali metal ion in the cavity.

In **1-3**, the alkali metal ions are bound to the cavity through two metal bound carboxylate oxygens (Figure 5.1). The average alkali metal ion to carboxylate distances (Table 5.2) increases from Na^+ (~ 2.36 Å), K^+ (~2.80 Å) to Cs^+ (~3.06 Å) commensurate with increasing ionic radii (ionic radii of Na^+ , 0.99; K^+, 1.38, Cs^+, 1.67 Å).[8] In addition to these bonds, Na^+ is bound to two methanol (in **1**), K^+ and Cs^+ are bound to acetate oxygen of the neighbouring molecule and water (in **2** and **3**) to have four oxygen donor around Na^+ & K^+ and six oxygen donor around Cs^+(Figure 5.2). Because of the electrostatic nature of alkali metal ions binding with oxygen atoms, the geometry around alkali metal ions are flexible and varies from almost planar in Na^+ to severely distorted geometry around Cs^+ (Figure 5.2).

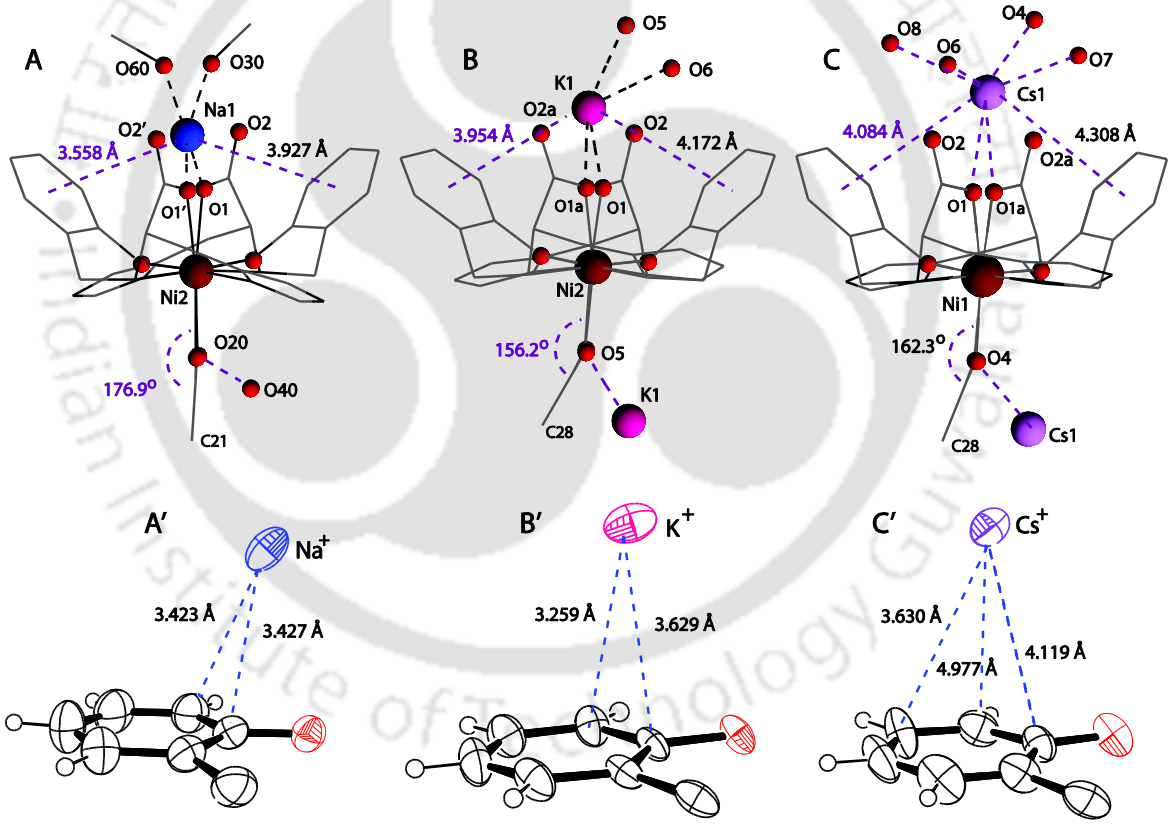

Figure 5.2 Comparison of cation-π interactions of the cations inside the cavity.

One of the two notable features in **1** to **3** is the observation of a possible cation-π interaction with one of the aromatic ring in **1** & **2** and with both the ring in **3**. The distances between alkali metal ions to one aromatic centroid varies from 3.558 to 4.082 Å (Figure 5.2) as the size of the alkali metal ion increases but the distance to both aromatic rings are not same except **3**, where larger ionic radius of Cs^+ allowed symmetric distance to both aromatic rings. The distance between Na^+ and K^+ with tyrosine phenol in a theoretically optimized structure were calculated by Rodger and co-workers found to be 2.619 and 3.022 Å respectively.[9] Na^+-π distances in structurally characterized complexes varies from 3.1 to 3.4 Å. Thus cation-π interactions are weaker in the present complexes. Closer inspection revealed that cation to one of the carbon of the ring is much shorter supporting the presence of interaction. This is reasonable because cavity is rigid and there is a limit on how much the aromatic ring can come closer without disturbing large number of H-bonded interaction that are present.

The other feature is the effect of K^+ and Cs^+ binding on the orientation of bridging acetate. The angle between the plane containing two Ni(II) & two acetate oxygen and the plane containing acetate oxygens and carbons varies from almost linear in **1** to 156.2° in **2** (Figure 5.2). This must have resulted from the alkali metal ions interaction with neighbouring acetate oxygen which is present only in **2** and **3** (Table 5.2). In the absence of this interaction in **1**, acetate coordination is linear which was also seen in other acetate bridged dinuclear complex.

Overall, presence of alkali metal ion inside the anionic cavity influences the crystal lattice formation considerably.

5.3.4 Ammonium and alkyl ammonium cation in the cavity.

Crystals of **4**-**6** diffracts but only **4** could be solved satisfactorily. While $[Ni_2(L^{l\text{-}his})_2(CH_3COO)]^-$ anion and location of the N of the ammonium in crystals of **5** and **6** could be resolved, the cation and some of the solvent molecules could not be refined well enough possibly due to disorder. Thus only general organization of the anionic cavity will be discussed for **5** and **6**.

The asymmetric unit of **4** contains two crystallographically non identical binuclear Ni(II) unit having similar geometry. One of the binuclear units along with guest is shown in Figure 5.3.

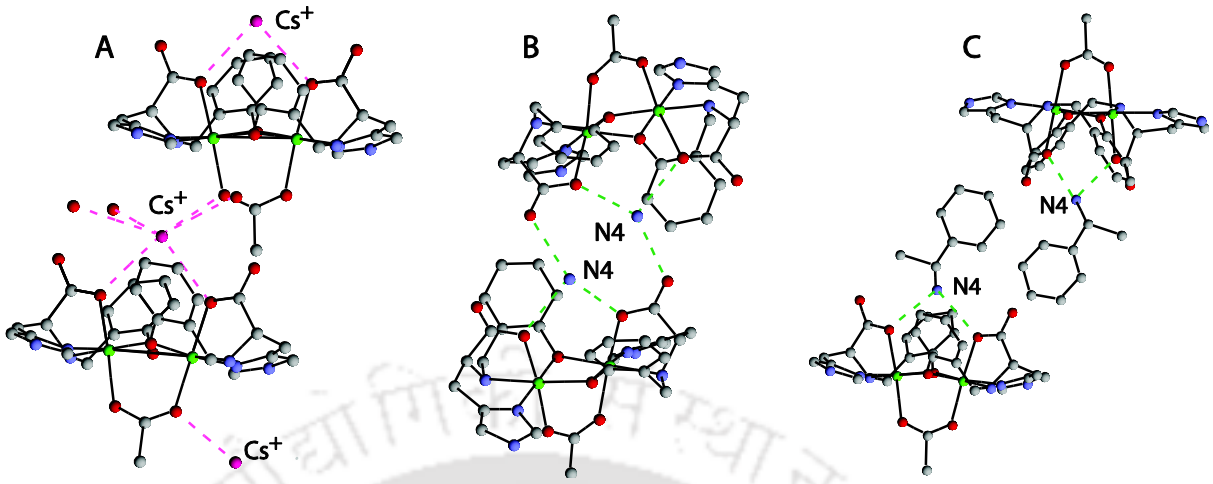

Figure 5.3 Head-tail and head-head arrangements of the binuclear unit w.r.t alkali metals and ammonium ions respectively.

In **4**, the tetrahedral ammonium ion is bound to two carboxylate oxygen of the same molecule, one carboxylate O from the neighboring molecule and one solvent oxygen through H-bonds. As the solvent and ammonium hydrogen could not be located or fixed, the presence of the H-bonds was determined from N and O distances. Differences between **4** and **1**-**3** are in two areas. First difference is that the mode of attachment of guest cation to carboxylate oxygen is through H-bonding. The other difference is that two ammonium nitrogen form bridges between carboxylates from neighbouring binuclear unit organizes cavity differently compared to **2** and **3** where K^+ or Cs^+ form the bridges because of their interaction with the acetate oxygen. This difference organizes cavities differently in the lattices (Figure 5.4).

In **5**, bulky substitution on the ammonium further modified this inter cavity interaction leading to formation of one dimentional channels (~17×14 Å) where disordered cationic guests are inside the channels (Figure 5.4D). Lattice of **6** contain identical channel formation where cations are trapped inside the channel.

5.3.5 Solution behavior of the Host-Guest adducts.

The solution conductance measurements were performed in both methanol and DMF to ascertain the stability of the host-guest adducts. In DMF, all the complexes behave as a non-

conducting solid indicating that the interactions are strong enough to exist as ion pair. In H-bond capable MeOH, complexes showed conductance but value is almost half compared to expect range for 1:1 electrolyte in MeOH (experimental section).[10] This indicates only partial ionization of the host-guest in MeOH.

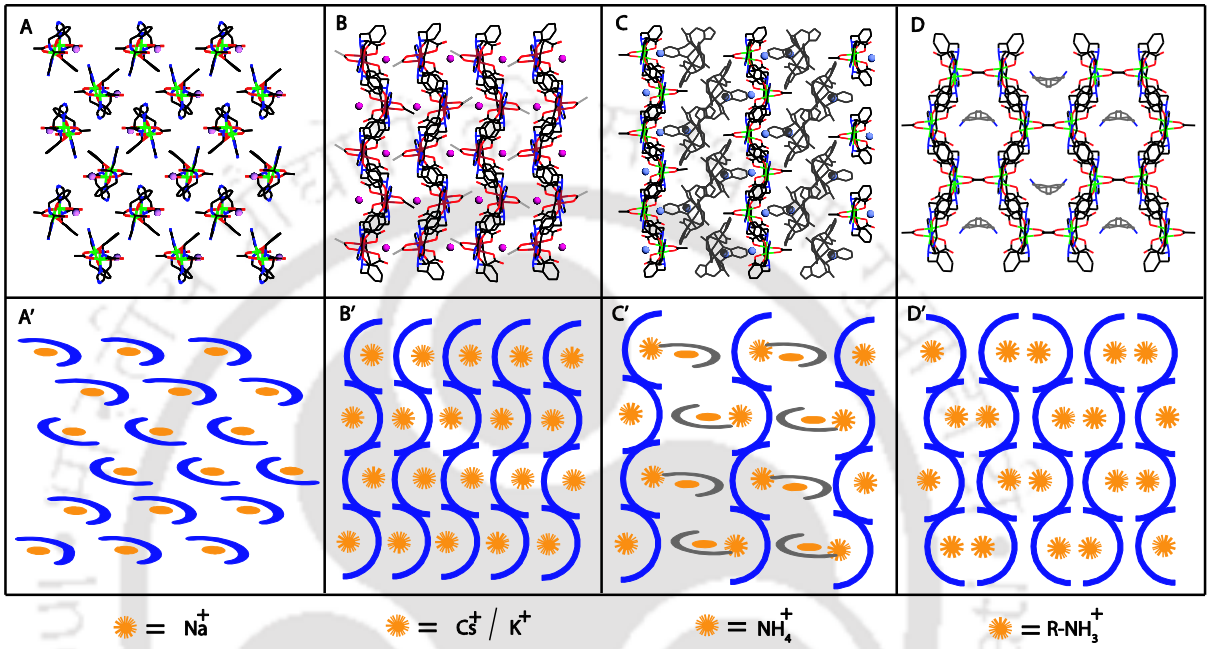

Figure 5.4 Lattice arrangements of the complexes.

5.4. Conclusion.

Structural characterization of a series of complexes having same binuclear Ni(II) anionic cavity with different cation allowed us to view the non covalent interactions possible between the cavity and different type of guests. Alkali ion as guest used carboxylate oxygen as binding post and showed additional cation-π interaction with the aromatic walls of the cavity (Figure 5.3). On the other hand, $R\text{-}NH_3^+$ cations H-bonds to two carboxylates and one oxygen either from neighbouring molecule (in **4**) or solvent (in **5**). Overall, alignment of two carboxylates surrounded by aromatic rings is a versatile cavity which can accommodate different type of cations through different type of non-covalent interactions. This along with anion-cation electrostatic interaction stabilizes the host-guest adducts large enough to prevent ionization in DMF.

The other interesting aspect of the study is the observation of size dependent effect of alkali metal ion on the lattice as well as on the geometry of the acetate bridge (Figure 5.4 A,B). On the other hand, ammonium cations have a quite different effect on the lattice organization (Figure 5.5) which eventually leads to formation of channels. However, quality of structures for **5** and **6** did not allow us to get finer details of the chiral interactions between two neighbouring guests.

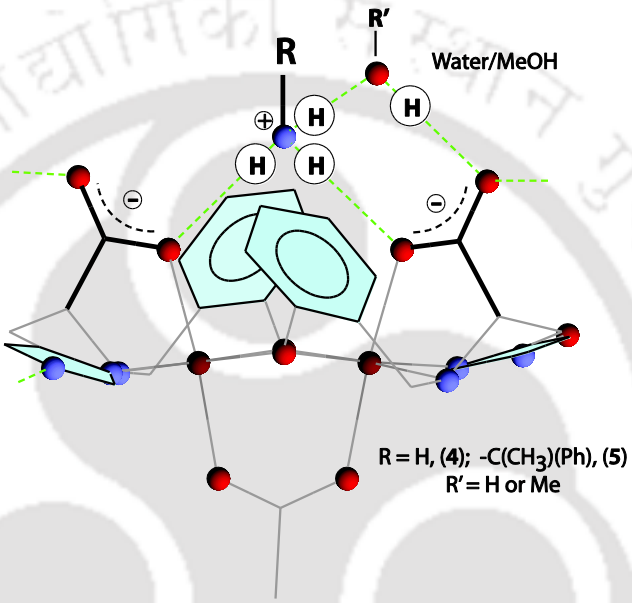

Figurer 5.5 Binding motif of the ammonium ions inside the binuclear cavity.

References:

1. Alam, M. A.; Netaji, M.; Ray, M. *Angew Chem., Int. Ed.* **2003**, *42*, 1940.

2. Alam, M. A. *Synthesis of Enantiomerically Pure Chiral Hosts using Amino Acid Derived Ligands with Fe(III), Ni(II) and Cu(II) ions*, Ph. D thesis, 2004, IIT Guwahati.

3. (a) Sheldrick, G. M. SHELXL-97, Program for the Solution of Crystal Structures, University of Göttingen, Göttingen, Germany, **1997**. (b) C. K. Johnson, ORTEP, Report ORNL-3794, Oak Ridge National Laboratory, Oak Ridge, TN, **1976**.

4. Nakamoto, K. *Infrared and Raman Spectra of Inorganic Compounds*, 5th ed.; Wiley Interscience: New York, **1997,** Part B

5. Koga, T.; Furutachi, H.; Nakamura, T.; Fukita, N.; Ohba, M.; Takahashi, K.; Okawa, H. *Inorg. Chem.* **1998**, *31*, 989.

6. Butcher, R. J.; O'Connor, C. J.; Sinn, E. *Inorg. Chem.* **1982**, *21*, 616.

7. Holligan, B. M.; Jeffery, J. C.; Ward, M. D. *J. Chem. Soc., Dalton Trans*. **1992**, 3337.

8. Shanon, R. D *Acta Cryst.* **1976**, A32, 751.

9. Ruan, C.; Rodgers, M. T. *J. Am. Chem. Soc.* **2004**, *126*, 14600.

10. Geary, W. J. *Coord. Chem. Rev.* **1971**, *7*, 81.

Chapter 6

In the previous chapter we have observed that binuclear Ni(II) complexes with $(L^{L\text{-}his})^{2-}$ have a chiral cavity where ammonium ion binds within the cavity. In this chapter we have synthesized a mononuclear complex which behaves as a chiral monobasic acid and it transforms to the binuclear Ni(II) complexes in the presence of a base. Employing amino alcohols as base we have been successful in separation of enantiomers of amino alcohols. We chose amino alcohols[1] as the target guest because of their structural similarity to adrenaline and nor-adrenaline, a hormone and neurotransmitter[2] respectively (Scheme 6.1). Another reason for choosing amino alcohols is the presence of two different H-bonding capable groups namely amine (ammonium after conversion) and alcohol. Thus binding with the host can be enhanced by electrostatic attraction between cationic ammonium guest and anionic host.

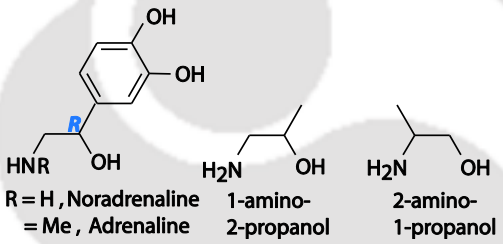

Scheme 6.1 Structures of racemic amino alcohols used along with the noradrenaline and adrenaline.

6.1 Experimental Section

6.1.1 Solvents and Reagents

Solvents used were purified prior to the use following standard literature procedure. Salicyaldehyde, racemic 1-Amino-2-propanol, (*S*)-(+)-1-amino-2-propanol and 2-amino-1-propanol were purchased from Aldrich Chemical Co. L-histidine monohydrochloride was purchased from Loba Chemicals Pvt. Ltd, India and used as received.

6.1.2 Measurements

The IR spectra were recorded on Perkin-Elmer Spectrum one FT-IR spectrophotometer with KBr discs in the range 4000-400 cm^{-1} and electronic spectra on Perkin-Elmer Lambda 25 UV-vis spectrophotometer. The ^1H NMR spectrum was recorded using Varian Mercury plus 400 MHz instrument. Solid-state magnetic susceptibility of the complexes at room temperature was recorded using Sherwood Scientific Magnetic balance MSB-1. Solution electrical conductivity

and solution pH were measured with Eutech Instruments CON 5/TDS 5 Conductivity Meter and Ecoscan pH meter respectively. Both the instruments were calibrated with standard solutions. Elemental analyses were performed on a Carlo Erba 1108 and also by using a Perkin-Elmer series II 2400 instrument. Optical rotations were measured using a Perkin-Elmer 343 polarimeter. Ligand $H_2L^{L\text{-}his}$ was prepared following the literature procedure.[3]

The single crystals were mounted on glass fibers. All geometric and intensity data for the crystals were collected at room temperature using a Bruker SMART APEX. CCD diffractometer equipped with a fine focus 1.75 kW sealed tube Mo-Kα (λ = 0.71073 Å) X-ray source, with increasing ω (width of 0.3° per frame) at a scan speed of 10 s per frame. SMART software was used for data acquisition and SAINT software for data extraction. Absorption corrections were not performed. The structures were solved and refined using SHELX-97.[4a] All nonhydrogen atoms were refined anisotropically. The hydrogen atoms wherever possible were located from the difference Fourier maps and were refined isotropically. Thus some of the C-H bonds will not be ideal and may vary. In some structures, hydrogen atoms attached to the lattice water molecules could not be located or fixed, thus calculated and reported formula differs. Selected crystallographic data and bond parameters are summarized in Table 6.1 and Table 6.2, 6.3 respectively. Perspective views of the complexes were shown using ORTEP.[4b]

6.2 Syntheses of Complexes

Detailed synthetic methodologies along with analytical data are given below

6.2.1 [Ni(HL$^{L\text{-}his}$)(OAc)(MeOH)](1)

The ligand $H_2L^{L\text{-}his}$ (0.500 g, 1.91 mmol) and $Ni(OAc)_2.4H_2O$ (0.475 g, 1.91 mmol) were mixed in 15 mL MeOH and kept for stirring. Within a while ligand was dissolved and a clear solution was formed. After 30 min of stirring a light-blue compound starts precipitating. The solid was filtered, washed with acetonitrile and dried under vacuum. Yield 82 %. Rod shaped X-ray quality crystals were obtained by slow evaporation of methanolic solution. Anal. calcd. for $[Ni(HL^{L\text{-}his})(OAc)(MeOH)]\cdot 2H_2O$. C, 44.51; H, 5.11; N, 10.14. Found: C, 44.50; H, 4.90; N,

10.29 %. IR (KBr, cm^{-1}): $\upsilon(COO)_{asym}$ 1603 (s), $\upsilon(COO)_{sym}$ 1457 (s), υ(phenolic CO) 1251(s). μ_{eff} (powder, 298K): 3.28 μB.M./Ni. Λ_M (ohm^{-1} cm^2 mol^{-1}): 26(MeOH), 7.0(DMF).

6.2.2 ((*S*)-1-ammonium-2-propanol)[$Ni_2(L^{L\text{-}his})_2(OAc)$](2)

A methanolic solution of racemic 1-amino-2-propanol (0.085 g, 1.13 mmol) was added to a stirred solution of **1** (0.500 g, 1.13 mmol) in 10 mL of MeOH. After stirring for 2 h, the precipitated solid was filtered, washed with acetonitrile and dried in vacuum. Yield 80 %. X-ray quality crystals as blue plate were obtained from methanolic solution after 4-5 days of keeping in refrigerator. Anal. Calcd for ((*S*)-1-ammonium-2-propanol)[$Ni_2(L^{L\text{-}his})_2$ (OAc)]·$6H_2O$: C, 42.42; H, 5.81; N, 11.17. Found: C, 42.86; H, 6.18; N, 11.08. IR (KBr, cm^{-1}): $\nu(COO)_{asym}$ 1593 (s), $\upsilon(COO)_{sym}$ 1454 (s), υ(phenolic CO) 1291 (s). μ_{eff} (powder, 298K): 3.21 μB.M./Ni. Λ_M (ohm^{-1} cm^2 mol^{-1}): 43 (MeOH), 3 (DMF).

6.2.3 ((*R*)-2-ammonium-1-propanol)[$Ni_2(L^{L\text{-}his})_2(OAc)$](3)

This was prepared from **1** following the procedure described for **2** using racemic 2-amino-1-propanol instead of 1-amino-2-propanol. Yield 75 %. Anal. calcd for ((*R*)-2-ammonium-1-propanol) [$Ni_2(L^{L\text{-}his})_2(OAc)$]·4MeOH.$2H_2O$: C, 46.00; H, 6.37; N, 10.50. Found: C, 46.03; H, 6.35; N, 10.58 IR (KBr, cm^{-1}): $\upsilon(COO)_{asym}$ 1593 (s), $\upsilon(COO)_{sym}$ 1452 (s), υ(phenolic CO) 1290 (s). μ_{eff} (powder, 298K): 3.38 μB.M./Ni. Λ_M (ohm^{-1} cm^2 mol^{-1}): 52 (MeOH), 1 (DMF).

6.2.4 K[$Ni_2(L^{L\text{-}his})_2(OAc)$](4)

The complex **2** (0.250 g, 0.273 mmol) was dissolved in 20 mL MeOH. A water-methanol mixture of excess KNO_3 (0.137 g, 1.36 mmol) was added to the above mixture. After stirring for 2 h the volume was reduced to 10 mL and kept in refrigerator. Blue block crystals were obtained after one week. The crystals were filtered, washed with acetonitrile and dried under vaccum. Yield 70 %. Anal. Calcd for K[$Ni_2(L^{L\text{-}his})_2(OAc)$]·2MeOH·$2H_2O$: C, 43.26; H, 4.92; N, 10.09. Found: C, 43.87; H, 5.01; N, 10.14. IR (KBr, cm^{-1}): $\upsilon(COO)_{asym}$ 1602 (s), $\upsilon(COO)_{sym}$ 1479 (s), υ(phenolic CO) 1254 (s). μ_{eff} (powder, 298K): 3.13 μB.M./Ni. Λ_M (ohm^{-1} cm^2 mol^{-1}): 58 (MeOH), 2.3 (DMF).

6.3 Quantitative estimation of 1-amino-2-propanol

Quantitative estimation of 1-amino-2-propanol was performed using a modification of the principle described for amines elsewhere.[5] The method utilizes spontaneous Schiff base formation of an amine with a chromogenic aldehyde following by determination of Schiff base using spectrophotometry. The formation of Schiff base of 1-amino-2-propanol with salicylaldehyde has been reported in the literature (Scheme 6. 2).[6]

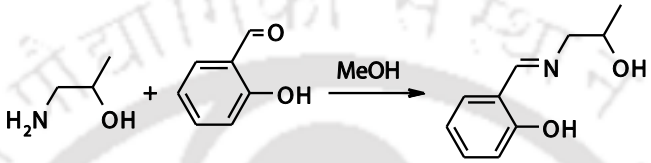

Scheme 6.2 Formation of the Schiff base.

Method. A series of methanolic solution of 1-amino-2-propanol (93 %, racemic, Aldrich) were prepared in presence of excess salicylaldehyde (~10 equiv.) in such a way that final concentration of the solution with respect to 1-amino-2-propanol lies between 0.2 to 1 mM. The solutions were warmed at ~50°C for 10 min and brought to room temperature before measurement. The spectra of the solution, free aldehyde and amine show an absorption maximum at 405 nm due to Schiff base which is absent in the reagents (Figure 6.1). Thus calibration plot for quantitative measurement was performed monitoring the absorption at 405 nm (Figure 6. 2).

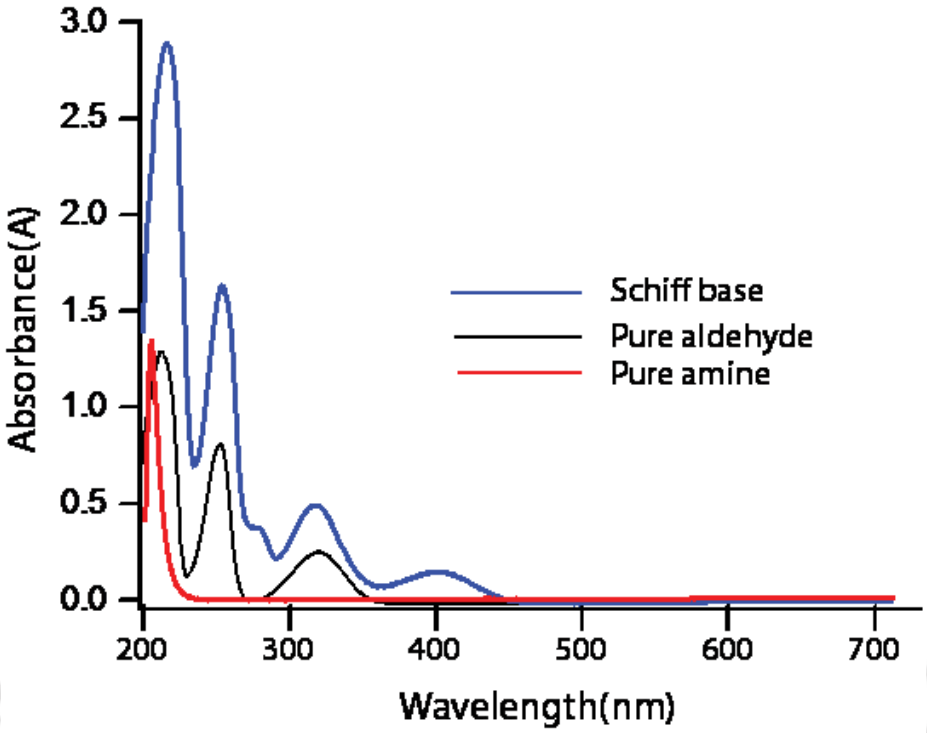

Figure 6.1 Comparison UV-vis plot of pure amine, pure aldehyde and Schiff base.

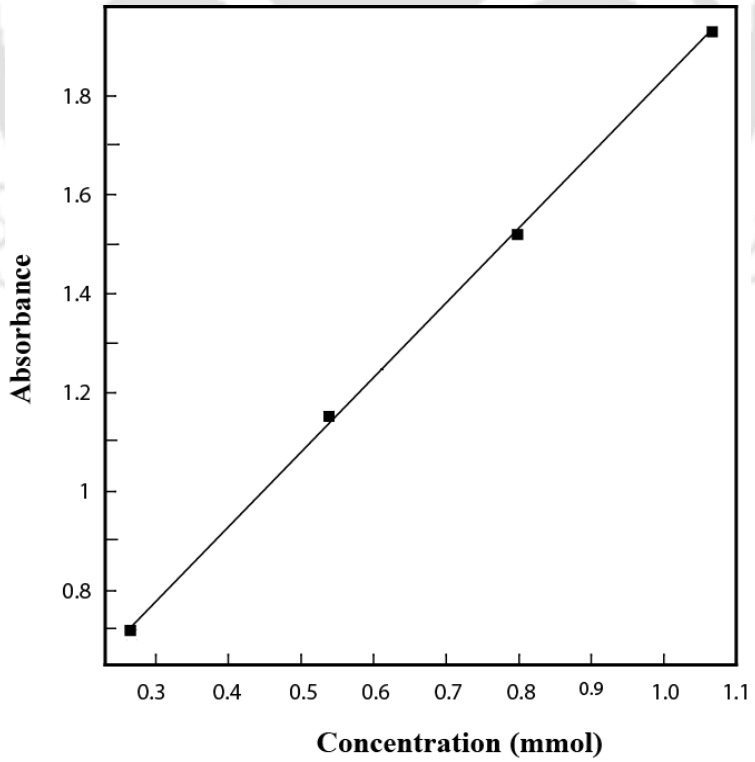

Figure 6.2 Calibration plot for Schiff base of 1-amono-2-propanol and salicyldehyde in MeOH.

6.4 Estimation of enantiomeric separation through HPLC

Chiral amines were extracted from reaction mixture and extent of chiral separation was measured using HPLC using Chiralcel OD-H coloumn attached with refractive index detector at a flow-rate of 1mL /min. Hexane and isopropanol in 93:7 ratio was used as eluent. The extraction procedure and organic derivative preparation (necessary for HPLC) and the detailed procedures and corresponding HPLC data plot (Figure 6.3) have been provided below.

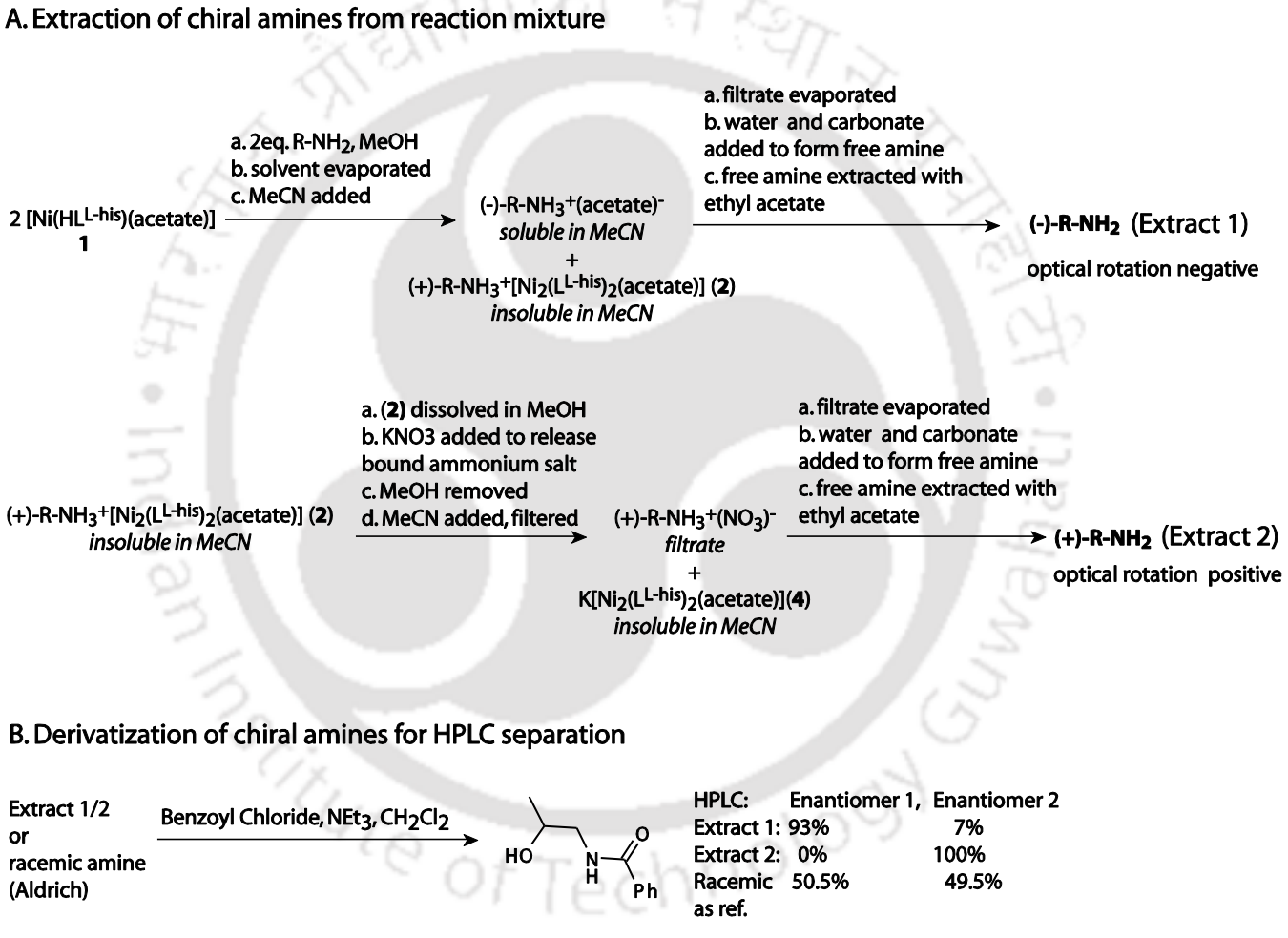

Scheme 6. 3 Methods of extraction (A) and organic derivative preparation (B) of chiral amines from reaction mixture.

6.4.1 Isolation of Amine from reaction mixture of 1-2 *(Extract 1 in Scheme 6. 3).*

Complex 1 (0.250 g, 0.56 mmol) was stirred in MeOH. Racemic 1-amino-2-propanol, (0.042 g, 0.56 mmol) was added to it. After 2-3 h stirring the solvent was evaporated to dryness. The solid was stirred with 20 mL of MeCN and filtered. The filtrate was evaporated, 5mL of water was added and pH maintained to 8-9. The solution was extracted three times with ethyl acetate. Ethyl acetate layer was separated and dried with anhydrous Na_2SO_4 and evaporated to dryness. Volume make up with MeOH (10 mL). Amount of free 1-amino-2-propanol was estimated and found (0.0176 g, 0.234 mmol). Yield 84% Optical rotation of the solution is -0.0425º ± 0.002. Specific Rotation is –24°±1°. Specific rotation was calculated using (S)-(+)-1-amino-2-propanol (Aldrich, e/e ≥ 98%) as reference ($[\alpha]_D^{25}$ –24 ±1°, calculated using same setup).

6.4.2 Isolation of Amine from reaction mixture of 2-4 *(Extract 2 in Scheme 6.3).*

Complex **2** (0.250 g, 0.27 mmol) was stirred in MeOH. KNO_3 (0.137 g, 1.35 mmol) was dissolved in minimum amount of water-MeOH mixture and added to the complex mixture. After stirring for 2-3 h, mixture was evaporated to dryness and was stirred with MeCN and filtered. The filtrate was evaporated, water 2 mL added and pH was maintained between 8-9. The solution was extracted three times with ethyl acetate. Ethyl acetate layer was separated and dried with anhydrous Na_2SO_4 and evaporated to dryness. Volume make up with MeOH (10 mL).

6.4.3 Derivatization of chiral amines reacting with bezoyl chloride

As the chiral coloumn (Chiralcel OD-H) we have used was not suitable to separate chiral amines, we have derivatized the chiral amines to corresponding amide derivative before subjected to HPLC run. All the derivatives were prepared identically and the derivatives were characterized using IR, ESI-Mass and ^{1}H NMR spectroscopy. Racemic form of the amino alcohol purchased from the Aldrich chemical Co. was used as reference. Detailed procedure and characterization data for one representative derivative is provided below.

Racemic-1-amino-2-propanol (0.1 g, 1.33 mmol) was taken in 5ml dichloromethane along with (0.134 g, 1.33 mmol) of triethylamine and kept for stirring in ice cold condition for 10 min. Benzoyl chloride(0.186 g, 1.33 mmol) in dichloromethane was added drop wise manner to the above mixture. After stirring for 5-6 h, ice cold condition was removed and mixture was

stirred at room temperature for another 2-3 h. The compound was extracted from dichloromethane in presence of saturated sodium chloride and compound was obtained as white solid after drying in vacuum. (ESI-MS, + ve) m/z 180.11 ($[M+H]^+$, 30%), 202.10 ($[M+Na]^+$, 100%), IR (KBr, cm^{-1}) 1644(s), 3329(s). ^1H NMR (400 MHz, $CDCl_3$): 7.78 (2H, d, *o*-C_6H_5), 7.41 (1H, t, *p*-C_6H_5), 7.34 (2H, t, *m*-C_6H_5), 7.12 (1H, br, NH), 3.96 (1H, m, CH) 3.58 (1H, dd, CH_2), 3.24 (1H, dd, CH_2), 1.16 (d, 3H, CH_3), mp 91-93 °C. Compounds were washed with diethyl ether and dried under vacuum before HPLC experiment.

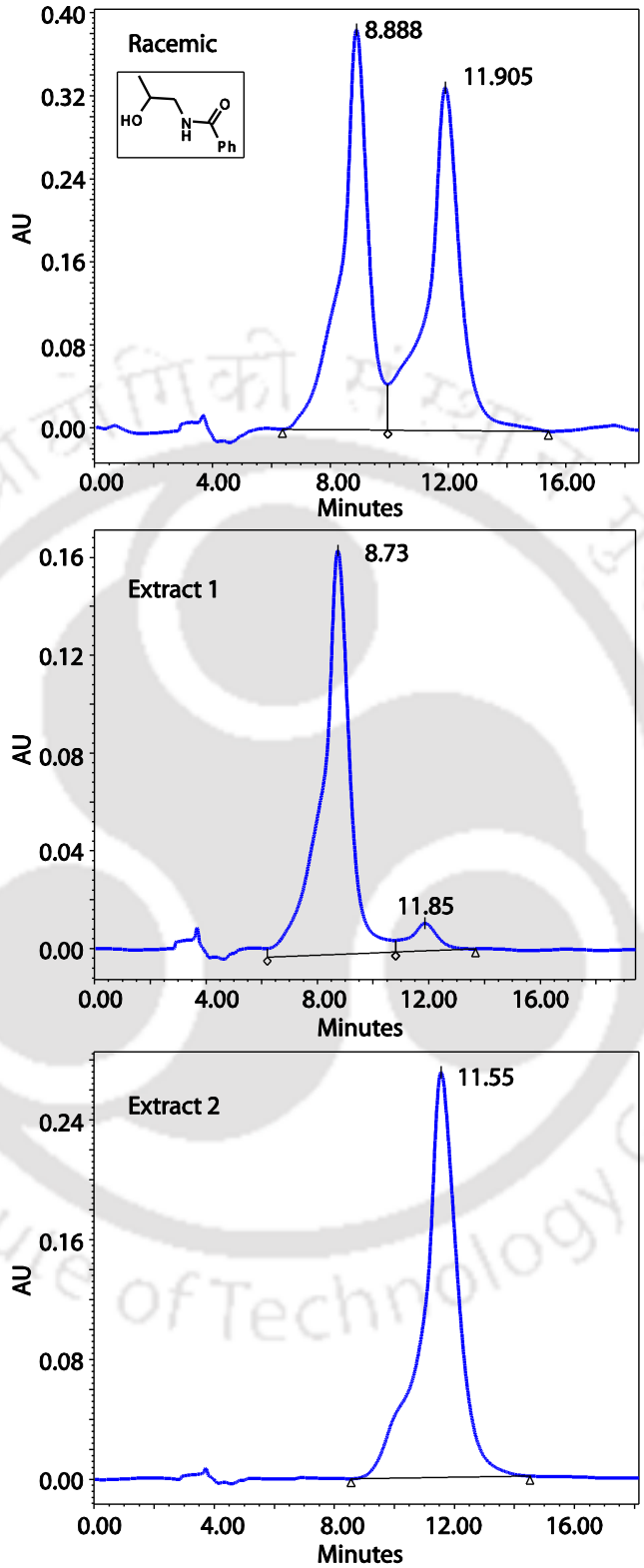

Figure 6.3 HPLC plots showing chiral separation for derivatives of racemic amine (top) and extracted amines after chiral separation using the metathesis.

6.5 Molecular Mechanics

Molecular Mechanics (MM3) calculations were performed using the structural parameter of **2** where we have inverted the chirality of the guest to simulate opposite enantiomer binding and then allowed the guest (locked host) to optimize (Figure 6.4). Molecular mechanics calculations were performed using Cache[@] software by Oxford molecular group using default MM3 parameter[7].

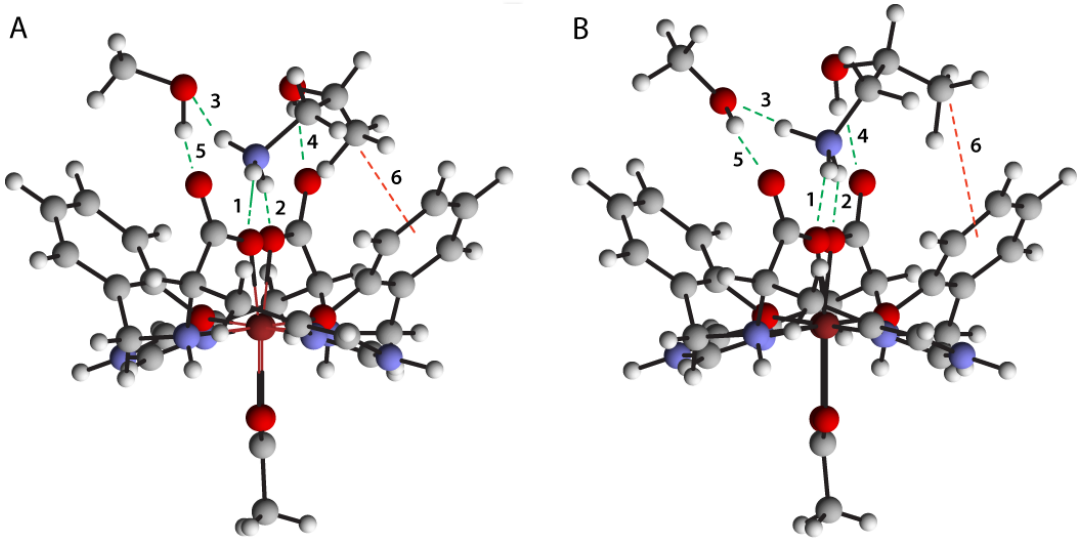

Changes in H-bond & CH..π interaction (in Å) within the cavity for (*R*)-1-amino-2-propanol

	before optimization	after MM3 optimization
1	2.738	2.988
2	2.823	3.013
3	2.818	2.860
4	2.672	3.108
5	2.767	3.112
6	3.055	3.873

Figure 6.4. (A) Figure showing structure of cavity with (*R*)-1-amino-2-propanol using the structural parameters of **2** (contained (*S*)-1-amino-2-propanol) and (B) after the optimization where cavity structure is locked.

Table 6.1 Selected crystallographic data for the complexes.

	1	**2**	**3**	**4**
Empirical formula	$C_{17}H_{25}N_3NiO_7$	$C_{35}H_{55}N_7Ni_2O_{14}$	$C_{35}H_{54}N_7Ni_2O_{13}$	$C_{29}H_{33}KN_6Ni_2O_{13}$
Formula weight (fw)	442.09	915.28	898.27	830.09
Wavelength(Å)	0.71073	0.71073	0.71073	0.71073
Crystal system	orthorhombic	orthorhombic	orthorhombic	orthorhombic
Space group	$P2_12_12_1$	$P2_12_12_1$	$P2_12_12_1$	$P2_12_12_1$
a, Å	8.5896(2)	11.1512(5)	11.3630(3)	12.7079(5)
b, Å	11.0668(2)	13.9822(6)	13.2943(4)	15.6471(6)
c, Å	21.3314(5)	27.8718(12)	27.8916(8)	19.2646(6)
α, β, γ, deg	α = β = γ = 90	α = β = γ = 90	α = β = γ = 90	α = β = γ = 90
V, Å^3	2027.75(8)	4345.7(3)	4213.4(2)	3830.6(2)
Z	4	4	4	4
Calculated density(ρ)	1.448	1.399	1.416	1.439
Abs. coefficient (μ)	1.00	0.936	0.962	1.157
Reflns collected	26049	51416	43131	26796
Indep. reflns	4998	6464	9609	7858
FLACK parameter	0.014(8)	0.05(2)	0.001(3)	-0.008(16)
GOF	1.005	1.078	1.063	0.960
Final R indices	R1 =0.0229,	R1 =0.0618,	R1 =0.0549,	R1 = 0.0481,
[I >2σ(I)]	wR2 = 0.0557	wR2 = 0.1588	wR2 = 0.1409	wR2 = 0.1076
R indices (all data)	R1 = 0.0266,	R1 = 0.0739,	R1 = 0.0633,	R1 = 0.0992,
	wR2 = 0.0567	wR2 = 0.1658	wR2 = 0.1452	wR2 = 0.1247

Table 6.2 Selected bond lengths (Å) and bond angles (°) for complex **1**.

Complex		**1**	
Ni1–O_{phenol}	2.0982(11)	O1–Ni1–N2	176.27(5)
Ni2–O_{phenol}		O2–Ni1–N1	177.83(5)
Ni1–$O_{carboxy}$	2.0802(11)	O3–Ni1–O4	170.46(5)
Ni1–N_{amine}	2.0708(12)	N1–Ni1–N2	91.99(5)
Ni1–N_{imid}	2.0449(12)	N1–Ni1–O4	79.42(4)
Ni1–$O_{acetate}$	2.0393(11)		

Table 6.3 Selected bond lengths (Å) and bond angles (°) for the complexes **2**, **3** and **4**.

	3		**2**		**4**	
Ni1–O_{phenol}	2.043(3)	2.037(3)	2.054(5)	2.063(5)	2.103(3)	2.000(3)
Ni2–O_{phenol}	2.011(3)	2.059(3)	2.030(5)	2.067(5)	2.078(3)	2.051(3)
Ni1/Ni2–$O_{carboxy}$	2.094(3)	2.102(3)	2.075(5)	2.091(4)	2.090(3)	2.113(3)
Ni1/Ni2–N_{amine}	2.076(4)	2.066(4)	2.084(6)	2.068(6)	2.076(4)	2.065(4)
Ni1/Ni2–N_{imid}	2.071(4)	2.051(4)	2.099(6)	2.045(7)	2.054(4)	2.096(4)
Ni1/Ni2–$O_{acetate}$	2.098(3)	2.076(3)	2.097(5)	2.094(5)	2.049(3)	2.112(3)
K–$O_{carboxy}$			2.054(5)		2.867(3)	2.734(3)
N2–Ni1–O3		176.52(14)		176.7(2)		178.37(16)
N1–Ni1–O3a		172.99(14)		174.1(2)		174.94(14)
O1–Ni1–O4		174.24(13)		174.4(2)		174.82(14)
N1–Ni1–N2		85.30(16)		86.1(2)		87.06(16)
N2a–Ni2–O3a		178.32(16)		179.0(2)		175.31(15)
N1a–Ni2–O3		175.47(15)		175.8(2)		173.62(13)
O1a–Ni2–O5		168.79(13)		172.4(2)		167.13(14)
Ni2–O3a–Ni1		96.14(13)		94.8(2)		97.93(16)

Table 6.4 H-bonding distances (Å) present in the crystals.

1	O5 ···O3	2.692	O4···N1	2.988
	O5···O6	2.737	O1···O7	2.483
2	N4···O1	2.738	N4···O1A	2.821
	N4···O7	2.817	O2A···O6	2.675
	O7···O2	2.755	O4···O9	2.714
	O9···O10	2.714	O5···O8	2.715
3	N4···O1	2.789	N4···O1A	2.771
	N4···O7	2.837	O7···O2A	2.735
	O6···O2	2.800	N3···O8	2.762
	O4···O10	2.662	O10···O9	2.711
4	O2···N3A	2.764	O2A···N3	2.831
	O4···O7	2.724	O3···O9	2.898

6.6 Result and discussion

6.6.1 Characterization of 1 and its behaviour as chiral monobasic acid.

A slurry of $Ni(OAc)_2$ and $H_2L^{L\text{-}his}$ in MeOH yielded light blue crystals of [Ni($HL^{L\text{-}his}$) (OAc)(MeOH)](**1**) in high yield (82%). Structural parameters have been provided in Table 6.1 and selected bond lengths and angles in Table 6.2 and 6.3. In **1**, Ni(II) is octahedrally coordinated by tetradentate $(HL^{L\text{-}his})^{1-}$, monodentate acetate and a methanol molecule (Figure 6.5). The conformation at the chiral carbon and amine N are *S* and *R* respectively. This phenomenon of opposite conformation preference at chiral carbon and amine N has been observed in all the previously characterized complexes of this ligand. Assignment of the conformation is supported by low value of Flack parameter (Table 6.1).

The notable feature of this structure is the very short H-bond[8] (O7…O1, 2.484Å) between acetate oxygen (O7) and phenolic oxygen (O1) (Figure 6.5). The location of the hydrogen determined from difference fourier map found to be closer to O7. Consideration of higher acidity of acetate (pK_a 4.75) compared to phenol (pK_a 9.95) we have concluded the formulation of **1** as [Ni($HL^{L\text{-}his}$)(acetate)(H_2O)] not [Ni($L^{L\text{-}his}$)(acetic acid)(H_2O)]. Further, Ni-O_{phenol} distance in **1** is comparable in a analogous situation (~2.15 Å).[9] Carboxylate oxygens, coordinated methanol, lattice methanol and amine took part in multiple H-bond formation (Table

6. 4). The elemental analysis, room temperature magnetic moment and solution conductance supports the formulation.

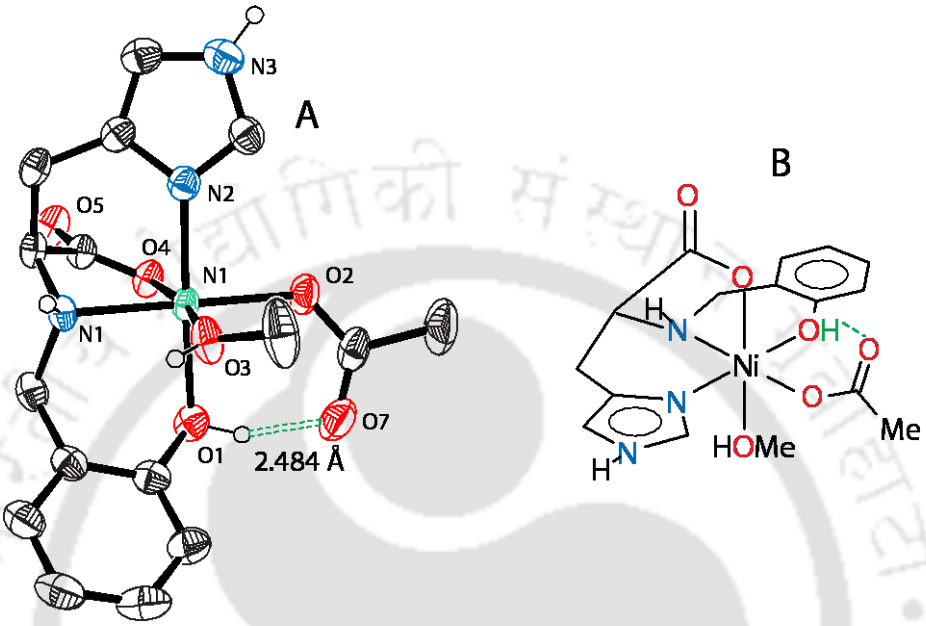

Figure 6.5 ORTEP of **1** with 50 % probability. Hydrogens are removed for clarity.

The coordination to metal along with strong H-bond, the proton bound to phenol (O1) is expected to be acidic. We have performed the pH titration of **1** with LiOH solution. We have avoided use of KOH or NaOH as these alkali ions have tendency to binds to carboxylates and form assembly having limited solubility (Chepter 5)[9] Due to solubility reason we have performed the titration in water/methanol mixture (9:1). As a reference we have measured the pKa of *o*-nitrophenol under the same condition and pKa found to be 7.2 (reported pKa 7.2 in water). The titration plots are shown in Figure 6.8. What is immediately apparent is that, **1** behaves as a monobasic weak acid. The pK_a of the phenolic proton presents in **1** was estimated to be ~6.6 (Figure 6.6) which is considerably lower than that expected for phenolic proton (range 8-10).

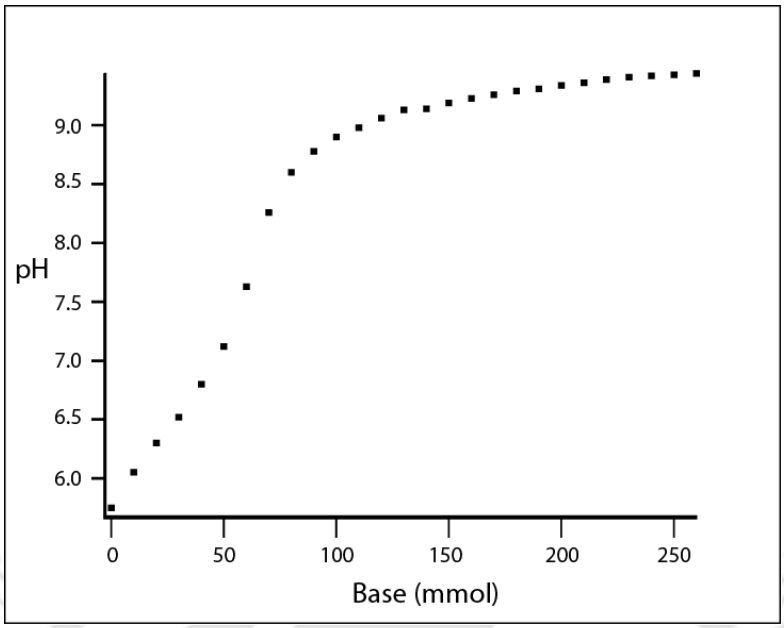

Figure 6.6 pH titration curve for complex **1** (water/methanol in 10:1).

6.6.2 Base induced mononuclear to binuclear transformation and chiral recognition

As the complex **1** behaves as a weak acid we have decided to use chiral amino alcohols as base to deprotonate **1**. Addition of 1 equivalent of racemic 1-amino-2-propanol to **1** yielded crystals of [(*S*)-NH_3^+][$Ni_2(L^{L\text{-}his})_2$(OAc)] (**2**) in high yield (80%), crystallized in the chiral space group $P2_12_12_1$. The structure of **2** showed that mononuclear **1** transformed into a dinuclear Ni(II) complex similar to those in the previous chapter, where (*S*)-1-amino-2-propanol as ammonium salt is bound inside the cavity, formed by the three dimensional orientation of the aromatic rings (Figure 6.7). The transformation has occurred as follows (eq. 1).

$$2\ [Ni(HL^{L\text{-}his})(OAc)](\mathbf{1}) + 2\ rac\text{-}NH_2 \rightarrow$$

$$[(S)\text{-}NH_3^+][Ni_2(L^{L\text{-}his})_2(OAc)](\mathbf{2}) + ((R)\text{-}NH_3^+)(OAc)^- \quad \text{..... (1)}$$

In **2,** the carboxylate groups from both the ligands were aligned next to each other inside the cavity in a way that two of the ammonium N-H from guest is H-bonded to two carboxylate oxygens (Figure 6.7). Alcoholic oxygen of the (*S*)-1-amino-2-propanol is H-bonded to the next available carboxylate oxygen. A solvent methanol molecule further stabilized the orientation of the guest in the cavity by forming additional H-bonds, bridging the N-H of the ammonium group with the remaining carboxylate oxygen. Recognition of both ammonium and alcohol group using aligned carboxylates in **2** is far simpler and effective compared to organic macrocyclic receptors employed in the literature for amine salt recognition[10] Additionally, a CH....π interaction was observed between chiral C-H and aromatic ring of the cavity (Figure 6.7) acting as a third point of recognition.

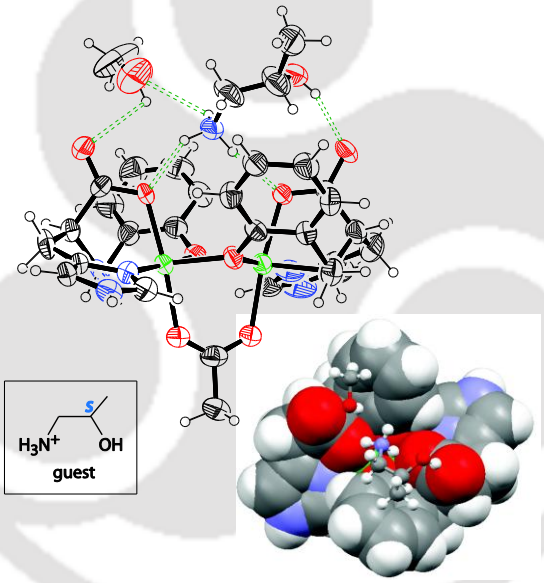

Figure 6.7 ORTEP of **3** with 50 % probability.

In order to check if this recognition process is reproducible for other amines, we choose 2-amino-1-propanol as a second guest where chiral centre has been shifted. Addition of racemic 2-amino-1-propanol to **1** yielded crystals of [(*R*)-NH_3^+][$Ni_2(L^{L\text{-his}})_2$(OAc)] (**3**). The structure of **3** (Figure 6.8) showed the binding of ammonium and alcoholic groups to the identical sites as in **2**. But unlike **2**, it is the *R* isomer of the 2-amino-1-propanol which is bound in **3** (Figure 6.9).

Comparison between **2** and **3** showed that the despite of the shift in position of the chiral centre, the CH....π interaction is preserved for the *R* enantiomer of the 2-amino-1-propanol.

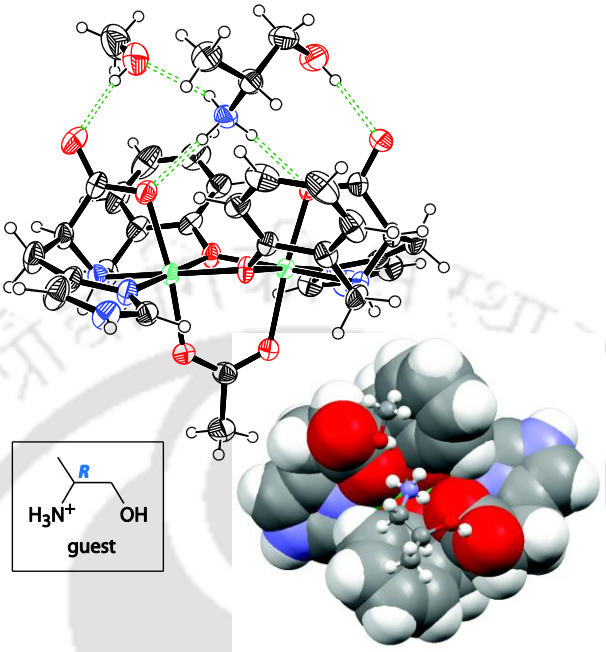

Figure 6.8 ORTEP of **2** with 50 % probability.

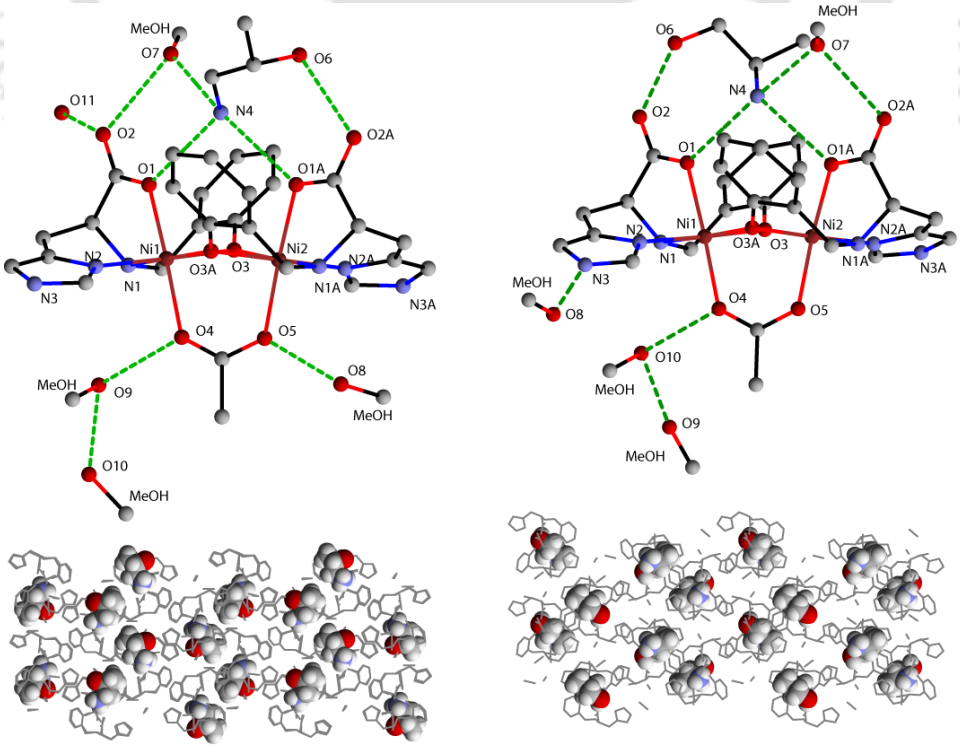

Figure 6.9 H-bonding schemes and space fill models of complex **2** (Fig. A, B) & **3** (Fig. C, D).

6.6.3 Role of CH.....π interaction in the recognition process

Recently, Martin and coworkers have reported that a single CH....π interaction was responsible for 70% chiral enhancement in a organic receptor characterized through NMR and molecular modelling[11] Previously Comba and coworkers also showed that 2 Kcal/mol difference in energy between two diastereoisomer is sufficient to shift the equilibrium to one diastereoisomer by 95%.[12] Further if we consider that the chirality of the guests are reversed (in Figure 6.10), the C-H....π interaction will be lost and the methyl group now will be very close to aromatic group, increasing the steric interaction considerably. The steric interaction can be relieved by moving the methyl group away from the aromatic ring. As the guest is already in a somewhat rigid orientation inside the cavity through four H-bonds and electrostatic interaction, it would require considerable reorganization of the H-bonds within the cavity to nullify the steric interaction. Molecular mechanics calculation supports this hypothesis (Figure 6.4).

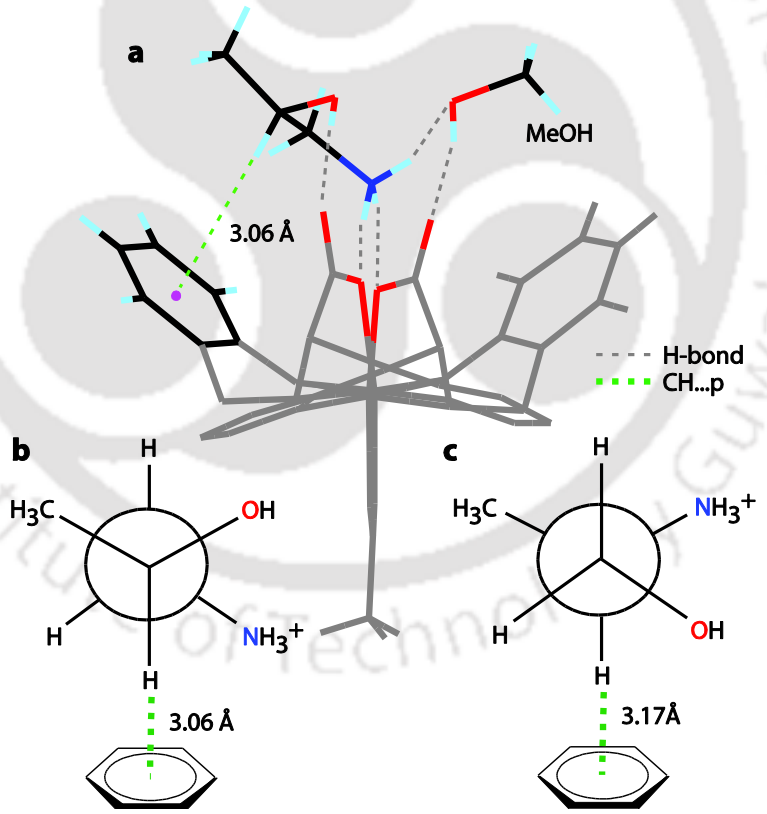

Figure 6.10 C-H….π interaction between the enantiomer and the aromatic ring of the cavity shown for **2**(A, B), and **3** (C).

We think that this steric constrain affect the packing of the molecule, where chirality of the guest has been inverted, into crystals. Attempt to synthesize cavity with pure (*S*)-2-amino-1-propanol (chirality reversed in **3**) resulted in sticky solid instead of crystal. This shows that even though the difference in recognizing enantiomer lies with a favourable CH...π interaction (< 2.7 Kcal/mol)[13] the rigidity of the metallocavity and rigid orientation of guest due to multipoint H-bonding within the cavity is sufficient to alter crystallization behaviour drastically resulting in the isolation of one diastereoisomer.

6.6.4 Solution behaviour

Strong host-guest interaction was also showed in solution behaviour of the complexes. Both **2** and **3** are remarkably stable in N, N′- dimethyl formamide (DMF) solution behaving as non electrolyte as revealed from molar conductance measurements (measured: 1-3 Ω^{-1} cm^2 mol^{-1}; expected for 1:1 electrolyte: 60-80 Ω^{-1} cm^2 mol^{-1}).[14] In H-bond capable MeOH the conductance values (40-50 Ω^{-1} cm^2 mol^{-1}, expected range 80-120 Ω^{-1} cm^2 mol^{-1}) shows only partial ionization. These results underline the strong nature of the H-bonds which are retained in DMF (partially in MeOH).

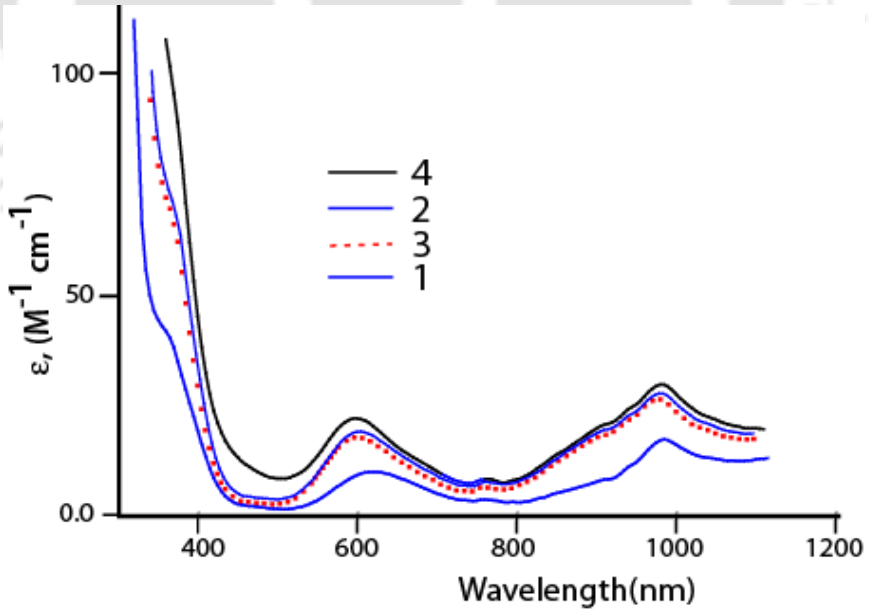

Figure 6.11 The UV-vis spectra of complex **1-4** in DMF.

6.6.5 Recovery of the chiral guest

From a practical point of view, recovery of the recognized guest would be useful. Taking cues from the metal bound carboxylates ability to bind alkali metal ion in the previous chapter, we have employed metathesis reaction with a potassium salt (Scheme 6.4). Isolation and structural characterization of **4** from **2** (yield, 70%) shows the replacement of chiral ammonium cation with K^+ in the cavity. The K^+ in **4** is bound to the central carboxylates (Figure 6.12). This metathesis highlights the advantages of non-covalent interactions for recognition facilitating easy recovery of the guest.

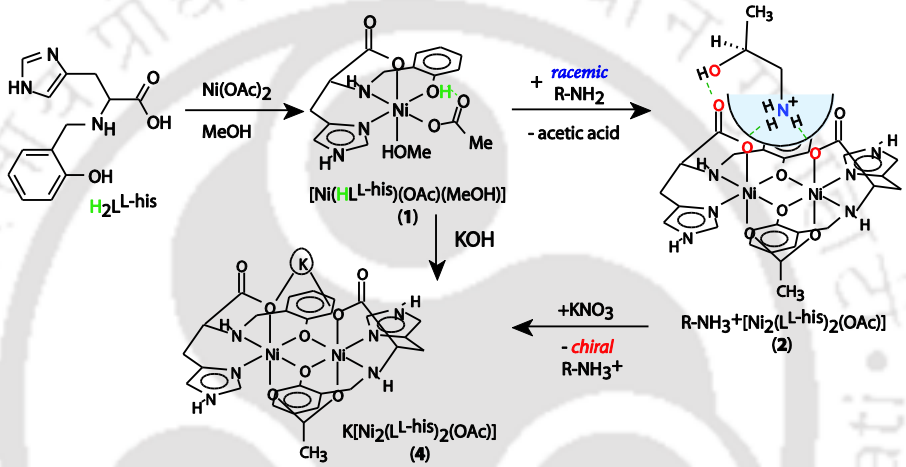

Scheme 6.4 Schematic representation of the sequence of reactions starting with monomer, its convertion to dinuclear cavity and eventual release of enantiomer after metathesis.

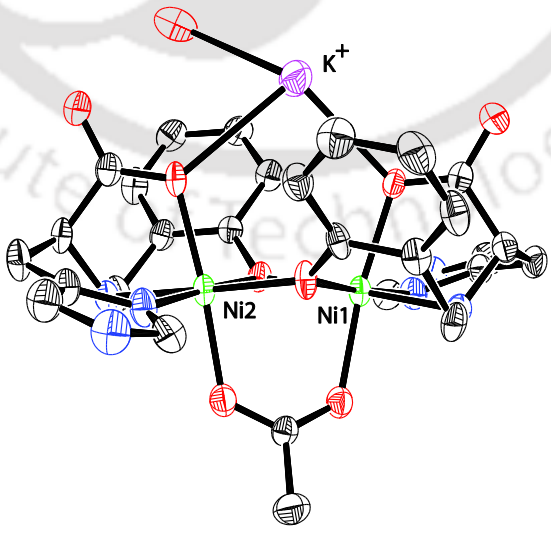

Figure 6.9 ORTEP of **4** with 50 % probability. Hydrogens are removed for clarity.

Unbound amines during transformation of **1** to **2** (Extract 1) and released amines after addition of potassium salt were extracted (Extract 2) in the free amine form, characterized through NMR and ESI-Mass. Spectrophotometric measurement of the isolated amine, provided an estimated yield of 84% for Extract 1 and 63% of (*S*)-(+)-1-amino-2-propanol for respective solution. Amines were then converted to corresponding amide using benzyl chloride and enantiomeric excess were measured through HPLC using chiral coloumn. Extract 1 showed presence of 93% *R* isomer and Extract 2 has 100% *S* isomer (Figure 6.3).

6.6.6 Conclusion

In conclusion, we have synthesized a medium sized rigid cavity incorporating sites to recognize amine and alcohol group in a very efficient way compared to macrocycles. The smaller size and the rigidity of the resulting hosts allowed us for the first time to identify the molecular interactions responsible for recognition inside a chiral cavity through structural characterization of the host-guest complexes. These structural informations helped identifying the presence of weak CH....π interaction with one enantiomer and disfavourable steric interaction over the other enantiomer and cavity can shift the solution equilibrium and crystallization behaviour between two diastereomeric host-guest complex to the extreme to facilitate chiral separation. The role of weak interaction and their effect on the quilibrium has been shown through indirect experiment has been shown by others,[11,12] but this is the first direct evidence through crystallography. The flexibility of the design regarding choice of different amino acids and substitution in the aromatic ring, used in the present process, opens up possibility of recognition and effective separation of other amino alcohols as well. Structures of **2** and **3** also showed aligned carboxylates inside the cavity along with a solvent molecule, acts as efficient receptor for amino alcohols compared to synthetically challenging organic designs.[10] Isolation of acidic **1** and its transformation were important as they provide a general route for relatively volatile chiral amines to trap directly in the cavity. This is completely different from the chiral organic acid salts which do not undergo any such transformation. For practical utility, the recognized enantiopure guest could be recovered through simple metathesis with KNO_3 which was not observed before.

References:

1. (a) Nandhakumar, R.; Soo, A. Y.; Hong, J.; Ham, S.; Kim, K. M. *Tetrahedron* **2009**, *65*, 666. (b) Tsukube, H.; Hosokubo, M.; Wada, M.; Shinoda, S.; Tamiaki, H. *Inorg. Chem.* **2001**, *40*, 740. (c) Schrader, T. *J. Org. Chem.* **1998**, *63*, 264. (d) Kubo, Y.; Maeda, S.; Tikita, S.; Kubo, M. *Nature* **1996**, *382*, 522. (e) Simonato, J.-P.; Pe´caut, J.; Marchon, J.C. *J. Am. Chem. Soc.* **1998**, *120*, 7363. (f) Wang, Q.; Chen, X.; Tao, L.; Wang, L.; Xiao, D.; Yu, X.-Q.; Pu, L. *J. Org. Chem.* **2007**, *72*, 97. (g) Tang, L.; Choi, S.; Nandhakumar, R.; Park, H.; Chung, H.; Chin, J.; Kim, K. M. *J. Org. Chem.* **2008**, *73*, 5996.

2. (a) Schrader, T. *Angew Chem., int. Ed*. **1996**, *35*, 2649. (b) Strader, C. D.; Fong, T. M.; Tata, M. R.; Underwood, D. *Annu Rev. Biochem*. **1994**, *63*, 101.

3. (c) Alam, M. A.; Nethaji, M.; Ray, M. *Angew. Chem., Int. Ed*. **2003**, *2*, 1940.

4. (a) Sheldrick, G. M. SHELXL-97, Program for the Solution of Crystal Structures; University of Göttingen: Göttingen, Germany. (b) Johnson, C. K. *ORTEP, Report ORNL-3794*, Oak Ridge National Laboratory, Oak Ridge, TN, 1976.

5. Nakatsuji, S.; Nakano, R.; Kawano, M.; Nakashima, K.; Akiyama, S. *Chem. Pharm. Bull*. **1982**, *30*, 2467.

6. Ho1pfl, H.; Sa´nchez M.; Barba, V.; Farfa´n, N.; Rojas, S.; Santillan, R. *Inorg. Chem.* **1998**, 37, 1679.

7. (a) Yahiro, N. *Chem. Lett*. **1982**, 1479. (b) Allinger, N. L. *J. Am. Chem. Soc*. **1977**, *99*, 8127

8. (a) *The weak hydrogen bond in structural chemistry and biology*. Desiraju, G. R.; Steiner, T. IUCr Monographs on Crystallography, Vol. 9, Oxford University press. (b) Kudava, S. S.; Blaser, D.; Bose, R.; Desiraju, G. R, *J. Org. Chem.* **1999**, *66*, 1621. (c) Pal, S.; Sankarnan, N. B.; Samanta, A. *Angew Chem., int. Ed*. **2003**, *42*, 1741. (d) Lioyd, G. O.; Atwood, J. L.; Barbour, L. J. *Chem. Commun*. **2005**, 1845.

9. Dubey, M.; Koner, R. R.; Ray, M. *Inorg. Chem.* **2009**, *48*, 9294.

10. (c) Zhang, X. X.; Bradshaw, J. S.; Lzatt, R. M. *Chem. Rev*. **1997**, *97*, 3313. (d) Kano, K. *J. Phys. Org. Chem.* **1998**, *10*, 286. (c) Gubitz, G. M.; Schmid, G. *Biopharm. Drug Dispos.* **2001**, *22*, 291. (d) Maier, N. M.; Lindner, W. *Anal. Bioanal. Chem*. **2007**, *389*, 377.

11. Carrillo, R.; Lopez-Rodriguez, M.; Martin, V. S.; Martin, T. *Angew Chem., Int. Ed*. **2009**, *48*, 7803.

12. Bernhardt, P. V.; Comba, P.; Gyr, T.; Varnagy, K. *Inorg. Chem*. **1992**, *31*, 1220.

13. (a) Levitt, M.; Perutz, M. F.; *J. Mol. Biol.* **1988**, *201*, 751. (b) Desiraju, G. R.; Steiner, T. *The Weak Hydrogen Bond in Structural Chemistry and Biology*; Oxford University Press: Oxford, 1999.

14. W. J. Geary, *Coord. Chem. Rev*. **1971**, *7*, 81.

List of publications

1. "Ferrocene substitution in amino acid strengthens the axial binding in Cu(II) complexes and separates the hydrophobic and hydrophilic region in the Crystals" Subash Chandra Sahoo and Manabendra Ray *Dalton Trans.* **2007**, 5148.

2. "Formation of a narrow chiral cavity in *bis*-copper(II) complexes of ferrocenylmethyl-L-tyrosine and its interaction with achiral guests".
   Subash Chandra Sahoo and Manabendra Ray *Dalton Trans.* **2009**, 3230.

3. "Chiral recognition and resolution of amino alcohols through well defined interaction inside metallocavity".
   Subash Chandra Sahoo and Manabendra Ray *Chemistry A European Journal*, 2010, 16(17), 5004.

4. "Effect of metal coordination and intramolecular H-bond on the acidity of phenolic proton in a set of structurally characterized octahedral Ni(II) complexes of L-histidine derivative".
   Subash Chandra Sahoo**,** Mrigendra Dubey,Md. Akhtarul Alam and Manabndra Ray**,** *Inorg. Chem. Acta*. **2010,** 363, 3055.

Manuscript to be submitted

5. "Effect of ligand chirality on structure and tuning of electrochemical properties of bis-Copper(II) complexes of ferrocenyl-methyl-L-leucine"
   Subash Chandra Sahoo and Manabendra Ray

6. " Cations inside a mettalocavity: Effect of cations size on structural diversity.
   Subash Chandra Sahoo, Md. Akhtarul Alam and Manabendra Ray